SU-SEL-67-051

Interplanetary Electron Content Measured Between Earth and the Pioneer VI and VII Spacecraft Using Radio Propagation Effects

by

Richard L. Koehler

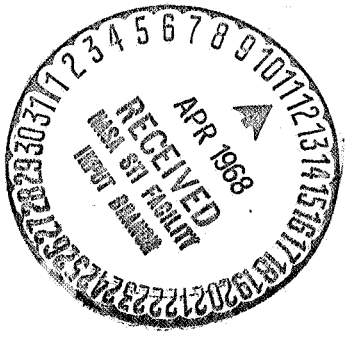

May 1967

Scientific Report No. 1
Prepared under National Aeronautics and Space Administration
Contracts NSR 05-020-109 and NAS 2-3908
Scientific Report No. 20
[redacted] NsG 377 (NASA GRANT)

RADIOSCIENCE LABORATORY
STANFORD ELECTRONICS LABORATORIES
STANFORD UNIVERSITY • STANFORD, CALIFORNIA

SEL-67-051

INTERPLANETARY ELECTRON CONTENT MEASURED BETWEEN EARTH AND THE PIONEER VI AND VII SPACECRAFT USING RADIO PROPAGATION EFFECTS

by

Richard L. Koehler

May 1967

Scientific Report No. 1
Prepared under
NSR 05-020-109

Scientific Report No. 1
Prepared under
NAS 2-3908

Scientific Report No. 20
Prepared under
NsG 377

Radioscience Laboratory
Stanford Electronics Laboratories
Stanford University Stanford, California

INTERPLANETARY ELECTRON CONTENT MEASURED BETWEEN EARTH AND THE PIONEER VI AND VII SPACECRAFT USING RADIO PROPAGATION EFFECTS

by Richard L. Koehler

ABSTRACT

Radio signals at 50 and 425 MHz are sent from Stanford to deep space probes to determine the electron number density, structure, and time variability of the interplanetary medium. The electron content (the number of electrons in a square meter column along the path of propagation) introduces a small difference in the time it takes the 50 and 425 MHz signals to reach the spacecraft; this time difference is caused by the frequency dependence of the velocity of propagation in a plasma. The time difference, determined from phase shift of the modulation on both signals, provides a measure of the total electron content in the path. In addition, the number of cycles of phase shift of the radio frequency carriers are counted to provide a high resolution measurement of the change in electron content along the path.

Total contents of up to 200×10^{16} el/m^2 have been measured, a substantial portion of which was located in the dense ionosphere surrounding the earth. To obtain the interplanetary content, the ionospheric portion must be subtracted. Differential doppler measurement of beacon satellite signals provide the ionospheric electron content several times during one Pioneer pass. Faraday rotation of signals from a geostationary satellite (Applied Technology Satellite) provides continuous measurement of electron content through the ionosphere. The interplanetary content is divided by the spacecraft range to give the average number density.

An average interplanetary number density of 4.3 el/cm^3 with an rms variation of ± 3.6 was determined from 125 Pioneer VI interplanetary electron content measurements, made from December 1965 through May 1966. The average determined from 170 Pioneer VII measurements made from August 1966 to March 1967 is 8.7 ± 4.0 el/cm^3. The higher average at the later date occurred because interplanetary space was filled more frequently with

denser plasma caused by increasing solar activity. The quiet level for Pioneer VII was about 5 el/cm^3, which is near the average for Pioneer VI; these values are in agreement with measurements made locally in interplanetary space by plasma probe experimenters. All of the above measurements apply to regions of interplanetary space which are within 20 percent of the distance of earth from the sun.

Three sudden, large increases in the electron content were observed: 24 October 1966, 10 November 1966, and 25 January 1967. They are explained by a model with a rectangular-shaped increase in electron number density with a spherical wavefront traveling radially from the sun at 300 to 400 km/sec. The increase in density ranged from 30 to 55 electrons/cm^3 above the background density, extending over a region from 5 to 10 $\times$ 10^6 km along a solar radial.

CONTENTS

CONTENTS (CONTD)

CONTENTS (CONTD)

TABLES

ILLUSTRATIONS

ILLUSTRATIONS (CONTD)

ILLUSTRATIONS (CONTD)

ACKNOWLEDGMENT

I would like to thank the many people who participated in this project: in particular, Prof. Allen M. Peterson who was my thesis advisor--especially for his extra encouragement at the end--, Prof. V. R. Eshleman who was the principal investigator and guided the research program, the Pioneer project office at the NASA-Ames Research Center who made this experiment possible, the operators who ran the transmitters and antenna, Blaine Craig who capably reduced the data with very little direction, H. Taylor Howard who managed much of the project at Stanford, Stan Hall for his cooperation in the use of his beacon satellite station, Roy Long and his team at Stanford Research Institute for the spacecraft receiver, TRW Systems, Inc. for their design of the Pioneer spacecraft, and Jet Propulsion Laboratory for receiving the Pioneer telemetry, and to Chris Tapley and Eleanore Perkins without whose help I would have been unable to complete this in time. The Pioneer project reported on was supported by National Aeronautics and Space Administration contract NAS 2-1759, NSR 05-020-109 and NAS 2-3908.

I INTRODUCTION

A. Purpose

The purpose of this experiment is to measure the electron content of the solar wind with radio propagation effects to determine the interplanetary electron number density and the structure and temporal behavior of the interplanetary plasma.

B. Previous Research

In the past, solar wind has been measured with plasma probes that detect proton and alpha particle (He^{++}) flux. [The first measurements of the solar wind plasma for an extended time were made on Mariner II on its voyage past Venus. Plasma velocities ranged from 400 to 700 km/sec. Estimates of plasma density, which were made for only a few spectra, were 2.5 and 4.5 protons/cc (Neugebauer and Snyder, 1962).]

Attemps to use plasma probes to measure the electron flux, however, have been unsuccessful. On the other hand, radio propagation methods have been successful for measuring ionospheric electrons for years. For example, radar reflections from the ionosphere have been used to determine the ionospheric electron profile up to the peak electron density. Earth satellites, beginning with the launch of Sputnik I in 1957, allowed radio methods to be extended from the ionospheric peak around 300 km to the satellite heights around 1000 km.

C. Area of Present Research

The work reported in this study extends the above-mentioned radio propagation techniques for detecting electrons into deep space--50 to 100 Gm (1 Gm = 10^9 m = 10^6 km) from the earth.

In this experiment, differential group path and phase path measurements are made on radio signals transmitted from earth to the Pioneer interplanetary spacecraft (Fig.1-1). The differential group path measurements are proportional to the number of electrons in a column (electron content) from the earth to the spacecraft, and when divided by the

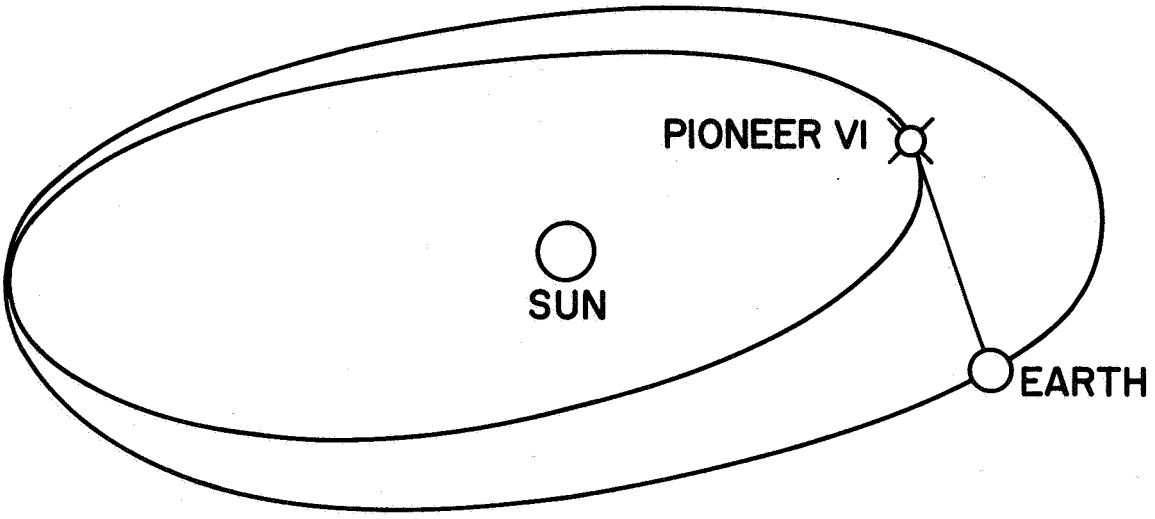

FIG. 1-1. PIONEER VI IN ORBIT AROUND THE SUN.

spacecraft range, give the average electron number density. The differential phase path measurements complement these results by providing more detail on the changes in content and density with time.

D. Contributions of the Experiment

The overall contributions of the experiment are

1. Determination of the average interplanetary electron number density in the vicinity of the orbit of the earth.
2. Detection and measurement of several very dense plasma pulses from the sun.

The author, in addition to his contribution to those listed above:

1. Determined the common type of model that describes the plasma pulses discovered in this experiment.
2. Supervised the ionospheric measurements and analyses necessary to make possible interplanetary electron content determination from Pioneer measurements. Conceived the establishment of a

second ATS receiving station to reduce the effect of spatial differences in the ionosphere.

3. Played a major role in the overall design of the spacecraft receiver and designed part of it in detail, including an in-flight modulation phase calibration system; he also wrote the receiver instructions manual (Koehler, 1965).

4. Increased the accuracy of the electron number density calculations by normalizing the data to 1 AU.

5. Confirmed that the divergence of group and phase path measurements was due to the neglect of second order terms in the Pioneer data analysis.

II METHODS USED TO MEASURE THE INTERPLANETARY ELECTRON CONTENT

This chapter briefly describes the interplanetary electron content experiment as conducted by SCRA* and the principles on which the experiment is based.

Nearly 4 years of intensive effort by a number of people at SCRA were required in preparation for the experiment. Measurements began in December 1965 with the launch of the Pioneer VI spacecraft.

A. Principle of Operation

Two high power transmitters on the ground transmit through SCRA's 150 ft "Big Dish" to the Pioneer spacecraft (Fig. 1-1). At the frequencies used, the large power required to span distances equal to half way to the sun precludes transmitting from the spacecraft. The experiment uses the equivalent of two pulses transmitted simultaneously on frequencies near 50 and 425 MHz from earth to the spacecraft. As the two pulses travel to the spacecraft, the low frequency pulse travels slower and falls behind the high frequency pulse. The time difference between the arrival of the two pulses at the spacecraft is proportional to the total number of electrons in a column along the propagation path. This time difference is measured at the spacecraft and telemetered back to one of the Jet Propulsion Laboratory's Deep Space Stations.

1. Group Velocity

The pulse described above travels at a group velocity v_g of

$$v_g = c\left(1 - \frac{40.3\ N}{f^2}\right) \qquad (2.1)$$

in a medium with a low ion (and electron) density; i.e., the second term in Eq. (2.1) is less than about 0.03. (MKS units are used in the equations

*SCRA (Stanford Center for Radar Astronomy) is a joint venture in radar astronomy and space science of Stanford University and Stanford Research Institute.

and for all quantities, except for the quoting of values of density which are conveniently expressed in number per cc.)

It is clear from this equation that the higher the electron density, N, the slower the group velocity. Also the change in group velocity is a function of frequency, which permits the measurement of the delay of the 50 MHz pulse relative to the 425 MHz pulse. Pulses are not actually used to determine the time delay; instead, the 50 and 425 MHz carriers are continuously modulated at 7.7 kHz (or at 8.7 kHz), and the time delay in the arrival at the spacecraft is proportional to the phase shift between the modulation signals. The modulation phase is quantized into 3° steps corresponding to about 2×10^{16} el/m^2 of electron content. For a 50 Gm propagation path and the 5 el/cc typical interplanetary background electron number density, the integrated electron content is 25×10^{16} el/m^2. The minimum resolution of 2×10^{16} el/m^2 would detect a change in density of 0.5 el/cc over this whole path.

2. Phase Velocity

The velocity of the waves of a radio wave is the phase velocity v_p

$$v_p = c\left(1 + \frac{40.3\ N}{f^2}\right) \qquad (2.2)$$

This is similar to the expression for the group velocity, except that v_p is slightly faster rather than slower than the speed of light. As the two carriers propagate from the earth to the spacecraft, the phase of the 50 MHz carrier advances faster than the 2/17 harmonic of the 425 MHz carrier (= 50 MHz). Thus, the increase in phase velocity appears as an RF phase advance at the spacecraft. The phase of the 50 MHz carrier is compared with the phase of the appropriate subharmonic (2/17) of the 425 MHz carrier and the number of cycles of phase difference are counted and telemetered back to earth.

One cycle of phase difference corresponds to about 0.04×10^{16} el/m^2, which is much finer resolution than can be used, since small changes in the ionospheric content mask interplanetary changes to about 0.5×10^{16} el/m^2. Over a 50 Gm propagation path, a change of about 0.01 el/cc along

the whole path can be detected, although changes in the ionosphere limit this resolution to about 0.1 el/cc. A 50 Gm path with a 5 el/cc electron density gives 25×10^{16} el/m^2 electron content, corresponding to 625 RF cycles of phase difference between the carriers. This large multifold ambiguity in the number of RF cycles precludes an absolute determination of content, but minute changes in content can be detected. The ambiguity can be removed by fitting the carrier phase (phase path) determination of electron content to the nonambiguous modulation phase (group path) determination of electron content. The fine resolution phase path determination of electron content then provides interpolation between the more coarsely spaced points of the group path determination of electron content. The group path and phase path provide two independent measurements of the same time-variable electron content, even though they use the same radio signals, and provide a very reassuring redundancy when an unusual event occurs.

While the problem of the ionospheric electron content intervening between the earth and the interplanetary electron content remains to be discussed, the techniques for subtracting the ionospheric content from the Pioneer content are deferred until after the interplanetary electron content measurements are contrasted with plasma probe measurements of the interplanetary medium.

B. Comparison of Integrated Electron Content with Plasma Probe Measurements

Plasma probes aboard the Pioneer spacecraft (Lazarus et al, 1966; Wolfe et al, 1966) measure protons and alpha particles at the point in interplanetary space occupied by the probe. The radio propagation method measures all the electrons along the propagation path from earth to Pioneer. Another dimension is added to the local plasma measurement, but it has the disadvantage that we do not know where the electrons are located along the path. Much can be learned by study of the plasma probe and integrated content data separately, but more can be gained by combining the data. For example, the breadth of a plasma pulse can be inferred from the electron content along the propagation path from earth to the Pioneer spacecraft, and from the proton density and velocity measured by the plasma probes aboard Pioneer.

The radio propagation method measures the electron content from the effect of the electrons themselves on the radio transmissions. The plasma probes do not measure the number of electrons directly; they only measure (positively charged) protons and alpha particles, and an equal number of electrons are inferred to satisfy space charge neutrality. Direct measurements of interplanetary electron density on a spacecraft have been obscured by photoemission, which can generate densities several orders of magnitude larger than the interplanetary density. Spacecraft charge can easily repel or attract the interplanetary electrons, since they have such low translational energy ($\approx$ 0.25 eV). Photoemission and spacecraft charge change the total number of electrons along the propagation path by only a microscopic amount.

Any protons with less energy than the minimum energy detectable by the plasma probes would remain undetected by the probes. The radio propagation method could detect the electrons associated with these low-energy protons, since the radio propagation effects are not dependent on the electron energy.

C. Subtraction of Ionospheric Content from the Pioneer Content

The ionosphere, a blanket of electrons (and ions) surrounding the earth, is included in the number of electrons measured between the earth and the Pioneer interplanetary spacecraft. The ionosphere must be measured separately so that it can be subtracted from the Pioneer earth-spacecraft content to obtain the interplanetary content. The vertical ionospheric content ranges from 4×10^{16} el/m^2 at night to 10 to 30 $\times 10^{16}$ el/m^2 during the day. A slant path through the ionosphere can increase this content by a factor of 3. A comparison with 25×10^{16} el/m^2 for a 50 Gm interplanetary propagation path at 5 el/cc shows the need to subtract the ionosphere.

1. Beacon Satellites: Differential Doppler Technique

Beacon satellites transmit on 40 and 360 MHz from a 1000 km height orbit above most of the ionosphere (Fig. 2-1). The differential doppler, caused by changes in phase velocity along the satellite's propagation path to earth, are measured just as in the Pioneer receiver.

The ionospheric electron content determined from the measurement of beacon satellite transmissions can be subtracted from the earth-interplanetary spacecraft Pioneer electron content wherever the beacon and Pioneer propagation paths are close together.

2. ATS Geostationary Satellite: Faraday Rotation Technique

The geostationary Applied Technology Satellite (ATS) transmits on 137 MHz from its fixed position in the sky. The plane of polarization of ATS's 137 MHz transmission is like a twisted ribbon between ATS and our ground-based receiver. Faraday rotation of the plane of polarization, or the twist of this ribbon is (approximately) proportional to the electron content along the ribbon, with the twisting being tighter where the density is higher. The ribbon is fixed at the satellite end, so a change in the total number of twists must turn off the ribbon at the ground receiver end. We continuously record the plane of polarization (the plane of the ribbon) on the ground, beginning at night when there is usually less than one-half turn, to midday when they typically reach a maximum of seven half-turns. The continuity of the record establishes the total number of turns that exist at midday.

The ATS Faraday rotation is converted to ionospheric electron content along Pioneer's slant ray path through the ionosphere, then subtracted from Pioneer's electron content to give a continuous record of the interplanetary electron content for the 12 hours each day that Pioneer is above the horizon. ATS went on station only in December 1966; since that time we have been able to measure time variations of the interplanetary content, which is far superior to the point measurements afforded by beacon satellites.

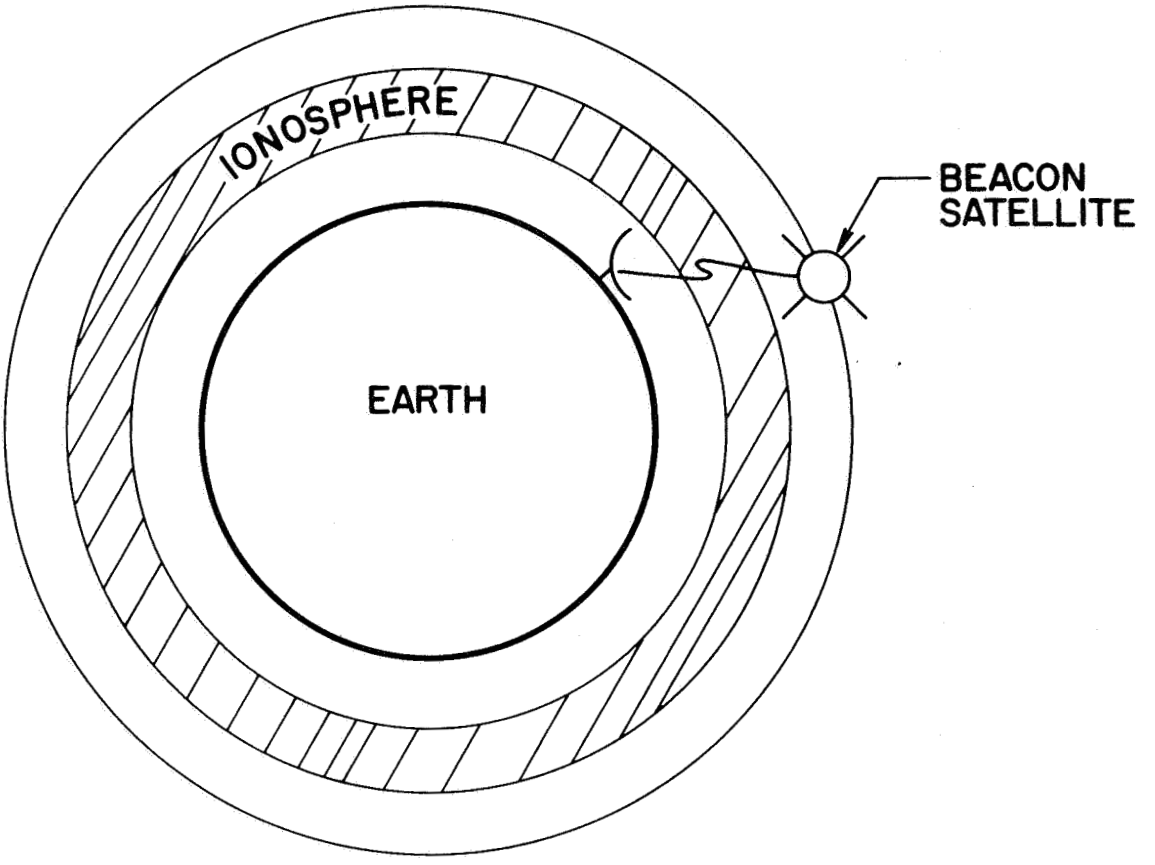

FIG. 2-1. BEACON SATELLITE IN ORBIT AROUND THE EARTH. Signals from the satellite are used to measure the ionosphere (the blanket of electrons around the earth).

III DERIVATION OF THE RADIO PROPAGATION EFFECTS ON WHICH THE EXPERIMENT IS BASED

Measurement of interplanetary electron content in this experiment is based on the effect that electrons have on the phase velocity of radio carriers (sent from earth to the Pioneer spacecraft in deep space) and on the group velocity of the modulation on those carriers. In this chapter both the phase and group velocity are derived from the Appleton-Hartree equation. The differential phase velocity is then used to linearly relate the integrated electron content to the measured RF phase shift between the 49.8 MHz carrier and the appropriate (2/17) harmonic of the 423.3 MHz carrier. The differential group velocity is used to linearly relate the integrated electron content to the phase shift between the 7.692 kHz (or 8.692 kHz) modulation on the 49.8 and 423.3 MHz carriers.

A. The Appleton-Hartree Equation for the Index of Refraction

1. Symbols Used in the Equation

The following symbols are used in the Appleton-Hartree equation [Ratcliffe, 1959], with rationalized MKS units.

n = wave refractive index

μ = real part of n

N = electron number density, in electrons/m^3

$f = \omega/2\pi$ = frequency of a radio wave, in Hz

e = charge on an electron = -1.602×10^{-19} coulomb

m = mass of an electron = 9.109×10^{-31} kg

ϵ_o = permittivity of free space = 8.85×10^{-12} farad/m

μ_o = permeability of free space = $4\pi \times 10^{-7}$ henry/m

c = speed of light = 2.998×10^{8} m/sec

H = magnetic intensity in A/m. At Stanford, the earth's magnetic intensity $\approx$ 40 A/m.

θ = angle between the wave normal and $\vec{H}$

ν = effective collision frequency between electrons and heavy particles, in sec^{-1}

$$\frac{e^2}{4\pi^2 \epsilon_o m} = 80.6 \text{ m}^3/\text{sec}^2$$

$$X = \left(\frac{e^2 N}{4\pi^2 \epsilon_o m}\right) \frac{1}{f^2} = \frac{80.6\ N}{f^2} = \frac{(\text{plasma frequency})^2}{(\text{wave frequency})^2}$$

$$|Y| = \left(\frac{\mu_o H |e|}{2\pi\ m}\right) \frac{1}{f} = \frac{(\text{gyro frequency})}{(\text{wave frequency})}$$

At Stanford and within the main ionospheric layer, $|Y| \approx \frac{1.4 \times 10^6}{f}$

$$\left.\begin{aligned} Y_L &= |Y \cos\theta| \\ Y_T &= |Y \sin\theta| \end{aligned}\right\}$$ Here, Y_L and Y_T appear as the square, or square root of the square, so the absolute value is used.

$$Z = \frac{\nu}{2\pi f} = \frac{1}{2\pi} \frac{(\text{collision frequency})}{(\text{wave frequency})}$$

The Appleton-Hartree equation for the square of the complex refractive index of a radio wave in a magneto-ionic medium, such as the ionosphere or interplanetary space, is

$$n^2 = 1 - \frac{X}{1 - iZ - \frac{\frac{1}{2} Y_T^2}{1 - X - iZ} \pm \sqrt{\frac{\frac{1}{4} Y_T^4}{(1 - X - iZ)^2} + Y_L^2}} \qquad (3.1)$$

2. High Frequency Approximation for the Radio Wave Index of Refraction

Equation (3.1) does not look very complex until it is used. Fortunately for our case, most of the terms are negligible for the range of values we use, which enables us to use the "high-frequency approximation." The worst-case (in the sense of the validity of the approximation) values for this experiment for Eq. (3.1) are

f = 50 MHz, our lowest frequency

$N = 10^{12}$ electrons/m^3, a very high value for the densest part of the ionosphere at the densest time of the day (noon to 3 p.m.)

ν = 1/sec, collision frequency at 300 km height

$\theta = 45°$, a typical value, and not worst case, because this parameter does not have a worst case

The above values give

$$X = 4 \times 10^{-2}$$

$$Y_L = Y_T = 2 \times 10^{-2}$$

$$Z = 5 \times 10^{-8}$$

By substituting these worst case values into Eq. (3.1) and crossing out the relatively small quantities, the terms which must be retained can be identified.

$$n^2 = 1 - \frac{(4 \times 10^{-2})}{1 - i(5 \times 10^{-8}) - \frac{\frac{1}{2}(4 \times 10^{-4})}{1 - (4 \times 10^{-2}) - i(5 \times 10^{-8})} \pm \sqrt{\frac{\frac{1}{4}(1.6 \times 10^{-7})}{\left[1 - (4 \times 10^{-2}) - i(5 \times 10^{-8})\right]^2} + (4 \times 10^{-4})}}$$

$$\approx 1 - \frac{4 \times 10^{-2}}{1 \pm 2 \times 10^{-2}}$$

Rewriting Eq. (3.1) with the terms retained above

$$n^2 \approx 1 - \frac{X}{1 \pm |Y_L|} \tag{3.2}$$

Taking the square root of n^2 from Eq. (3.2), using the binomial expansion, we obtain the index of refraction μ

$$\mu \equiv n = \underbrace{1}_{\substack{0 \\ \text{order}}} - \frac{1}{2} X \underbrace{(1}_{\substack{1\text{st} \\ \text{order}}} \pm \underbrace{|Y_L| - \frac{1}{4} X)}_{\substack{2\text{nd} \\ \text{order}}} \approx 1 - \frac{1}{2} X \tag{3.3}$$

Inserting the worst-case numbers into Eq. (3.3) shows that the terms labeled second order are truly negligible.

$$\mu \approx 1 - 0.02(1 \pm 0.02 - 0.01) \approx 1 - 0.02$$

The terms labeled "2nd order," while small, are even smaller in regions other than the peak density of the ionosphere or at times other than the middle of the day. However, ray bending more seriously affects the phase path than these second order terms in μ by themselves, when at low elevation angles (below 20°) during the middle of the day. The second order effects and bending are treated more thoroughly in Appendix A.

B. Phase Path and Electron Content

The phase path P for a radio wave going between a transmitter at $\ell = 0$ to a receiver at $\ell = s$ is

$$P = \int_0^s \mu \, d\ell = \int_0^s \frac{c}{v_p} \, d\ell = c \, t_p \tag{3.4}$$

where v_p is the phase velocity and t_p is the transit time. The phase path is not a physical path but the distance that a wave crest would have traveled in free space (at the velocity of light) in the transit time. The change $\Delta\ell$ in the phase path length from its free space value, caused by electrons along the path, is obtained by subtracting the physical path length s from the phase path P of Eq. (3.4). The right-hand side of Eq. (3.3) for μ is used.

$$\Delta\ell \equiv P - s = \int_0^s (\mu - 1) \, d\ell = -\frac{1}{2} \int_0^s X \, d\ell = -\frac{80.6}{2} \frac{1}{f^2} \int_0^s N \, d\ell$$

$$\Delta\ell = -\frac{80.6}{2} \frac{1}{f^2} I \tag{3.5}$$

where

$$I \equiv \int_0^s N \, d\ell$$

The incremental phase path $\Delta\ell$ is proportional to the integrated electron content I and inversely proportional to the frequency squared. Notice that the phase path P is shorter than the physical path s, that is, $\Delta\ell$ is negative.

The $\Delta\ell$ cannot be measured directly because the physical path length s, which is on the order of 10^{10} m, is not known to a wavelength of the order of 10 m. However, the frequency dependence of $\Delta\ell$ permits us to measure the difference ΔP between the phase path at two different frequencies.

$$\Delta P \equiv P_L - P_H = \Delta\ell_L - \Delta\ell_H = -\frac{80.6}{2}\left(\frac{1}{f_L^2} - \frac{1}{f_H^2}\right) I$$

$$\Delta P = -\frac{80.6}{2}\frac{1}{f_L^2}\left(1 - \frac{f_L^2}{f_H^2}\right) I \qquad (3.6)$$

where subscript L refers to the lower frequency and subscript H refers to the higher frequency. Solving Eq. (3.6) for I and inserting our frequencies of $f_L = 49.8$ MHz and $f_H = 17/2 \times 49.8 = 423.3$ MHz we get

$$I = \frac{1}{\left(\frac{80.6}{2}\right)} \frac{f_L^2}{\left(1 - \frac{f_L^2}{f_H^2}\right)} (-\Delta P) = 0.624 \times 10^{14} (-\Delta P)$$

P is measured in the number d of 49.8 MHz wavelengths $\lambda_{49.8}$.

$$I = 0.624 \times 10^{14} (\lambda_{49.8}\, d) = 3.755 \times 10^{14}\, d \qquad (3.7)$$

Equation (3.7) is used to convert the measured phase difference in cycles between the 49.8 MHz carrier and the appropriate (2/17) harmonic of the 423.3 MHz carrier to obtain the integrated electron content.

A +5 Hz bias is added to the 49.8 MHz carrier at the transmitter to resolve the sign of the change in the number d (or I or ΔP). Changes in I cause a change in frequency less than 0.5 Hz in all experiments to date.

The ratio f_L/f_H does not matter as long as it is less than about 0.7, and that both frequencies can be coherently compared at some common frequency. The 49.8 MHz frequency, already licensed to us and within

the range of our 20 to 64 MHz 250 kW transmitter, is low enough to provide a very high resolution of phase path, and high enough to be insignificantly affected by ionospheric refraction when the elevation is above 20°.

C. Group Velocity and Group Refractive Index

The equation for the group refractive index is

$$\mu' \equiv \frac{c}{v_g} \frac{c}{\left(\frac{d\omega}{dk}\right)} = \frac{d\,(\mu\omega)}{d\omega} = \mu + \omega \frac{d\mu}{d\omega} \tag{3.8}$$

where v_g is the group velocity and $k = 2\pi/\lambda$. Substituting Eq. (3.2) for μ into (3.8) we get

$$\mu' = \underbrace{1}_{\substack{0 \\ \text{order}}} + \frac{1}{2} X \underbrace{(1}_{\substack{1\text{st} \\ \text{order}}} \mp \underbrace{2Y_L + \frac{3}{4} X)}_{\substack{2\text{nd} \\ \text{order}}} \approx 1 + \frac{1}{2} X \tag{3.9}$$

Using the worst-case numbers in Eq. (3.9),

$$\mu' = 1 + 0.02\ (1 \mp 0.04 + 0.03)$$

The error from neglecting the second order terms is considered further in Appendix A. The maximum error is 7 percent of the ionospheric content, and usually less.

D. Group Path and Electron Content

A radio wave pulse travels at the group velocity. As in the case of the phase path, group path P' is defined relative to the transit time of a radio wave pulse sent from a transmitter at $\ell = 0$ to a receiver at $\ell = s$

$$P' = \int_0^s \mu\, d\ell = \int_0^s \frac{c}{v_g} = c\, t_g \tag{3.10}$$

where t_g is the group transit time. The group path is the distance that the pulse would travel in free space in the transit time; it is not a physical path. The change $\Delta\ell'$ in the group path from its free space

value, caused by electrons along the path, is obtained by subtracting the physical path length from the group path P' of Eq. (3.10), and using the right-hand side of Eq. (3.9) for μ'.

$$\Delta\ell' \equiv P' - s = \int_0^s (\mu' - 1)\, d\ell = \frac{1}{2} \int_0^s X\, d\ell = \frac{80.6}{2} \frac{1}{f^2} \int_0^s N\, d\ell$$

$$\Delta\ell' = \frac{80.6}{2} \frac{1}{f^2} I = -\Delta\ell \qquad (3.11)$$

The change in group path length is equal and opposite to the change in phase path length. In the same way as for phase path, $\Delta\ell'$ is measured by measuring the difference between group paths at two different frequencies.

$$\Delta P' = P'_L - P'_H = \Delta\ell'_L - \Delta\ell'_H = \frac{80.6}{2} \left(\frac{1}{f_L^2} - \frac{1}{f_H^2} \right) I$$

Solving for I and inserting the frequencies $f_L = 49.8$ MHz, $f_H = 17/2 \times 49.8 = 423.3$ MHz, we obtain

$$I = \frac{1}{\left(\frac{80.6}{2}\right)} \frac{1}{\left(\frac{1}{f_L^2} - \frac{1}{f_H^2}\right)} \Delta P' = 0.624 \times 10^{14}\, \Delta P' \qquad (3.12)$$

The differential group path $\Delta P'$ is proportional to the phase shift between the modulation signal on the low and high frequency carriers. $\Delta\phi$ degrees of modulation frequency f_m have a path length of

$$\ell_\phi = \frac{\lambda_m}{360} \Delta\phi = \frac{\left(\frac{c}{f_m}\right)}{360} \Delta\phi$$

Substituting ℓ_ϕ for $\Delta P'$ in Eq. (3.12) for I,

$$I = \left[\frac{1}{\left(\frac{80.6}{2}\right)} \frac{1}{\left(\frac{1}{f_L^2} - \frac{1}{f_H^2}\right)} \right] \left[\frac{\left(\frac{c}{f_m}\right)}{360} \Delta\phi \right] = \frac{5.20 \times 10^{19}}{f_m} \Delta\phi \qquad (3.13)$$

Equation (3.13) is used in the computer to convert Pioneer receiver modulation phase measurements to integrated electron content.

In equation (3.13) the modulation phase shift $\Delta\phi$ is in degrees. The receiver modulation phase meter analog output is quantized into 3.15° increments for Pioneer VII by the spacecraft analog-to-digital converter and is slightly different for Pioneer VI (see Table 3-1). At the 8.692 kHz modulation frequency, the 3.15° phase increment has a 302 m path length representing an electron content of 1.89×10^{16} el/m^2. Table 3-1 lists lengths and electron content for a number of pertinent quantities.

1. Modulation Phase Ambiguity Resolution

A single modulation frequency has an ambiguity every 360°. The use of the second modulation frequency resolves the multiple cycle ambiguity out to about 10 cycles, or an electron content of 2000×10^{16} el/m^2. The largest electron content we have measured is about 200×10^{16} el/m^2, corresponding to about one cycle of modulation phase.

2. Relation of Phase Path to Group Path

The total number of cycles of differential phase path is unknown; only the change in phase path each day while the spacecraft is above the horizon can be measured. This unknown number of cycles is determined by fitting the electron content determined from the phase path measurements to the unambiguous electron content determined from the group path measurement.

The overall electron content is determined with a 2×10^{16} el/m^2 resolution by the group path with fine interpolation provided by the 50 times finer resolution of the phase path of 0.04×10^{16} el/m^2.

TABLE 3-1. GROUP PATH LENGTH AND ELECTRON CONTENT

Path Length / Modulation Frequency		7.692 kHz	8.692 kHz
1 modulation frequency wavelength	length content	39,000 m 243.5×10^{16} el/m^2	34,600 m 222×10^{16} el/m^2
1° of 1 modulation frequency wavelength	length content	108 m 0.677×10^{16} el/m^2	96 m 0.599×10^{16} el/m^2
Pioneer VI modulation phase increment	phase length content	3.025° 328 m 2.05×10^{16} el/m^2	3.185° 306 m 1.91×10^{16} el/m^2
Pioneer VII modulation phase increment	phase length content	3.150° 341 m 2.31×10^{16} el/m^2	3.150° 302 m 1.89×10^{16} el/m^2
1 wavelength of 49.8 MHz	length content	6.02 m 0.03755×10^{16} el/m^2	

IV PERFORMING THE INTERPLANETARY ELECTRON CONTENT EXPERIMENT

The performance of this experiment required the launch of a receiver far into deep space, the means for transmitting to it from earth, and the monitoring of the ionosphere. The techniques, equipment, and operations used for the experiment are described in this chapter.

A. Trajectory of Pioneer VI and Pioneer VII

The Pioneer spacecraft, bearing the SCRA receiver, was launched into trajectory around the sun by an augmented Thor-Delta vehicle. The nighttime launch of Pioneer VI from Cape Kennedy in December 1965 is shown in Fig. 4-1. The trajectories are plotted in Fig. 4-2, where the ecliptic (plane of the earth's orbit) lies in the plane of the figure, with the ecliptic viewed from the north ecliptic pole. The trajectories are essentially in the ecliptic. This plot is centered on the earth, with the sun stationary, beyond the bottom of the plot.

The most significant feature for this experiment is the spacecraft's position and geocentric range, which is used to compute the interplanetary electron number density from the measured electron content.

The Pioneer VI trajectory is on the left-hand half of Fig. 4-2, with the geocentric range and the time (in months) marked along the trajectory as the spacecraft goes away from the earth. Pioneer VI traveled in toward the sun, as can be seen by comparison with the earth's 1 AU* (149.6 Gm) orbit, and reached a perihelion (point nearest the sun) of 0.8 AU (120 Gm). Pioneer VI was tracked out to 75 Gm from the earth for the 6 months from December 1965 through May 1966, until our signal became too weak to be detected at the spacecraft.

Pioneer VII was launched 9 months after Pioneer VI, on 16 August 1966. Its trajectory, on the right-hand half of Fig. 4-2, shows the outward launch that carried the spacecraft to an aphelion (point farthest from the sun) of 1.12 AU (168 Gm). Notice the cusp at 100 Gm range where Pioneer VII lingers for 6 months, allowing us to make measurements for a

*An AU (Astronomical Unit) is the average distance from the earth to the sun.

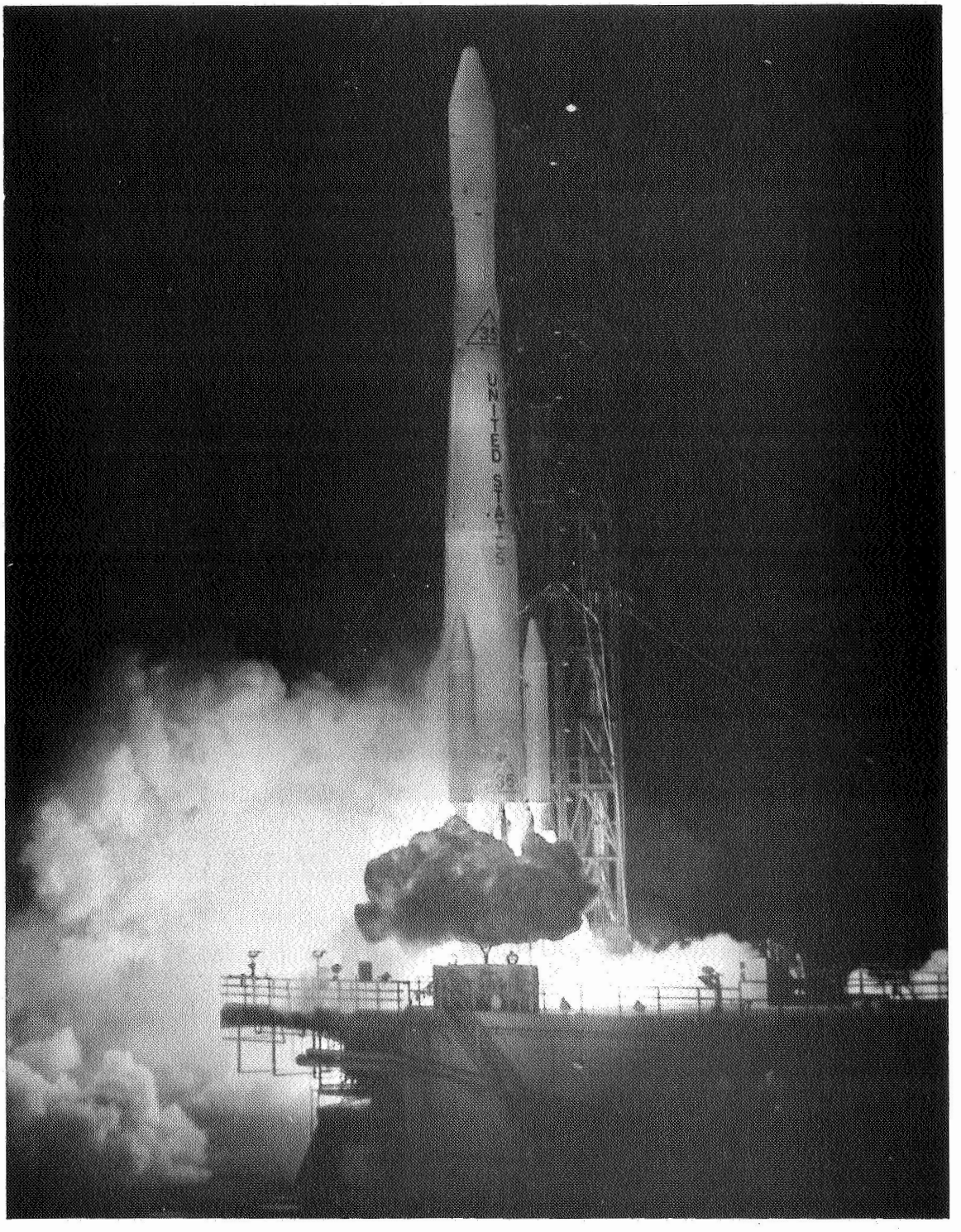

FIG. 4-1. NIGHTTIME LAUNCH OF PIONEER VI BY A THRUST-AUGMENTED THOR-DELTA LAUNCH VEHICLE FROM CAPE KENNEDY.

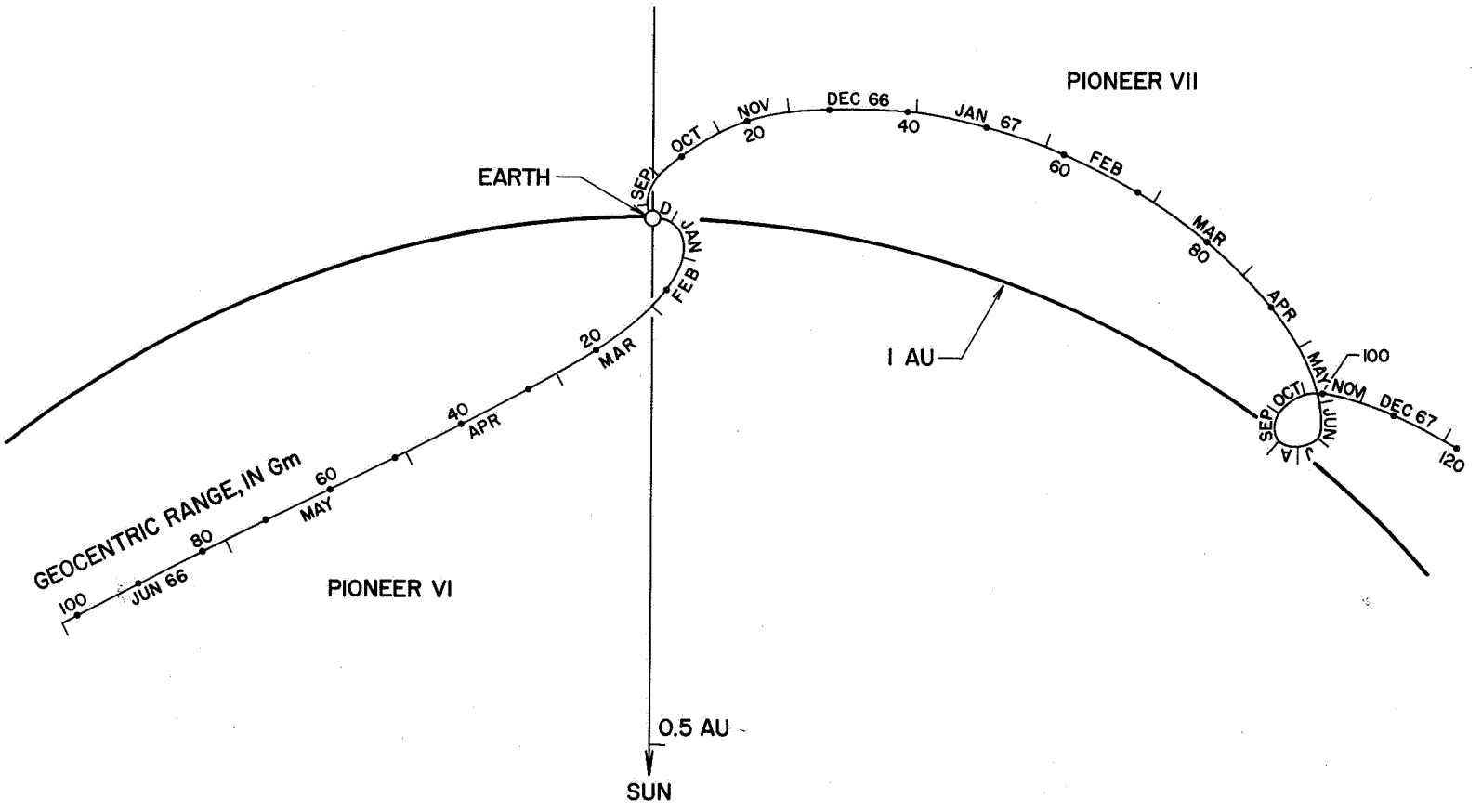

FIG. 4-2. TRAJECTORY OF PIONEER VI AND PIONEER VII IN AN EARTH-CENTERED COORDINATE SYSTEM. The earth-sun line is vertical.

long time over this long propagation path. Transmissions to Pioneer VII started in August 1966, and will continue through January 1969 (a total of 17 months), when it will be out beyond 120 Gm.

B. The Pioneer Spacecraft

The 140 lb (63 kg) Pioneer spacecraft carried Stanford's receiver into deep space. The solar cells covering the drum-shaped spacecraft (Fig. 4-3) powered our receiver from its 52 watt supply. The spacecraft spins at 1 rps to stabilize its spike-shaped telemetry antenna toward the south ecliptic pole. The antenna concentrates the telemetry power into a 6°-wide disc lying in the plane of the ecliptic. The 2.3 GHz TWT telemetry transmitter produces 8 watts.

SCRA's receiver on board the spacecraft receives the radio transmissions from earth through the whip antennas mounted on the opposite end of the spacecraft from the telemetry antenna. The 49.8 MHz antenna is a (short) quarter wave whip, mounted at the edge of the drum and inclined toward the center of the spacecraft. The 423.3 MHz folded dipole is mounted on the tip of the 49.8 MHz whip and centered on the spin axis.

C. Ground-Based Radio Transmission Equipment and Operation

The transmitters and associated equipment generate coherent 49.8 and 423.3 MHz transmissions, phase modulate them at either 7.692 or 8.692 kHz, and transmit them to the spacecraft.

1. Ground Antenna

Both the 49.8 and 423.3 MHz transmissions to the spacecraft are radiated from SCRA's 150 ft (46 m) Big Dish (Fig. 4-4). The 423.3 MHz transmission is radiated from a horn at the focus of the parabolic dish. The 49.8 MHz radiator is a crossed, folded dipole and reflector mounted below the horn. The wider beamwidth at 49.8 MHz permits the 49.8 MHz radiator to be offset from the focal point occupied by the 423.3 MHz horn.

The Big Dish is controlled by a PDP 8 computer (Fig. 4-5) which, once each second, interpolates between ephemeris points; these ephermis points are spaced five minutes apart and are read from a punched paper tape.

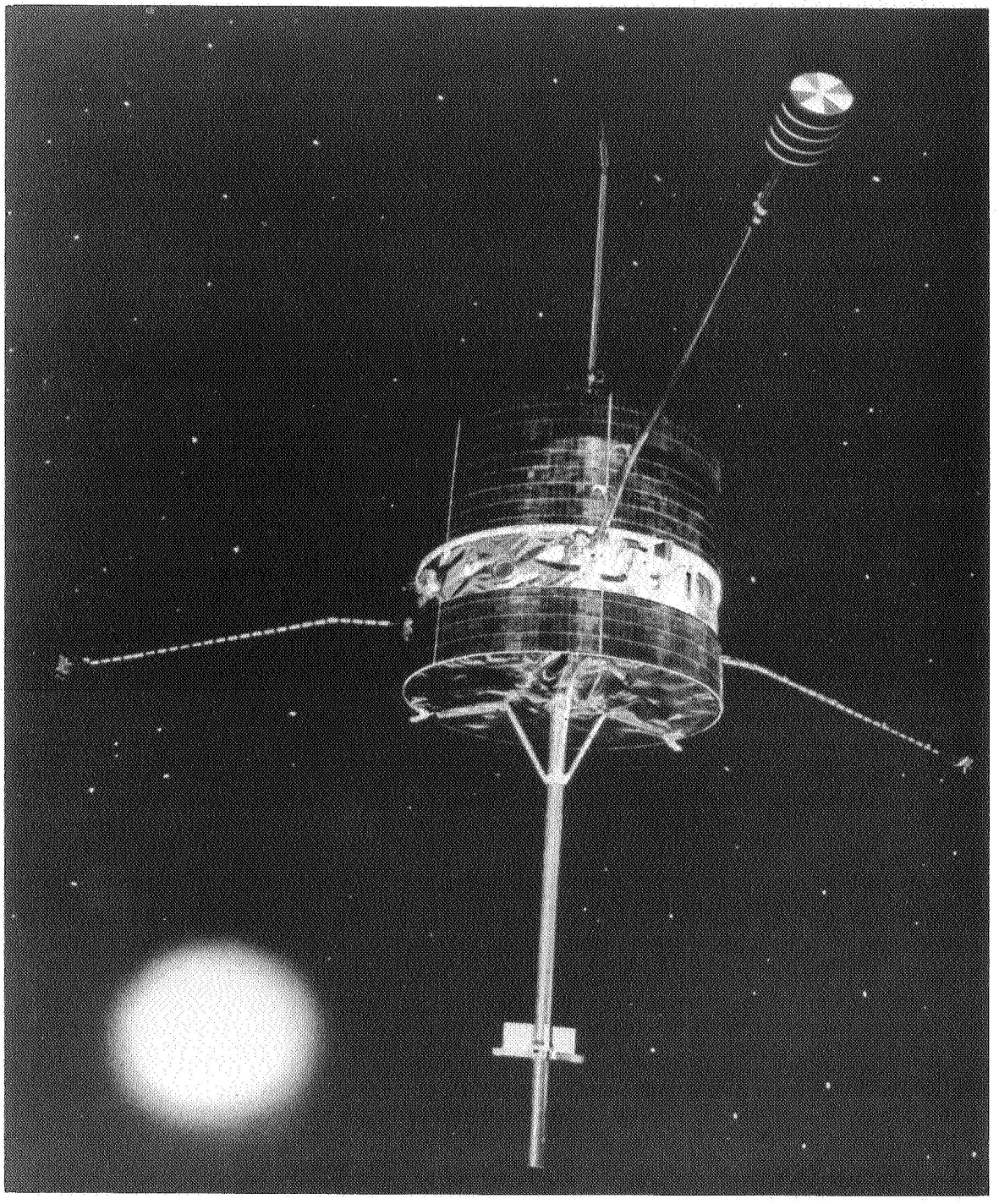

FIG. 4-3. PIONEER SPACECRAFT. The Stanford receiving antenna is mounted on the top edge of the drum.

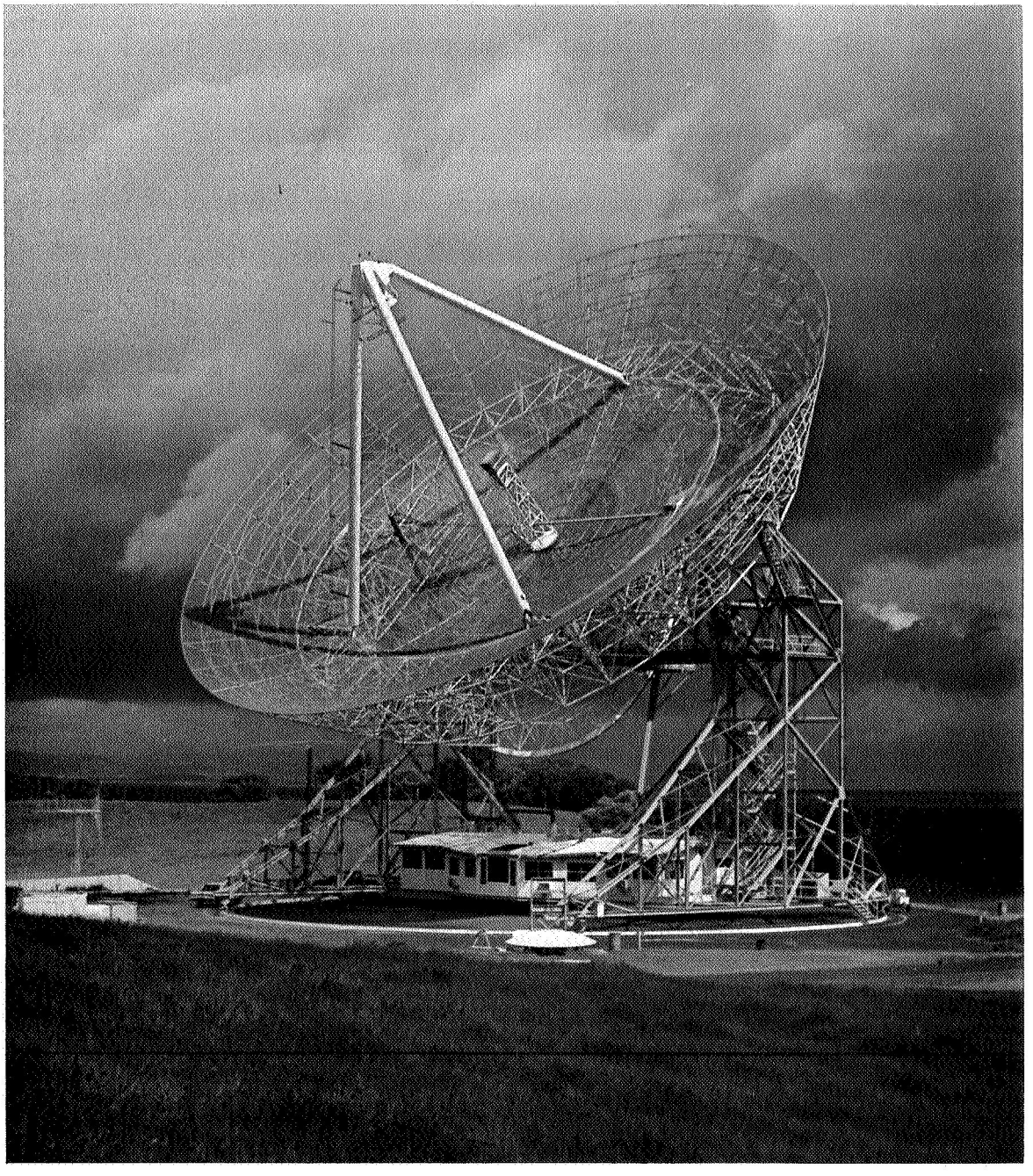

FIG. 4-4. THE 150-FT BIG DISH AT STANFORD USED TO TRANSMIT 49.8 AND 423.3 MHz SIGNALS TO THE PIONEER SPACECRAFT IN DEEP SPACE.

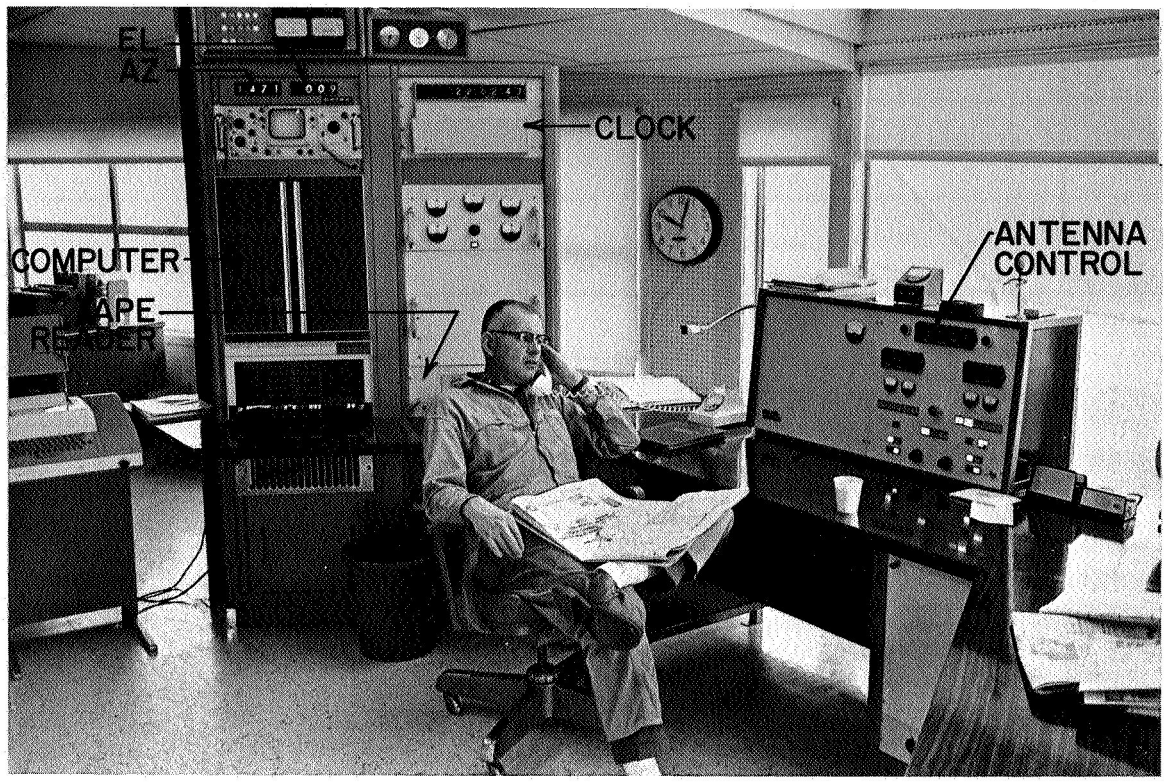

FIG. 4-5. THE COMPUTER CONTROL FOR THE POINTING OF THE SCRA 150-FT BIG DISH. The operator takes over at the control console in case of trouble.

2. Transmitters

The Big Dish is fed by powerful transmitters on 49.8 and 423.3 MHz. The 423.3 MHz 30 kW klystron transmitter is pictured in Fig. 4-6. The 49.8 MHz 50 kW linear amplifier transmitter (Fig. 4-7) is used until the spacecraft reaches a range of about 10 Gm, where the 50 kW transmission is no longer strong enough for the best quality data; then the 250 kW linear amplifier transmitter (Fig. 4-8) is switched into operation. The main features of the transmitters are listed in Table 4-1. Figure 4-9 shows the maximum power that the transmitters can transmit to a dipole at the spacecraft versus spacecraft range. The equation for this graph is

$$P_r = \frac{P_t \eta \, G_t \, A_r p}{4\pi \, R^2}$$

Table 4-1. TRANSMITTER CHARACTERISTICS

Transmitter frequency	49.8 MHz	423.3 MHz
Type of transmitter	Triode linear amplifier	Klystron
Maximum power output	250 kW 84.0 dBm	30 kW 74.7 dBm
Antenna	46 m diameter parabolic dish	
Antenna gain, $\eta = 1$	26.4 dB	45.0 dB
3 dB beamwidth	6.0°	1.0°
Antenna efficiency, η (est.)	0.50	0.50
Polarization Pioneer VI Pioneer VII	Left-hand eliptical 5.5 dB axial ratio 3.5 dB axial ratio	Right-hand circular
Polarization loss Pioneer VI Pioneer VII	Varying with Faraday rotation -1.1 to -6.6 dB -1.6 to -5.1 dB	-3 dB
Area of receiving dipole on spacecraft	4.7 m^2	0.65 m^2
Modulation frequency	7.692 or 8.692 kHz	
Modulation phase	Continuously adjustable through 360°	Fixed
Fraction of power in modulation sidebands	0.5	
Maximum total available power (carrier + sidebands) from dipole at 75 Gm (0.5 AU) Pioneer VI Pioneer VII	Varying with Faraday rotation -115.3 to -120.8 dBm -116.0 to -119.5 dBm	 -126.6 dBm -126.6 dBm

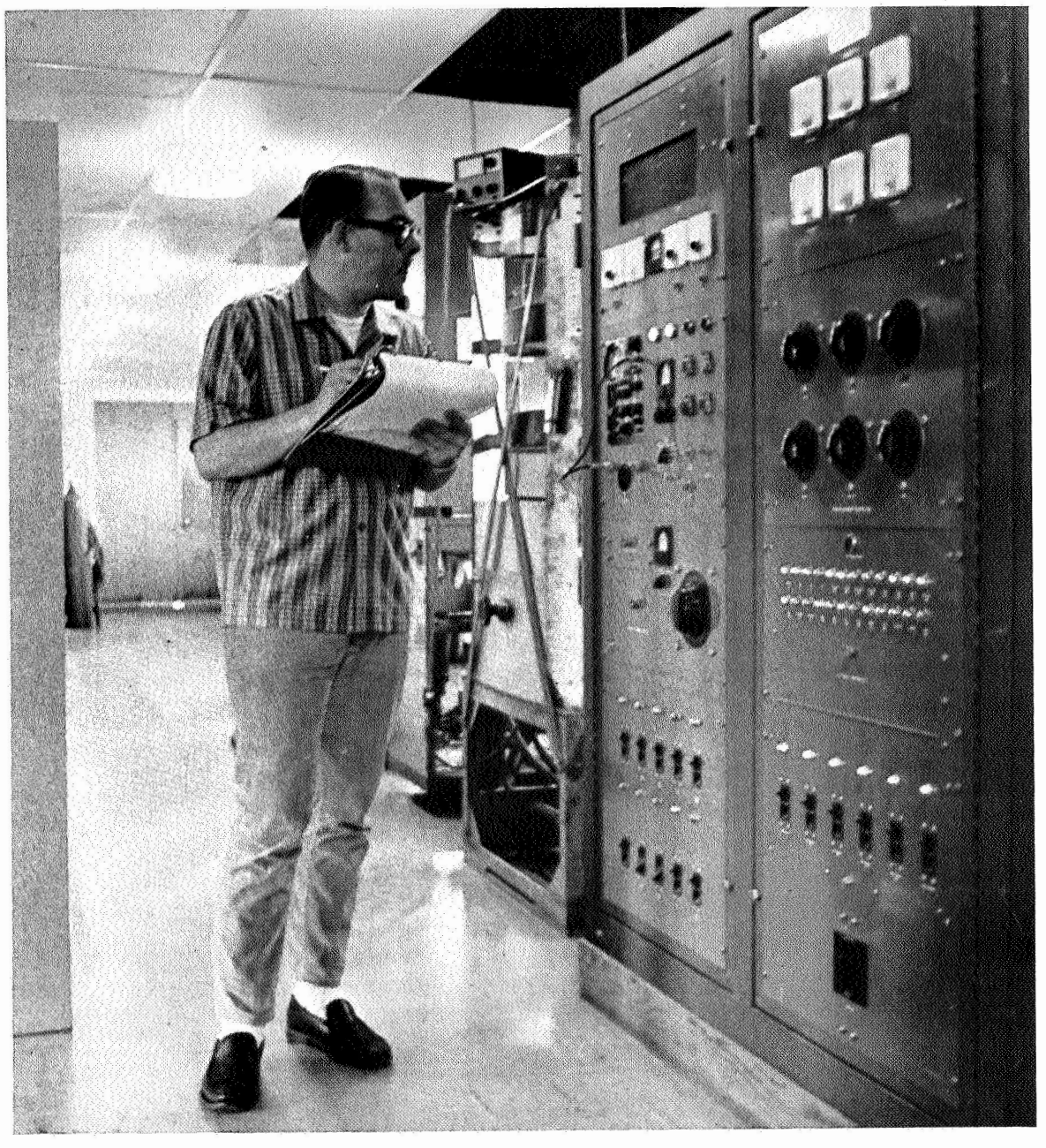

FIG. 4-6. THE 423.3 MHz 30 kW KLYSTRON TRANSMITTER, WHICH IS IN THE BUILDING UNDER THE BIG DISH.

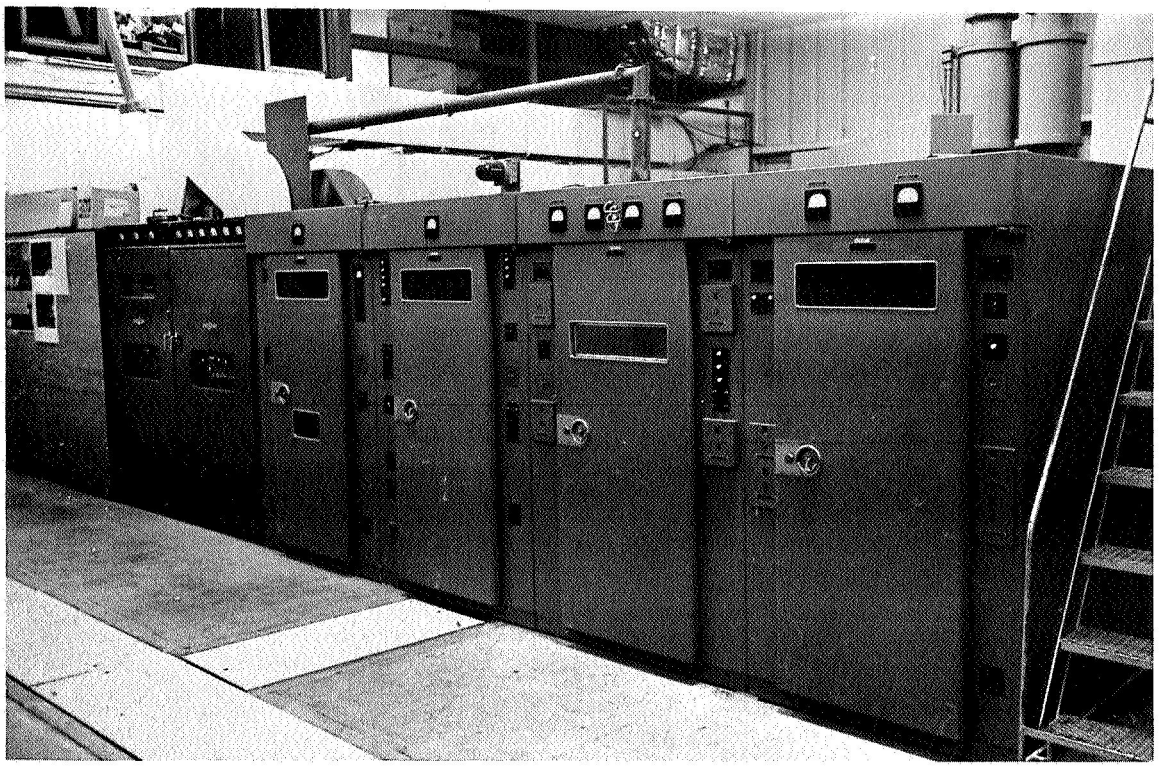

FIG. 4-7. THE 49.8 MHz 50 kW LINEAR AMPLIFIER TRANSMITTER, WHICH IS USED UNTIL PIONEER IS ABOUT 10 Gm FROM EARTH.

where A and G are related by

$$A = \frac{G \lambda^2}{4\pi}$$

P_r = power available at the receiving antenna terminals, in watts

P_t = power radiated from the transmitting antenna, in watts

G_t = transmitter antenna gain (see Table 4-1 for values)

A_r = area of the receiving antenna, in m^2 (see Table 4-1 for values)

R = distance between transmitting and receiving antennas, in meters

p = polarization loss multiplier

G = antenna gain. For a dipole, G = 1.64

η = antenna efficiency, generally 0.5 for parabolic dishes

A = antenna area, in m^2. For our transmitting antenna, A is the area of the 45.8 m diameter parabolic reflector

λ = radio wavelength, 6.02 m for 49.8 MHz, 0.71 m for 423.3 MHz

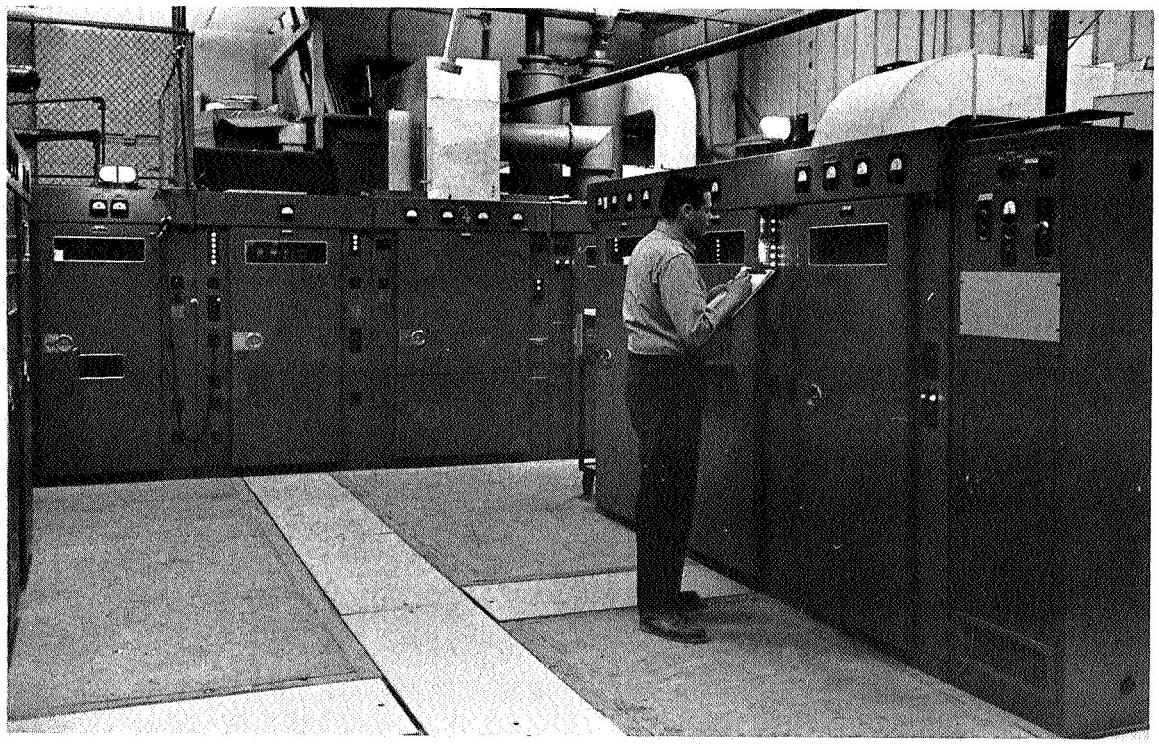

FIG. 4-8. THE 49.8 MHz 250 kW LINEAR AMPLIFIER (BACK); 16 kW DRIVER (RIGHT). They are used when Pioneer is farther than 10 Gm from earth.

3. Exciter

The transmitting system block diagram (Fig. 4-10) starts with a 1 MHz crystal frequency standard, common to both the 49.8 and 423.3 MHz channels. The 49.8 MHz channel HP 5100A synthesizer output is phase modulated at a low phase modulation index for linearity, then multiplied 4 times to 49.8 MHz to obtain a larger modulation index. The 423.3 MHz channel synthesizer output is phase modulated, then multiplied 16 times to 423.3 MHz to extend the synthesizer frequency beyond its 50 MHz limit.

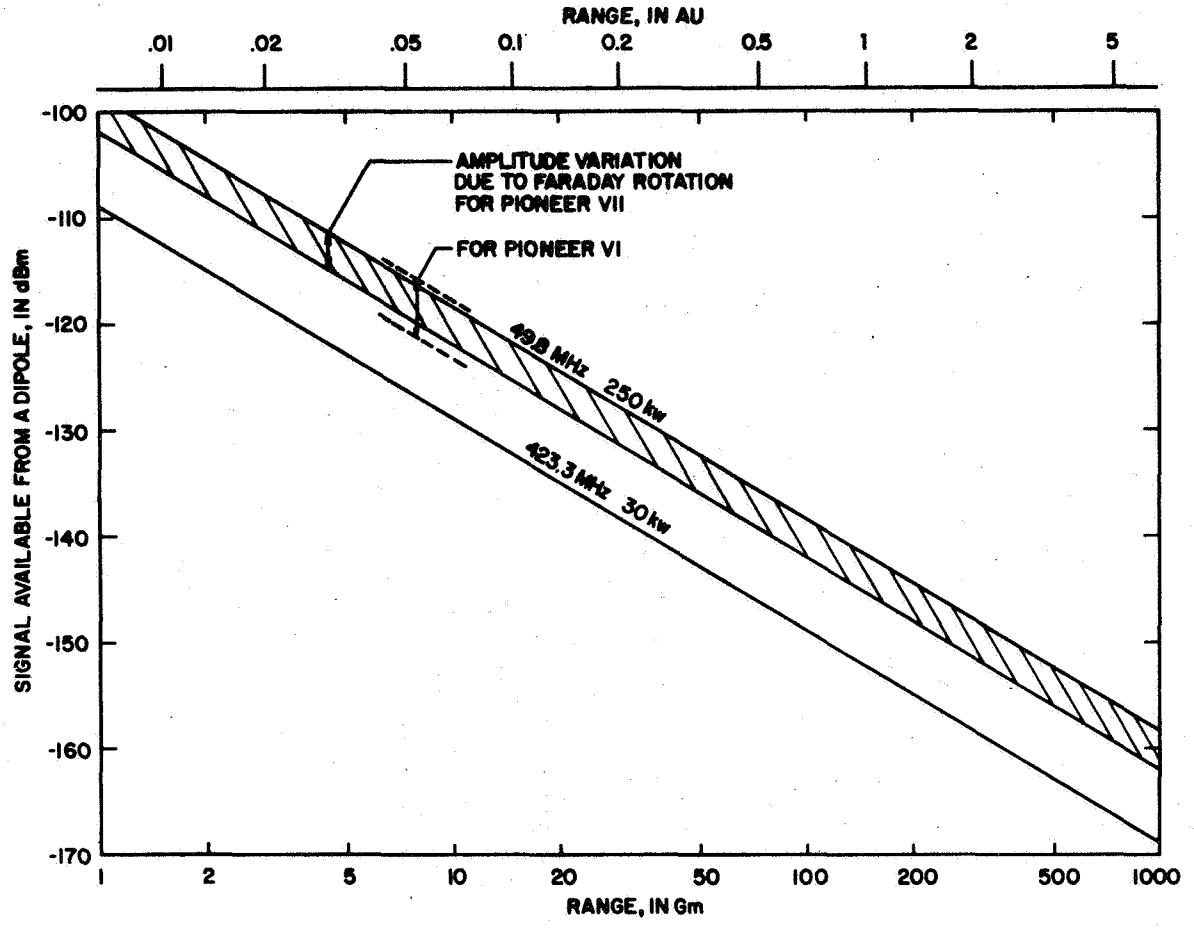

FIG. 4-9. THE POWER RECEIVED IN A DIPOLE (INCLUDING SIDEBANDS) AT THE SPACECRAFT VERSUS EARTH-SPACECRAFT RANGE. The power transmitted on 49.8 MHz is 250 kW and the power on 423.3 MHz is 30 kW.

The 423.3 MHz carrier is set to exactly 17/2 times the 49.8 MHz carrier; then a +5 Hz bias is added to the 49.8 MHz signal. This bias allows the sign of the RF phase difference for the phase path measurement to be determined at the spacecraft. The synthesizers are used to compensate for any static frequency error at the receiver, as well as for the doppler shift. For example, a 12 kHz doppler shift compensation is required on the 423.3 MHz carrier when the spacecraft is at 75 Gm range.

Both carriers are phase modulated at 7.692 kHz (or 8.692 kHz) for differential group path measurement. The second modulation frequency is available for resolution of more than 1 cycle of modulation phase in

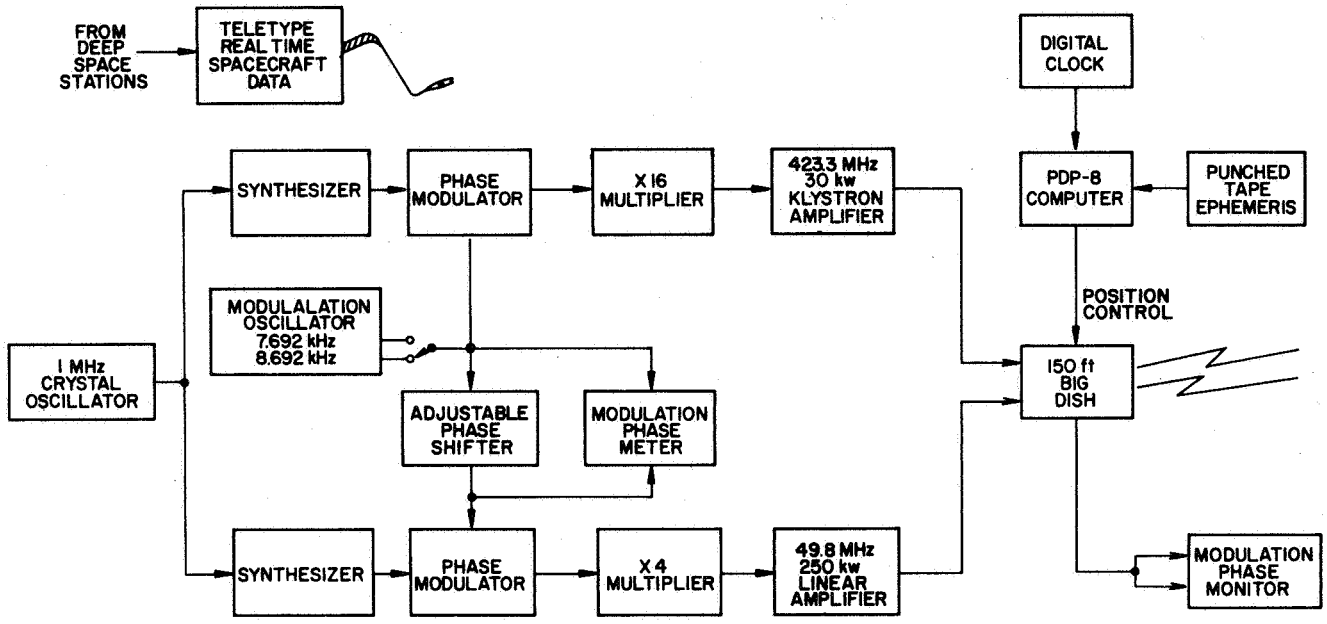

FIG. 4-10. TRANSMITTING SYSTEM BLOCK DIAGRAM.

the interplanetary medium. Thus far, the maximum phase shift due to the medium has been one cycle of modulation phase.

The continuously adjustable phase shifter controls the phase shift between the modulation on the two carriers. The real time data teletype shows the operating point of the spacecraft phase meter. This information is used to keep the spacecraft modulation phase meter output on its positive slope, by adjustment of the modulation phase shifter. The slope of the phase meter output is determined by noting whether the output (see Fig. 4-11) goes up or down when the phase shifter is increased 20°. The modulation phase shifter is used to calibrate the spacecraft phase meter once every two or three weeks to produce a curve as in Fig. 4-11. The details of this in-flight modulation phase calibration are described in Appendix B.

The phase modulated carriers from the exciter drive the 49.8 and 423.3 MHz transmitters, which in turn feed the 150 ft Big Dish. The

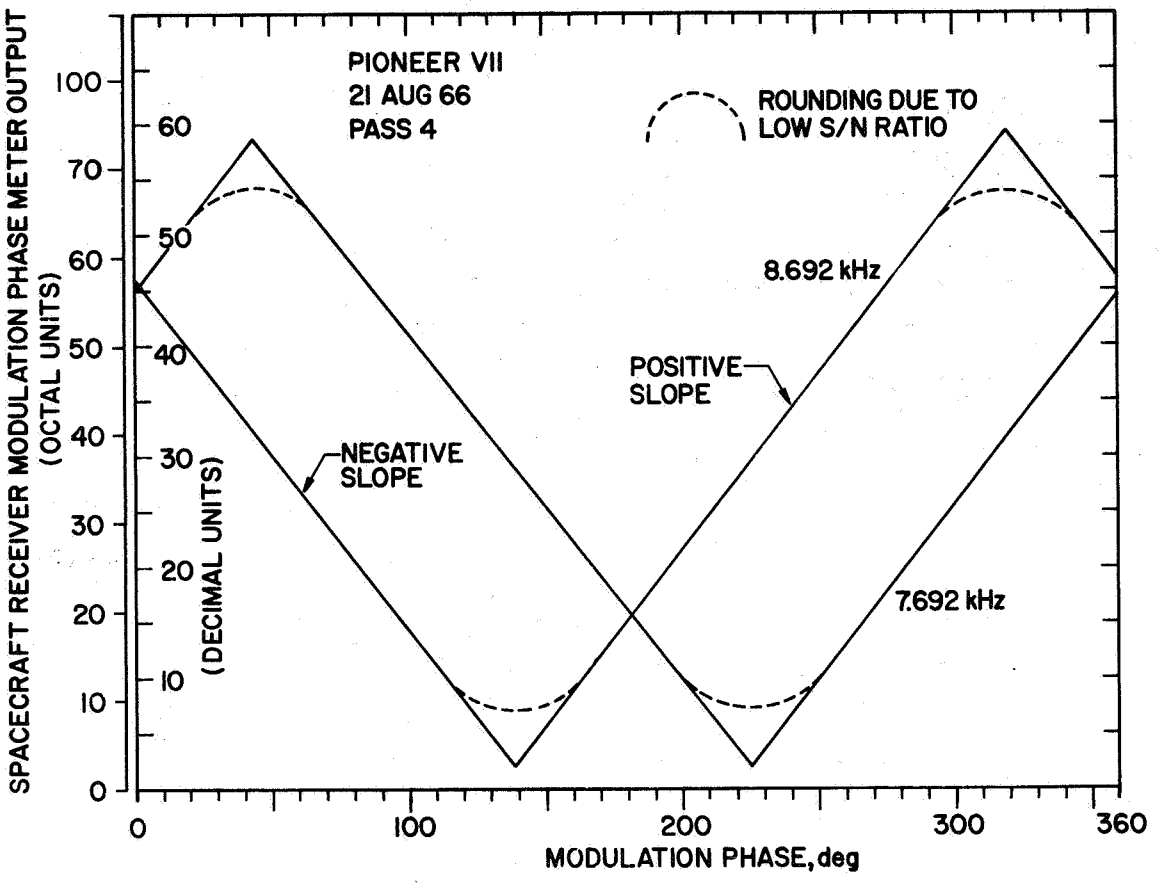

FIG. 4-11. MODULATION PHASE METER CALIBRATION CURVE FOR THE RECEIVER ABOARD PIONEER VII. Quantized phase meter output is on the vertical scale; the horizontal scale is the phase of the modulation on 49.8 MHz (phase lead is positive) with the modulation of 423.3 MHz used as the reference. The curve for Pioneer VI is similar.

exciter is located in the 49.8 MHz transmitter control room, shown in Fig. 4-12, along with the real time data teletype.

A pickup loop at the base of the Big Dish is connected to the phase monitor receiver in the control room (Fig. 4-12), where the monitor measures the modulation phase of the transmitted signals. The monitor has shown that the transmitted modulation phase of the 49.8 MHz signal lagged the 423.3 MHz signal by 5° relative to the phase measured at the modulators at the input to the transmitters, during most of Pioneer VII's flight.

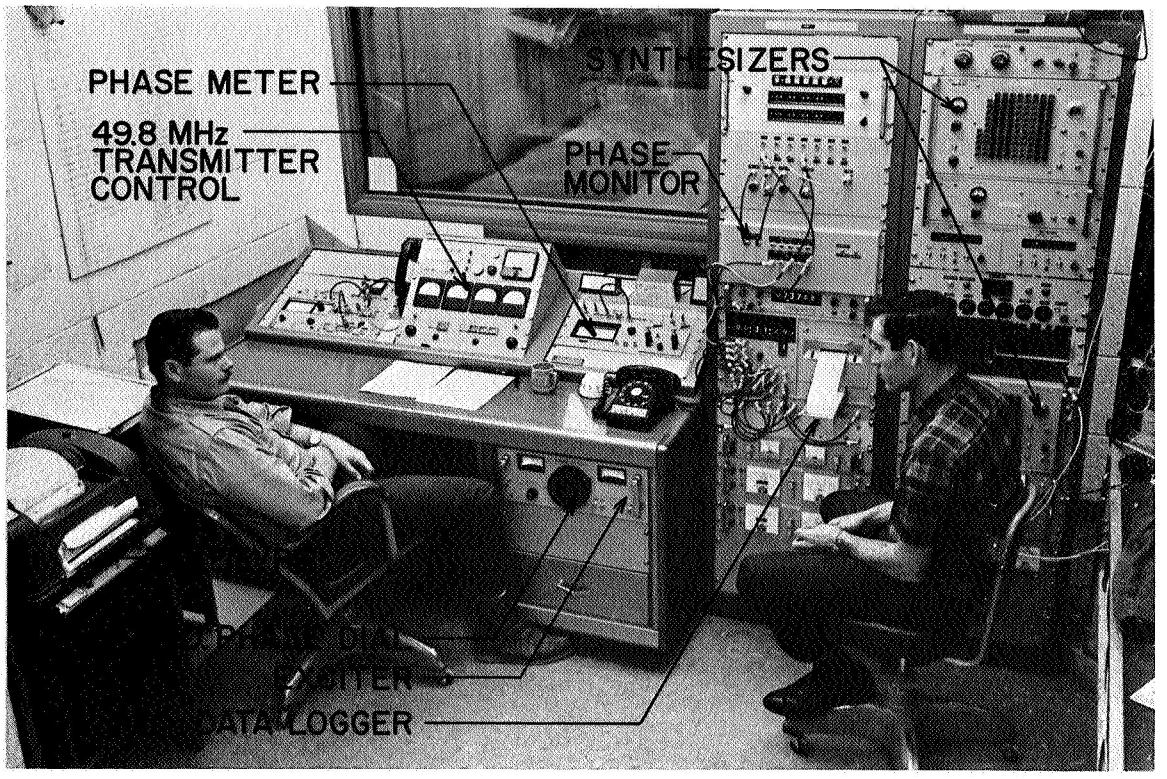

FIG. 4-12. THE CONTROL ROOM FOR THE 49.8 MHz TRANSMITTER. The transmitter exciter, the real time data teletype, and the modulation phase monitor are also located here.

D. Dual Frequency Receiver Aboard the Pioneer Spacecraft

The 49.8 and 423.3 MHz transmissions from earth are received by SCRA's receiver (Fig. 4-13) aboard the Pioneer spacecraft in interplanetary space. The receiver measures the RF phase shift between the 49.8 and 423.3 MHz carriers; the shift is caused by electrons along the earth-Pioneer transmission path (the phase path measurement). The receiver also detects the 7.692 or 8.692 kHz phase modulation on the two carriers and measures the phase difference between them. The modulation phase shift is caused by these same electrons (the group path measurement).

The receiver is briefly described in the block diagram in Fig. 4-14, and the reader is referred to the receiver final report (Koehler, 1965) for further details.

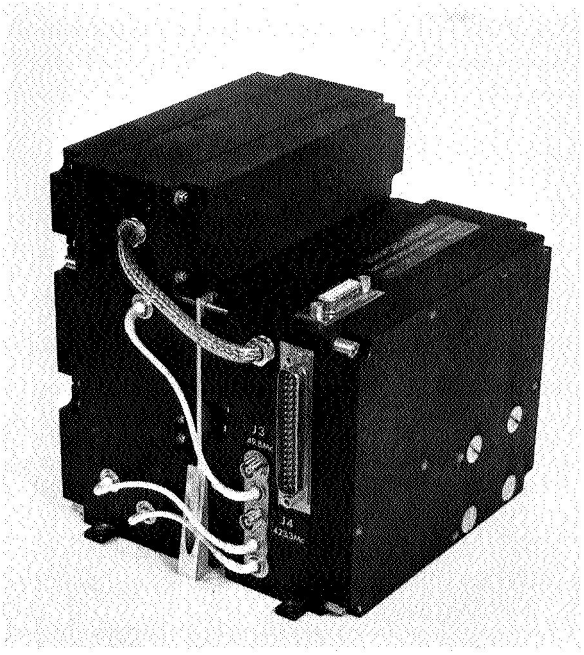

FIG. 4-13. THE SCRA DUAL CHANNEL RECEIVER WHICH IS USED ABOARD THE PIONEER SPACECRAFT. The receiver is about 6 inches on a side, weighs 5 lb, and uses only 1.5 watts of power.

The receiver parameters are listed in Table 4-2. The dual receiver is composed of two separate coherent phase-locked receivers, with part of the local oscillators in common. The main reasons for phase lock design are to increase the sensitivity of the receiver and to detect the difference in RF cycles between the 49.8 MHz and the 2/17 harmonic of the 423.3 MHz carrier (to normalize it to 49.8 MHz).

The difference in cycles between these normalized carrier frequencies equals the difference in cycles between the two VCOs detected in the Δf mixer. The Δf mixer output is the same frequency whether the frequency difference is positive or negative. The frequency difference is forced to have one sign by biasing the 49.8 MHz carrier 5 Hz high at the transmitter. The 10 bit counter accumulates the Δf difference in cycles, and the counter is sampled periodically, without destroying the count. The sample rate depends on the spacecraft telemetry bit rate, as listed in Table 4-3.

The modulation is detected at the loop phase detector for each channel. The 7.692 or 8.692 kHz modulation is mixed with the 8.192 kHz local oscillator frequency (available from the spacecraft) so that the mixer output is 500 Hz, regardless of which modulation frequency is present. A VCO, phase locked to the 500 Hz mixer output, is cross-correlated

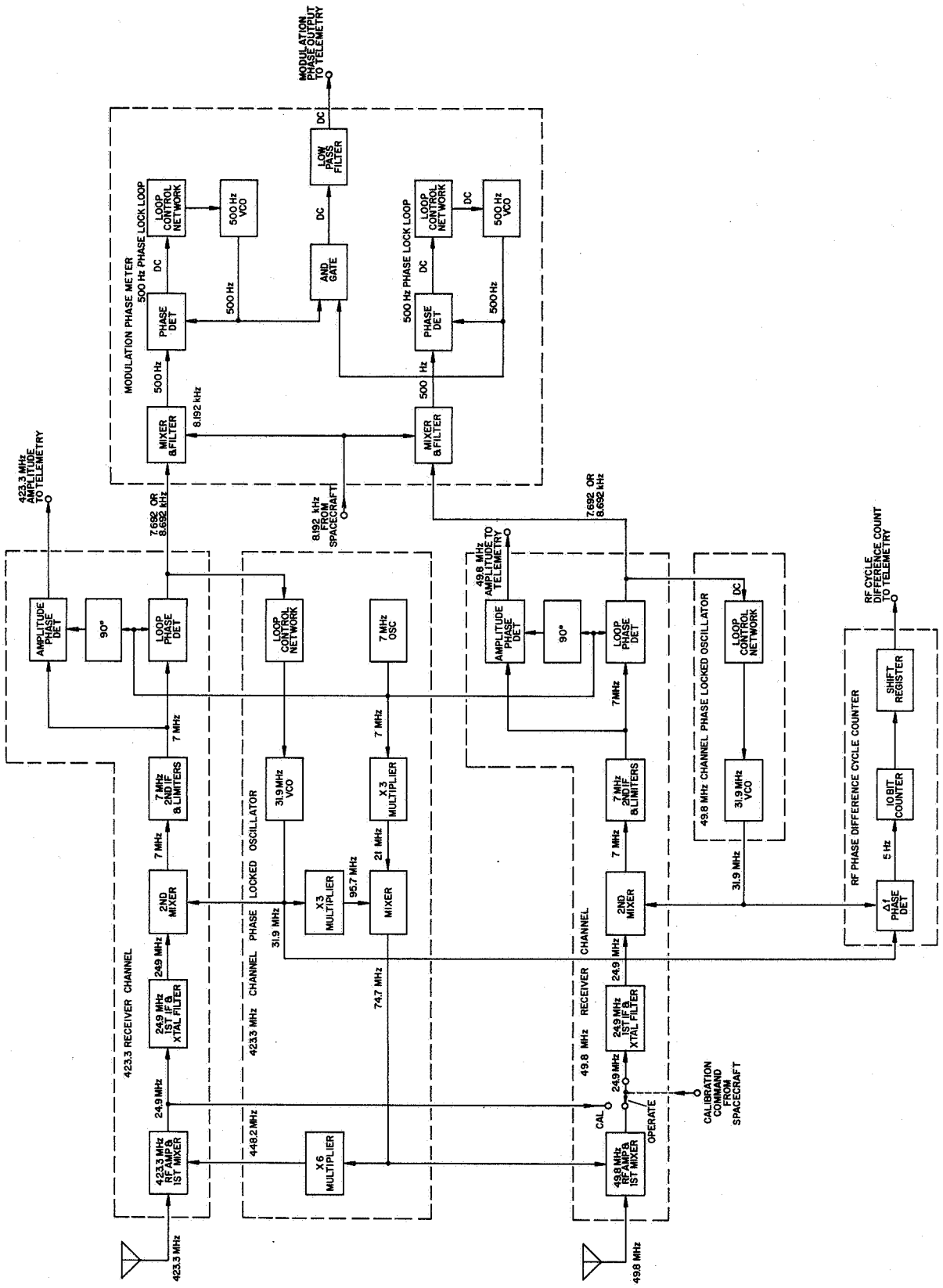

FIG. 4-14. SCRA DUAL CHANNEL SPACECRAFT RECEIVER BLOCK DIAGRAM.

Table 4-2. RECEIVER PARAMETERS

Frequency	49.8 MHz	423.3 MHz
IF bandwidths		
3 dB bandwidth	40 kHz	
Noise bandwidth	45 kHz	
Receiver input noise (including image)		
Noise figure	3 dB	7 dB
Noise temperature	300°K	1200°K
Cosmic noise (in a dipole with axis parallel to galactic axis)	8000°K	100°K
Spacecraft noise plus cosmic noise for Pioneer VII		
Noise temperature	50,000°K	1600°K
Noise in 45 kHz noise bandwidth	-105 dBm	-120 dBm
Minimum signal/noise in 45 kHz IF noise bandwidth for which phase lock is maintained for 1 hour	-21 dB	-19 dB
Corresponding receiver input signal in spacecraft noise environment	-126 dBm	-139 dBm
Signal level at 0.5 AU (75 Gm) from transmitter	-116.0 to -119.5 dBm	-126.6 dBm
Margin available* for safety, fading, and/or additional range	6 dB	13 dB
Modulation frequencies for phase meter	7.692 or 8.692 kHz	
Modulation phase accuracy	Digitized to approximately 3.15° digit; additional error estimated to be ±2°	
Differential phase path	Quantized to 1 cycle of RF phase difference at 49.8 MHz	

*This may seem like a large margin, but on many nights, especially from 10 p.m. to 4 a.m., PST, while Pioneer VII was less than 4 Gm from earth, 49.8 MHz scintillation fading of 10 to 15 dB was common. Margin is also required to take care of uneven antenna response.

in an AND gate with the other channel's 500 Hz VCO. The smoothed AND gate output provides the triangular output of voltage versus modulation phase difference between the inputs, shown in Fig. 4-11.

The zero phase is established by moving the calibrate switch in the receiver to the "CAL" position, by ground command. The calibrate switch connects the signal from the first mixer of the 423.3 MHz channel into the 49.8 MHz channel; the same signal goes down both channels to establish the phase meter output for 0° modulation phase input. The zero calibration procedure is necessary because the phase scale of the in-flight calibration (discussed under Exciter) is shifted by the phase shift introduced by the interplanetary medium.

E. Telemetry

The data from the SCRA receiver (and from five additional experiments) are telemetered by the Pioneer spacecraft's 2.3 GHz telemetry system to Jet Propulsion Laboratory's (JPL) Deep Space Station (DSS) on earth. Deep Space Station complexes are located roughly every 120° longitude around the world to make continuous coverage of an interplanetary spacecraft possible. The telemetry data are recorded at the DSS, such as DSS 12 at Goldstone, shown in Fig. 4-15. The tapes are mailed to Ames Research Center for processing into separate digital tapes for each of the six Pioneer experimenters.

Real time data are also sent from the DSS to Stanford via teletype, so the transmitter frequencies, power, and modulation phase offset can be adjusted for best operation of the receiver aboard the spacecraft. At the design range of 75 Gm, it takes 8 minutes from the time a change is made at the transmitter to the time the change appears on the teletype.

When the spacecraft is near the earth, the data rate is 512 bps and is gradually decreased to 8 bps in steps as the range increases. Table 4-3 lists the maximum communication range for each bit rate and the time interval between data points for the several types of data at each bit rate. The range refers to the 85 ft DSS dish capability. The 210 ft dish at Goldstone DSS 14 has 10 dB more sensitivity, which enables a 10 times higher bit rate to be used.

Table 4-3. TIME FOR A NUMBER OF TELEMETRY FRAMES VS BIT RATE
(IN SEC AND MIN:SEC)

QUANTITIES SAMPLED			Phase Path		Group Path		Amplitude; Loop Stress	Eng. Subcom Frame
FRAME INTERVAL		1	2	4	8	16	32	64
Communication Range (Gm)	Bit Rate (bps)							
12.5	512	0.44	0.88	1.75	3.5	7	14	28
17.5	256	0.88	1.75	3.5	7	14	28	56
35	64	3.5	7	14	28	56	112 (1:52)	224 (3:44)
70	16	14	28	56	112 (1:52)	224 (3:44)	448 (7:28)	896 (14:56)
100	8	28	56	112 (1:52)	224 (3:44)	448 (7:28)	896 (14:56)	1,796 (29:52)

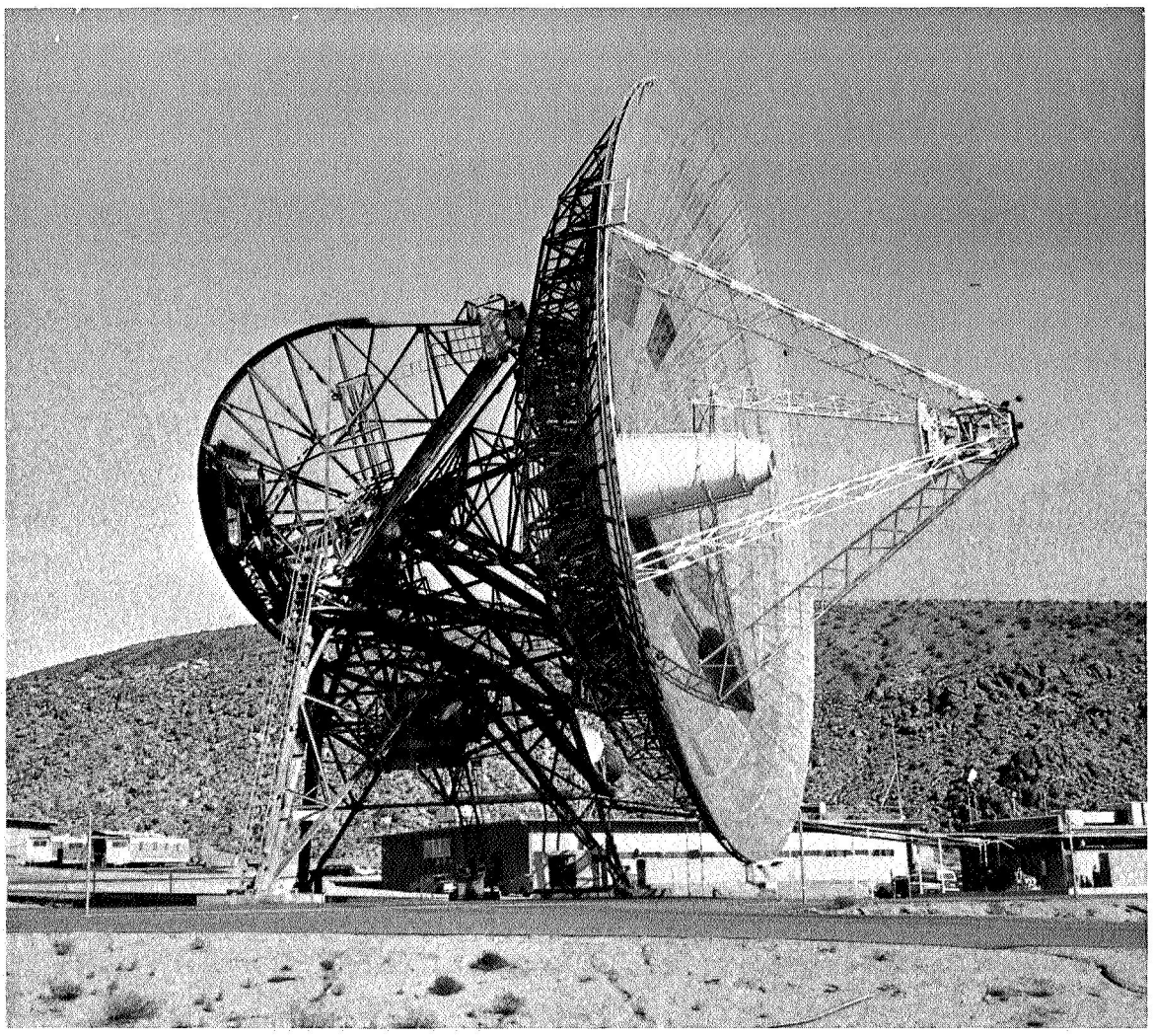

FIG. 4-15. THE 85 FT DISH AT DEEP SPACE STATION 12 (GOLDSTONE), WHICH RECEIVES PIONEER TELEMETRY SIGNALS. A maser receiver is located near the cassegrainian feed.

F. Ionospheric Measurement

1. Beacon Satellite Differential Doppler Measurement System

Two beacon satellites, BE-B and BE-C (Fig. 4-16) are used to measure the ionospheric electron content (Martin, 1964; Garriott and DeMendonça, 1963). We use the 40 MHz 0.25 watt and 360 MHz 0.1 watt coherent transmissions to measure changes in the differential phase path as the satellite sweeps across the sky (in about 15 minutes). A large bar

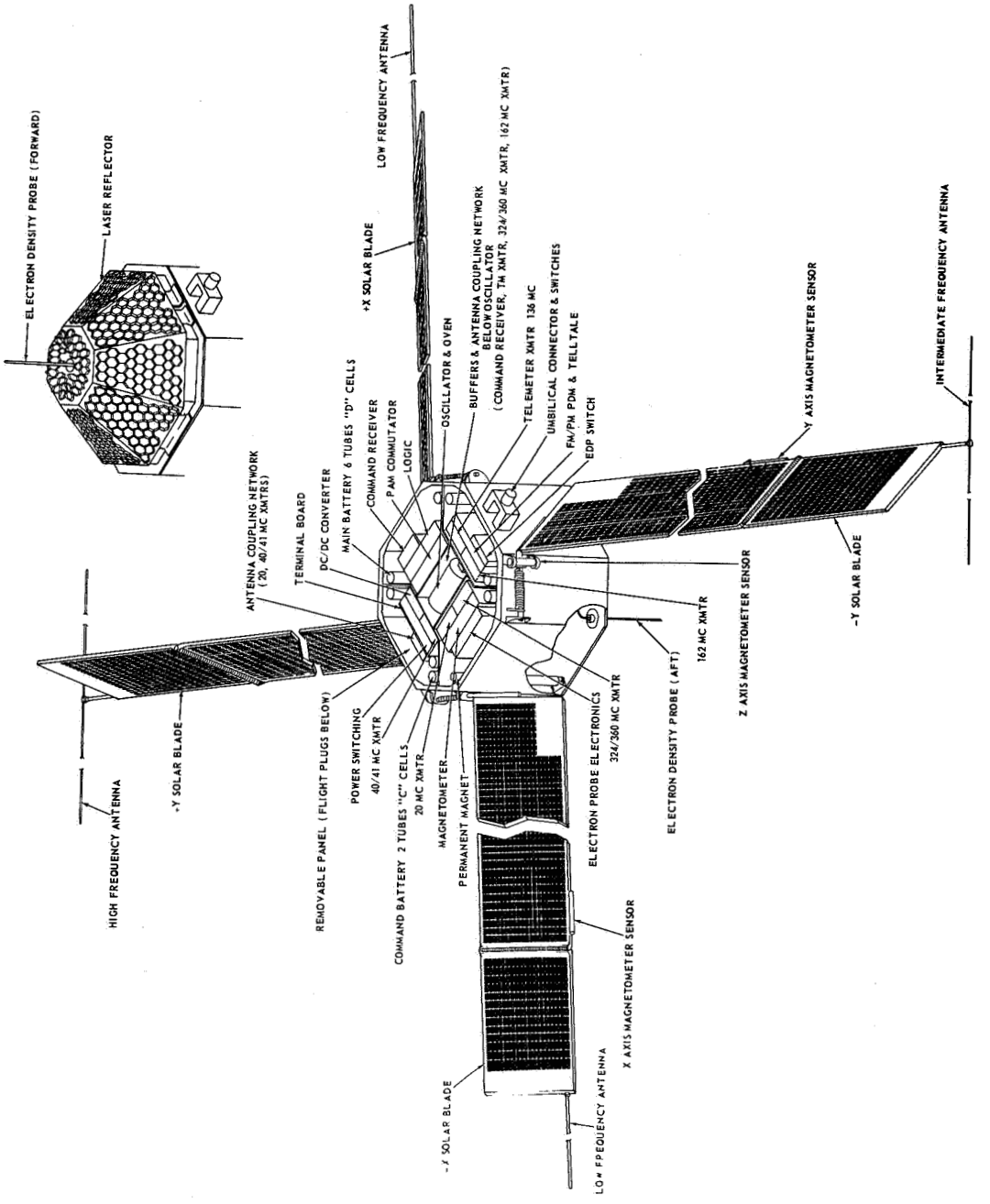

FIG. 4-16. THE BEACON SATELLITE, CUTAWAY VIEW.

magnet keeps one axis of the satellite aligned with the earth's magnetic field.

Both satellites are in a 1000 km height orbit, with a 110 minute period. The 1000 km height includes most of the ionosphere. BE-B is in a near polar orbit with an inclination of 80° with the equatorial plane. BE-C's orbital plane has a 40° inclination.

Figure 4-17 shows the manually controlled azimuth-elevation antenna for receiving the beacon satellite transmissions, which is located about 1 mile from the 150 ft Big Dish. The four 360 MHz right-hand circular helices have 22 dB gain and a 10° beamwidth. A 360 MHz low noise preamplifier is mounted on the movable part of the antenna. The four 40 MHz crossed yagis have 14 dB gain and a 40° beamwidth. They are combined to provide left-hand circular polarization for the differential doppler (phase path) receiver.

The beacon receiver, operating in the same manner as the Pioneer receiver, is a two-channel phase locked receiver which divides the 360 MHz carrier by 9 and compares it with the 40 MHz carrier (Fig. 4-18). The carriers are beat down to about 10 kHz and phase compared in an audio phase meter. The slope of the sawtooth-shaped phase meter output indicates the sign of the frequency difference; the sign may change several times throughout one pass. The data are recorded on a chart recorder.

2. ATS Faraday Rotation Measurement System

The Applied Technology Satellite (ATS) is fixed in the sky in synchronous orbit, 37° above Stanford's horizon. The Faraday rotation of ATS's 137 MHz beacon transmission is measured to obtain a continuous measurement of the ionospheric electron content. The ionospheric content along Pioneer's ray path is subtracted from the Pioneer content, giving a continuous record of interplanetary electron content for the 12 hours the Pioneer is above our horizon each day. This ATS measurement went into operation when ATS was launched in December 1966, and covers most of the useful life of Pioneer VII.

The Faraday rotation of ATS's 137 MHz linearly polarized transmission is proportional to the ionospheric electron content. The 137 MHz antenna in Fig. 4-19 points at ATS, and rotates at 1/2 rpm about the antenna axis. The receiver output from this antenna makes a sinusoidal

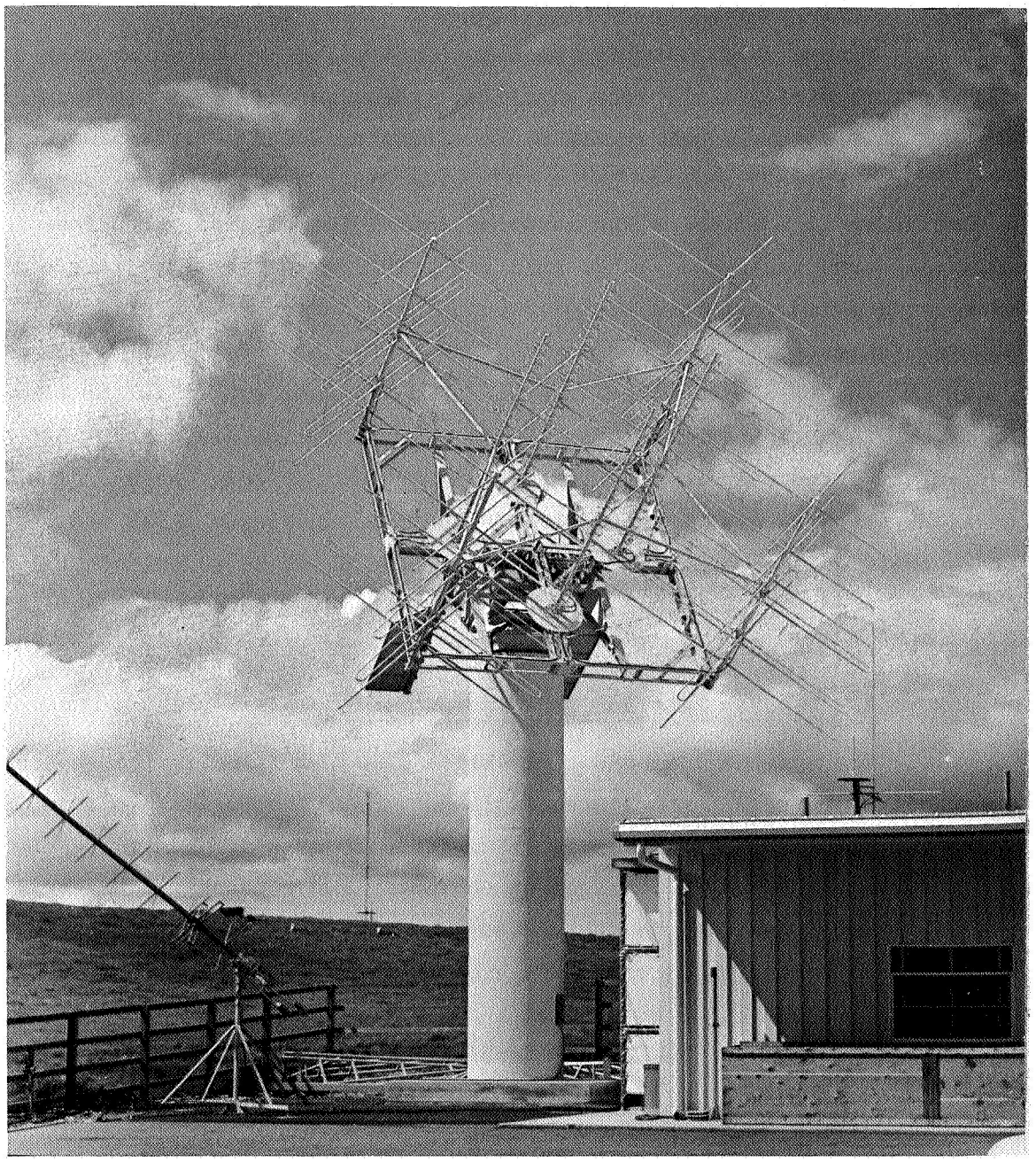

FIG. 4-17. BEACON SATELLITE TRACKING ANTENNA FOR 40 AND 360 MHz. The antenna is controlled manually.

FIG. 4-18. THE BEACON SATELLITE TRACKING STATION AT STANFORD. The operator is reading azimuth and elevation from an ephemeris, and pointing the antenna. ATS receiver and chart recorder are also located here.

pattern on a chart record as the antenna rotates. The received signal is minimum when the antenna plane is perpendicular to the received plane of polarization. The angular position of this minimum (null), measured from the position where the antenna plane is vertical, is the Faraday rotation angle.

Another Faraday rotation measurement system, which reduces the manual data reduction time, is now in operation. A second system is under development, similar to the 2 Hz phase meter used by Titheridge (Titheridge, 1966, pp. 1136-1139).

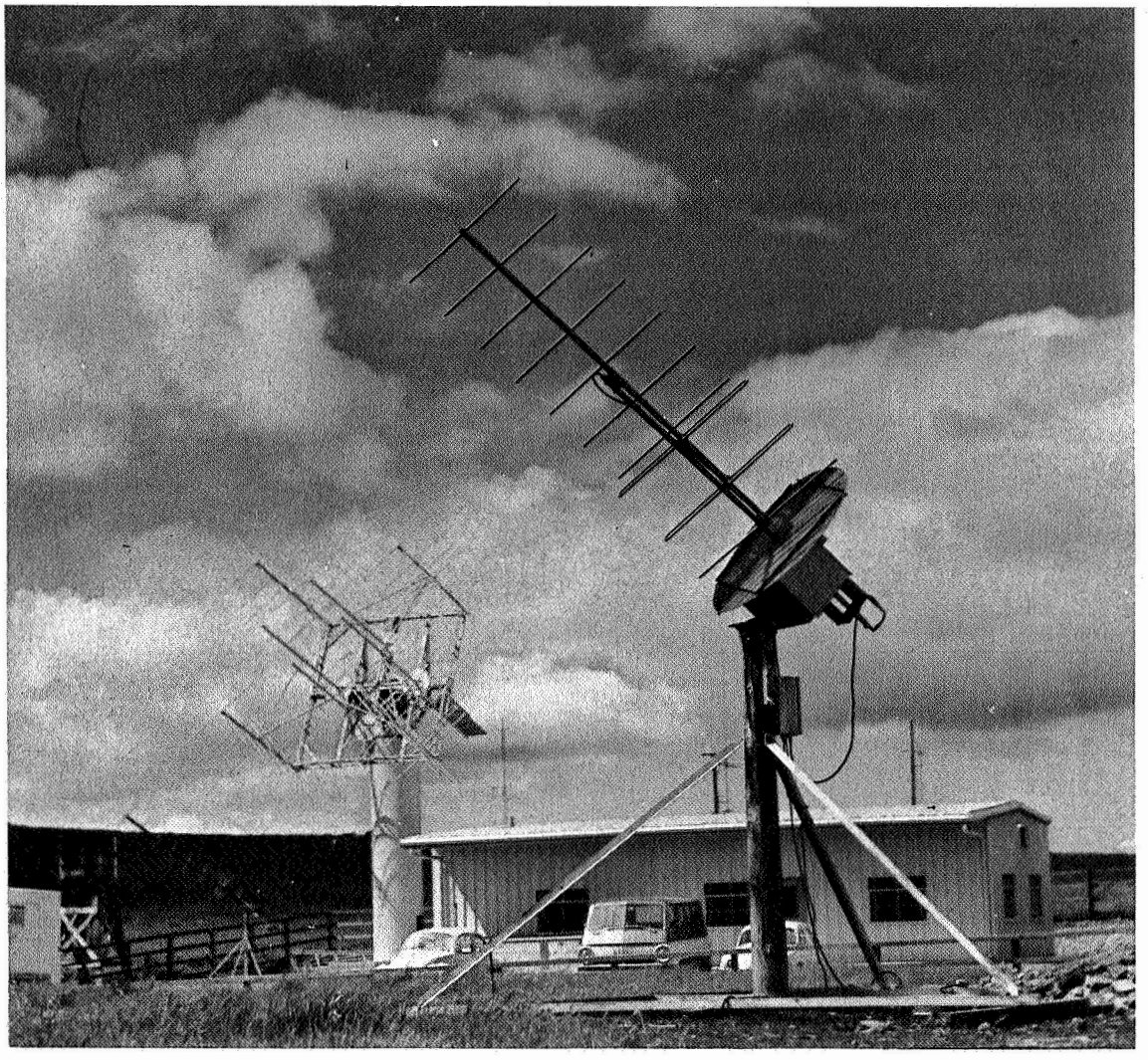

FIG. 4-19. THE ATS 137 MHz RECEIVING ANTENNA POINTS AT THE ATS SATELLITE, AND ROTATES AT 1/2 RPM TO MEASURE THE PLANE OF POLARIZATION OF THE RECEIVED ATS SIGNAL.

V ANALYSIS AND RESULTS OF THE INTERPLANETARY ELECTRON CONTENT MEASUREMENTS

This chapter discusses the Pioneer data reduction method, the average interplanetary electron density and its variation, and several large plasma pulses.

A. Plotting Pioneer Data

SCRA's data from the Pioneer spacecraft are processed onto digital data tapes at NASA Ames Research Center; then, at Stanford, each day's data are processed by an IBM 7090 and the results plotted on a Cal Comp plotter to produce a chart. Figure 5-1 is an example of a computer drawn chart.

1. Variables Plotted by the Computer

In Fig. 5-1 the Pioneer integrated electron content is plotted at the bottom of the chart. The horizontal axis is UT time in hours, with the day and the year noted at the beginning and at 0000 hrs, when the day changes.

The integrated electron content plotted on the bottom graph in the figure has a vertical scale with tick marks each 10×10^{16} el/m^2. The electron content curve determined from group path measurements appears as a series of steps, because of the relatively coarse group path quantization interval. The electron content determined from the phase path measurements is the solid curve and has a very fine (high resolution) quantization level of 0.04×10^{16} el/m^2.

The other two graphs on the chart, the (carrier) amplitude at the top and the rate of change (of electron content) in the middle, are not used in this discussion; however, they are described in Appendix C. Faraday fading is apparent in the 49.8 MHz carrier amplitude. Appendix C includes discussion of the problems that limit its use for measurement of the ionosphere.

2. Pioneer Data Processing

The data processing, while simple in concept, required a long time to evolve. Ames Research Center required four months to learn how

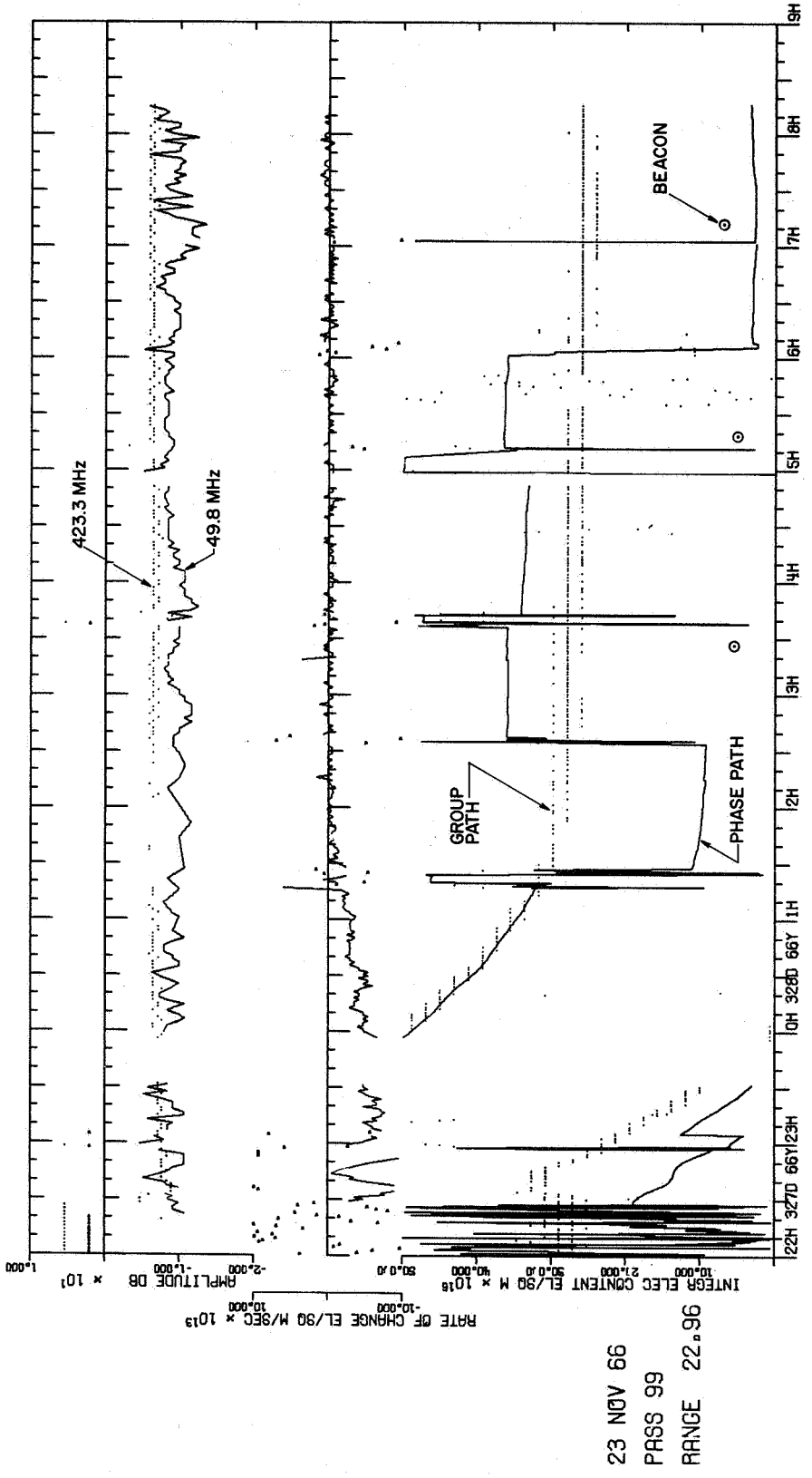

FIG. 5-1. COMPUTER DRAWN CHART OF PIONEER DATA FOR A TYPICAL DAY. The horizontal axis is UT time, in hours.

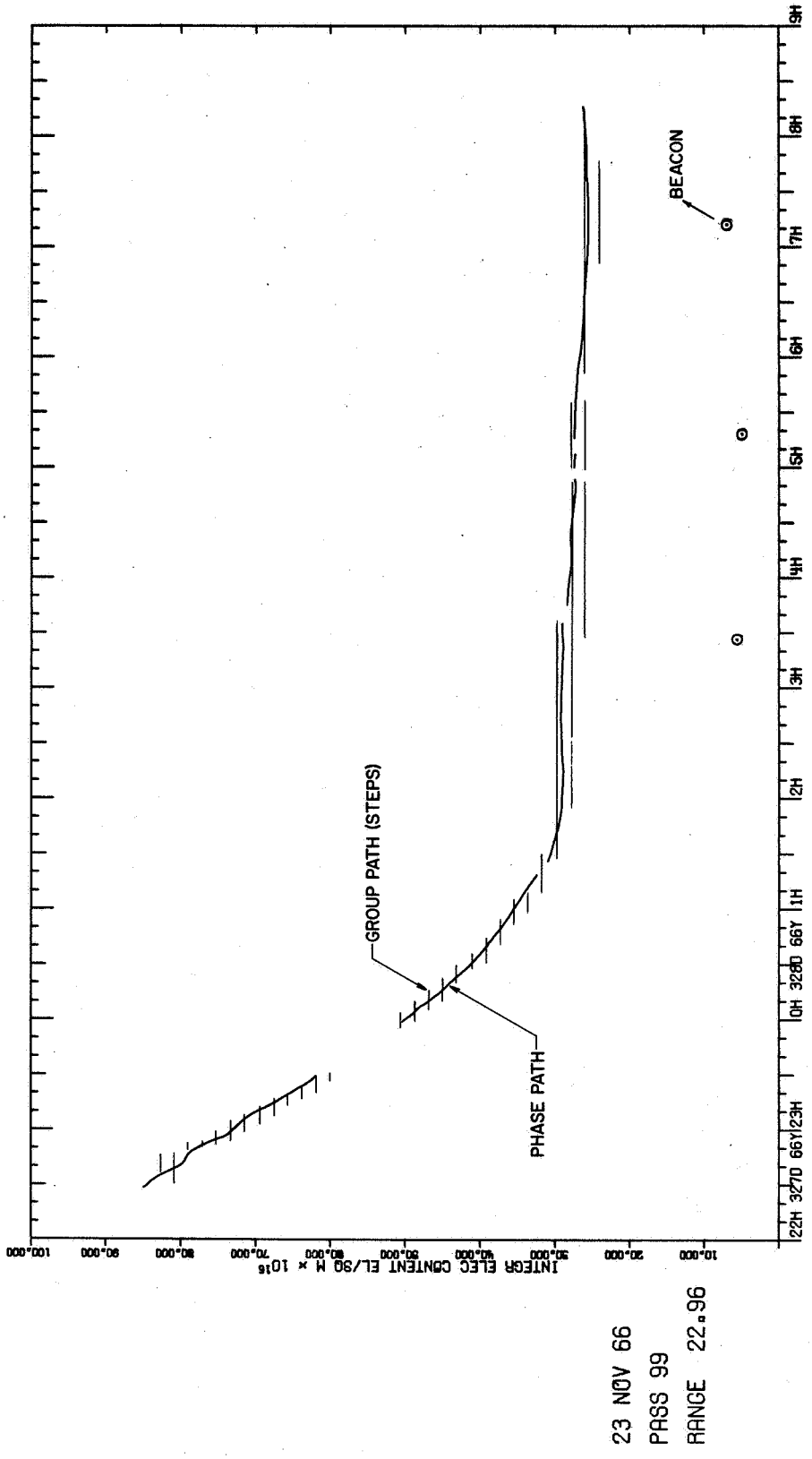

FIG. 5-2. THE PHASE PATH DETERMINATION OF ELECTRON CONTENT HAS BEEN RECONSTRUCTED FROM THE ELECTRON CONTENT DATA OF FIG. 5-1, AND FITTED TO THE GROUP PATH DETERMINATION OF CONTENT.

to put the Pioneer data on a digital tape and we required three months to learn how to take the data off. The plotting program first selects data from the magnetic tape in the desired time interval, then unpacks and assigns the data to their respective variables, and computes the time for each data point.

a. Group Path Data Processing

The modulation phase measured by the receiver aboard the spacecraft is read from the digital data tape. The transmitter modulation phase, which was added by the adjustable modulation phase shifter, is read from cards and added to the receiver modulation phase to obtain the total modulation phase shift caused by the medium. This total phase shift is converted to integrated electron content by multiplying by the appropriate constant--0.599×10^{16} el/m^2-deg for the 8.692 kHz modulation frequency, or 0.677×10^{16} el/m^2-deg for 7.692 kHz. The conversion equation used is presented in Appendix B.

The electron content determined from group path (modulation phase) is plotted as dots in the bottom graph in Fig. 5-1. The curve appears as a series of steps about 2×10^{16} el/m^2 high, which results from the digital quantization of the modulation phase into approximately 3° levels for telemetry transmission.

The program has a plot protection feature that not only prevents the curve from going off scale, but continues the curve from the opposite end of the scale, thus effectively expanding the scale length.

b. Phase Path Data Processing

The counter in the spacecraft receiver counts cycles of phase difference between 49.8 and 423.3 MHz carriers. The count is modulo 2^{10} (1024) because of the 10 bit length of the counter. The 5 Hz offset frequency added to the 49.8 MHz carrier at the transmitter causes the counter to overflow approximately every 3.5 minutes. The counter is sampled, without being reset, by the spacecraft telemetry system and split into two telemetry words for telemetering to earth. The telemetry words are unpacked in the computer, where they are reformed into the 10 bit counter word and corrected for the modulo 2^{10}

which occurred each time the counter overflowed. Then the 5 Hz bias, which was added at the transmitter to allow us to determine the sign of the phase path change, is subtracted from the count, leaving the net phase path in cycles. The net phase path, which results from changes in the medium, is multiplied by a constant (0.03755×10^{16} el/m^2-cycle) to convert it to integrated electron content.

The electron content determined from phase path measurements is plotted as a continuous curve in the bottom graph of Fig. 5-1. The resolution of phase path gives about 250 quantization steps for each division (10×10^{16} el/m^2) of the vertical scale. This curve is occasionally interrupted by discontinuities, which are caused by gaps of more than 3.5 minutes in the data, or by a loss of lock in the spacecraft receiver. The receiver VCOs run at their rest frequency when unlocked, and a meaningless count is accumulated in the counter, which in turn causes an erroneous jump in the electron content curve. The receiver loses lock when the signal gets too small, usually due to momentary failure of the 49.8 MHz transmitter (crowbar), or sometimes because of scintillation fading of the 49.8 MHz signal. Plot protection keeps the curve on scale, just as for the group path content curve.

c. Reconstruction of the Phase Path Electron Content Curve

The electron content curve determined from phase path measurements (continuous curve at the bottom of Fig. 5-1) is made up of a number of segments separated by discontinuities. The electron content of each segment is determined within an unknown additive constant; therefore, the discontinuous segments of phase path electron content curve can be aligned to make a continuous curve. The unknown additive constant is determined by fitting the aligned phase path electron content curve to the group path content curve, as shown in Fig. 5-2. The group path electron content curve in the figure has been copied from Fig. 5-1.

When the phase path data are missing for more than 10 to 20 minutes--for example, near the beginning of the curve in Fig. 5-2--the phase path electron content curve can no longer be pieced together. In that event, the separated portions of the phase path electron content are independently fitted to the group path curve.

B. Interplanetary Electron Density from Pioneer and Beacon Electron Content Measurements

The several circled points in Fig. 5-2 are the ionospheric electron content along the Pioneer propagation path, as determined from beacon satellite measurements of the ionospheric electron content. The difference between the Pioneer electron content and the ionospheric electron content is the interplanetary electron content. Nearly 300 of the interplanetary electron content points from Pioneer VI and VII have been averaged to obtain both the interplanetary electron content and density and the variation in the density.

1. Beacon Satellite Data Reduction

Beacon satellites pass over Stanford, going from horizon to horizon in about 15 minutes. The harmonically related 40 and 360 MHz beacon satellite transmissions are received on the ground and the changes in phase path (differential doppler) are recorded. The phase path data are processed in a computer. The thickness and horizontal density gradient of a wedge shaped ionosphere are fitted (least squares) to the phase path data to obtain the total phase path at the proximal point.* The computed phase path at the proximal point is added to the phase path data to obtain the slant electron content all along the satellite's subionospheric† path. The slant content is corrected to vertical. (See Garriott and de Mendonça, 1963, pp. 4920-4921, for a more detailed description of the technique.)

The beacon satellite's subionospheric path is plotted in Fig. 5-3 along with Pioneer's subionospheric point. Pioneer's position is

---

*The proximal point is where the incremental phase path is minimum (in magnitude), and is near the point of closest approach to the ground station. The proximal point is identified by a reversal in the sign of the differential doppler.

†Imagine a sphere concentric with the earth with a radius 350 km greater than that of the earth. The intersection of the ray path with this sphere is the ionospheric point, and its projection on the earth is the subionospheric point. The ray path's zenith angle at the ionospheric point is called χ.

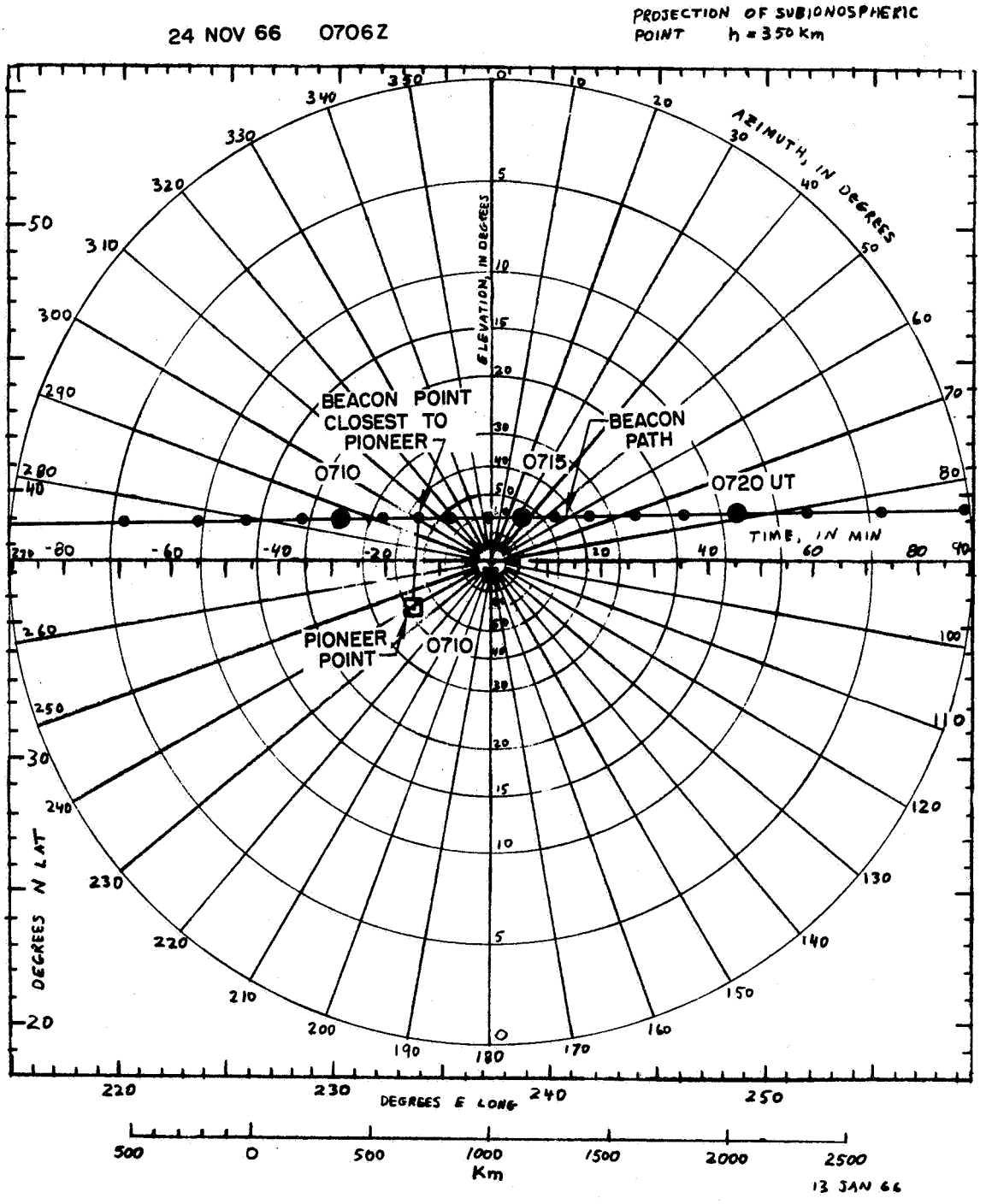

FIG. 5-3. THE SUBIONOSPHERIC PATH OF A BEACON SATELLITE ON 24 NOVEMBER 1966, PLOTTED ON AZIMUTH-ELEVATION COORDINATES. The Pioneer subionospheric point at 0710 is shown. This beacon measurement of the ionospheric content, projected along the Pioneer propagation path, is plotted as a circled dot at 0712 in Figs. 5-1 and 5-2.

assumed fixed during the 15 minute period that the beacon satellite is above the horizon. The ionospheric content measured at the point on the beacon's subionospheric path closest to Pioneer is multiplied by Pioneer's secant angle to account for Pioneer's slant path through the ionosphere. This slant ionospheric content is plotted on the Pioneer electron content curve (Fig. 5-2) as a circled dot if it is a "good point," otherwise it is plotted as a cross. Experience has shown that a beacon pass must meet the following requirements to be a "good point": (1) beacon transit elevation $\geq 30°$; (2) beacon and Pioneer ray paths have an elevation $\geq 25°$ at their closest approach to each other; and (3) the beacon and Pioneer subionospheric points $\leq$ 500 km apart (this can be relaxed at night).

2. Analysis of the Interplanetary Electron Content

a. The Interplanetary Density with Uniform Density Distribution

An interplanetary electron content point is obtained from plots of Pioneer electron content (Fig. 5-2 is an example) whenever there is a beacon measurement of the ionosphere to subtract from the Pioneer content. These interplanetary electron content points are plotted versus range in Fig. 5-4 for Pioneer VI. If the electron number density in interplanetary space were constant during the flight of Pioneer, and the density were uniform in space, the electron content in a 1 m^2 column between the earth and the spacecraft would increase linearly with range. The content would appear as a straight line on the interplanetary electron content plot, with a slope proportional to the interplanetary electron number density. The intercept of the line at zero range would be due to the part of the ionospheric content that had not been removed from the Pioneer content, i.e., the protonosphere (ionosphere above the 1000 km height of the beacon satellite orbits).

The dashed line (almost covered by the solid curve) in Fig. 5-4 is the best fit (least squares) straight line to the Pioneer VI electron content data versus range. The slope gives an interplanetary electron number density of 5.74 el/cc, which is averaged over space (each

point) and over time (all the points). The near-earth component of electron content (the intercept) is 8.37×10^{16} el/m^2, and the rms variation in density is ±4.1 el/cc.

The electron number density averaged over the 1 m^2 column for each electron content point is obtained by first subtracting the constant near-earth component from the interplanetary electron content, then dividing by the range. The plot of density versus range is shown in Fig. 5-6 for Pioneer VI. The straight line is the average density derived from the slope of the line in the electron content versus range plot (Fig. 5-4).

A plot of the Pioneer VII interplanetary electron content measurements is in Fig. 5-5, with the line which is fitted to the data drawn as a dashed line. The slope of this line gives an average electron number density of 8.02 el/cc with an rms variation of ±3.8 el/cc. The intercept is -1.41×10^{16} el/m^2. The Pioneer VII measurements of interplanetary electron number density are plotted versus range in Fig. 5-7. Further discussion about the density is deferred to section B.d., where the density data are corrected for the radial expansion of the solar wind.

b. The Intercept and the Protonosphere

The straight line fitted to the Pioneer VI interplanetary electron content data (Fig. 5-4) only grazes the top of the cluster of points in the 0 to 10 Gm range interval. Higher solar activity during the first 30 Gm of the flight, followed by low solar activity for the remainder of the flight, biased the line too high near zero range. The straight line, which was fitted to the ionospheric content data in the 0 to 10 Gm range, had an intercept of 4.8×10^{16} el/m^2, a content more like that expected in the late afternoon protonosphere. Referring to Fig. 4-2, it can be seen from the trajectory that the Pioneer VI propagation path passed through the late afternoon ionosphere at transit during the first 10 Gm of the flight.

The straight line fitted to the Pioneer VII electron content data (Fig. 5-5) goes through the middle of the cluster of points in the 0 to 10 Gm range. However, the burst of large electron content points at 60 Gm range has tilted this line so that the intercept is below zero, at -1.5×10^{16} el/m^2. The line fitted to electron content data in the

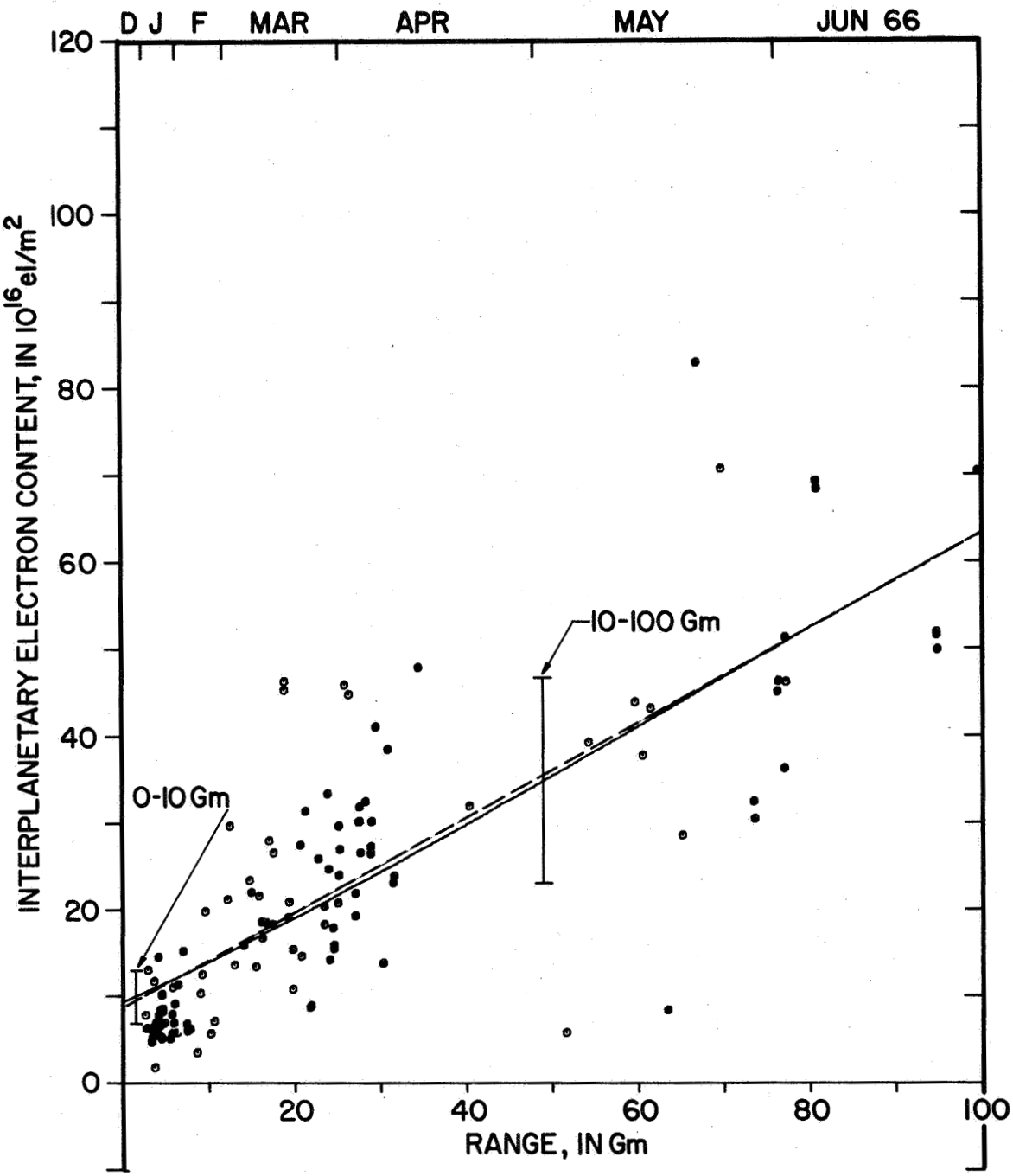

FIG. 5-4. PIONEER VI INTERPLANETARY ELECTRON CONTENT VERSUS (GEOCENTRIC) SPACECRAFT RANGE. The time scale across the top indicates when the measurements were made.

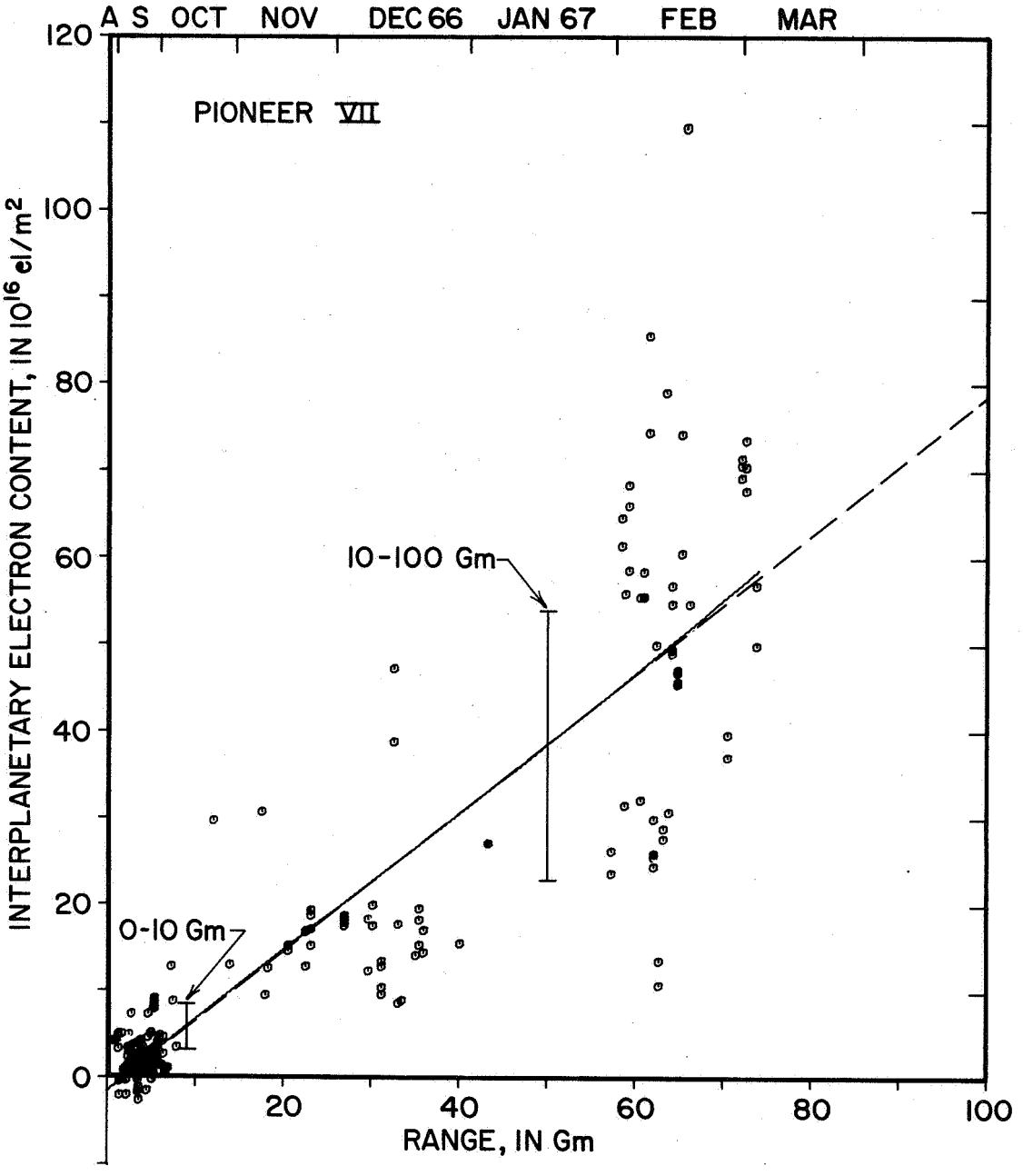

FIG. 5-5. PIONEER VII INTERPLANETARY ELECTRON CONTENT VERSUS SPACECRAFT RANGE. The time scale across the top indicates when the measurements were made.

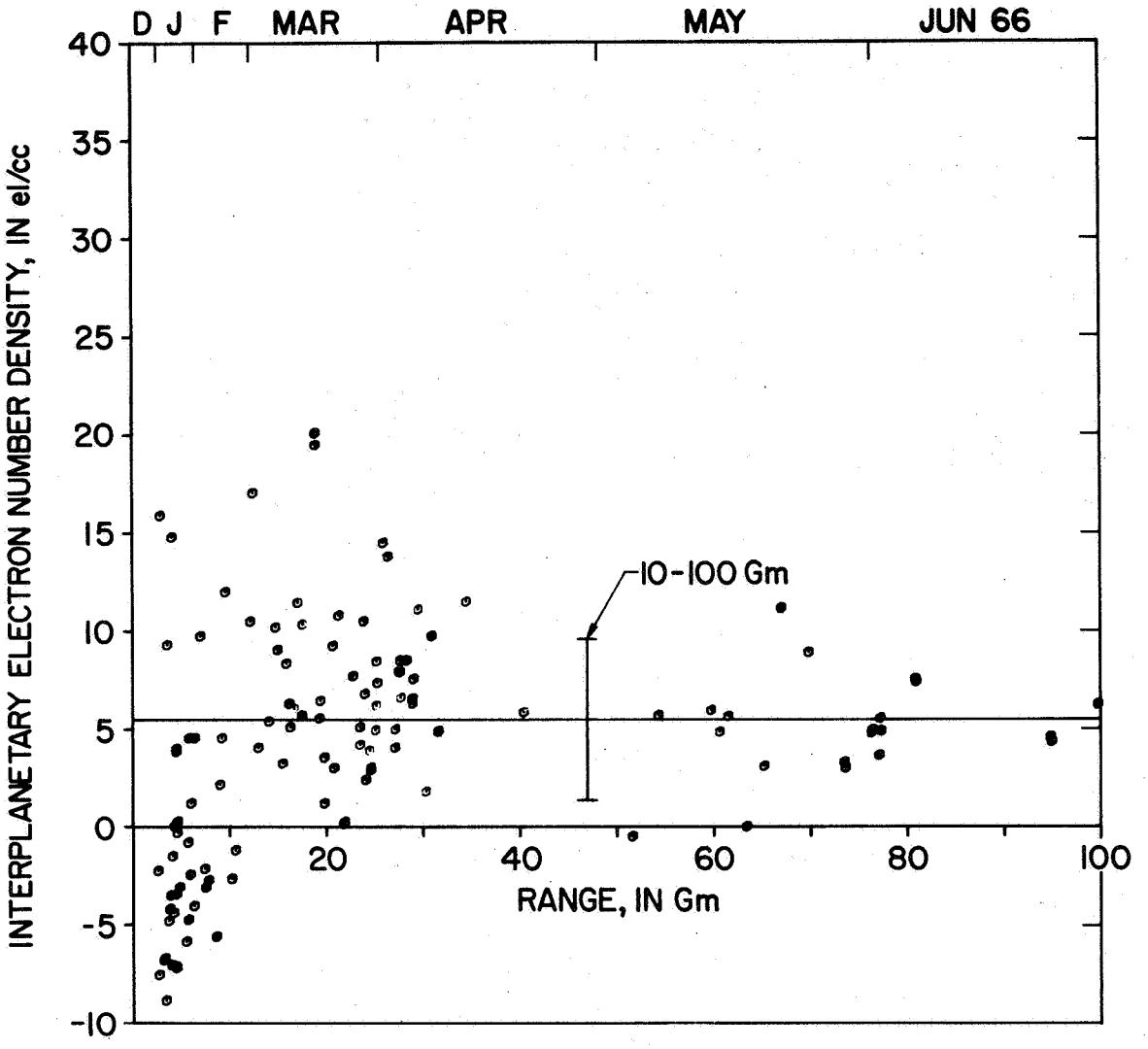

FIG. 5-6. PIONEER VI INTERPLANETARY ELECTRON NUMBER DENSITY VERSUS SPACECRAFT RANGE, ASSUMING A UNIFORM ELECTRON NUMBER DENSITY DISTRIBUTION. The 5.5 el/cc average is shown by the horizontal curve.

0 to 10 Gm range had an intercept of 0.72×10^{16} el/m^2, certainly a better value for the nighttime protonosphere than -1.5×10^{16} el/m^2. Again, reference to the trajectory in Fig. 4-2 shows that for the first 10 Gm of Pioneer VII's mission, the propagation path passed through the nighttime ionosphere.

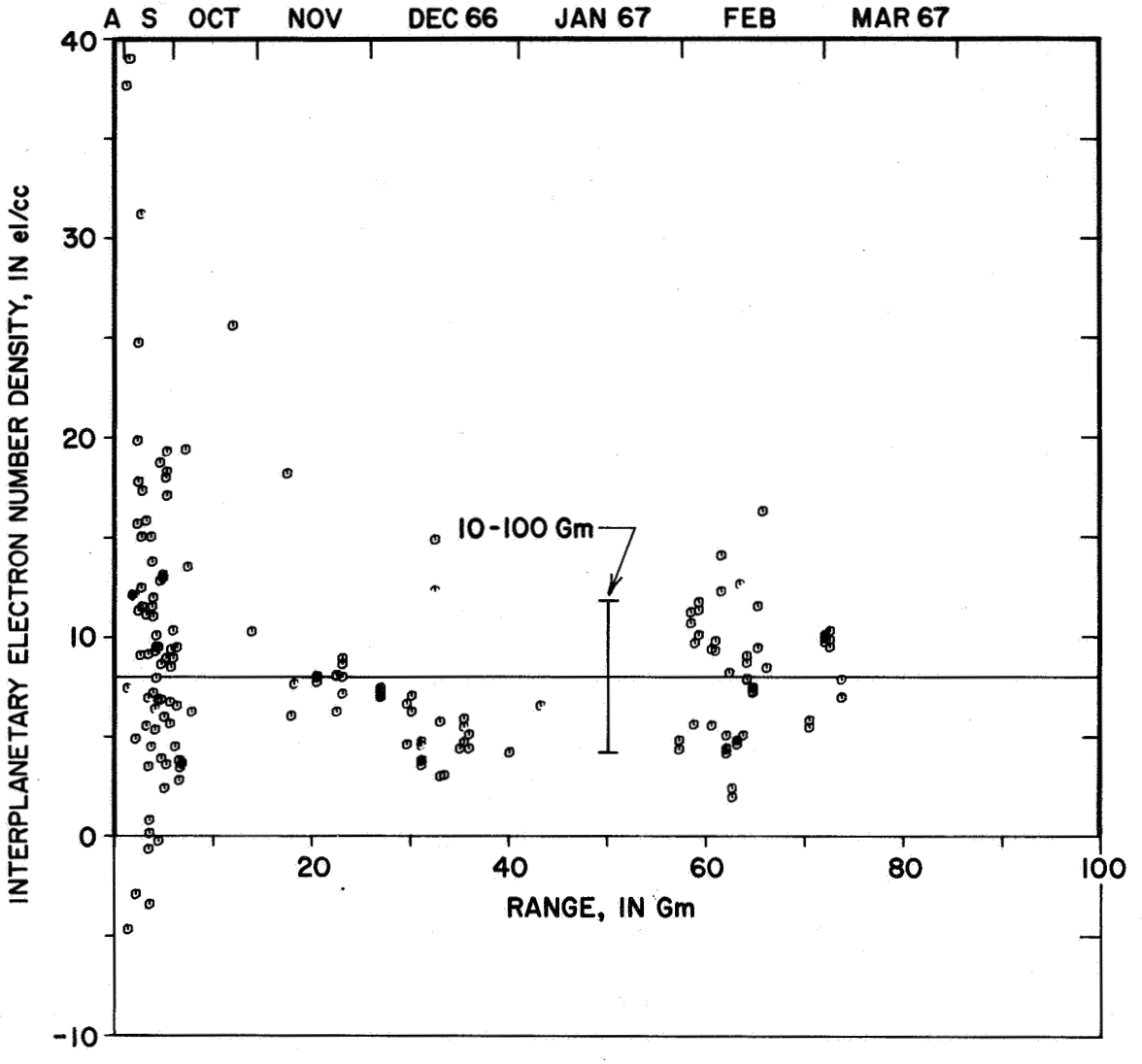

FIG. 5-7. PIONEER VII INTERPLANETARY ELECTRON NUMBER DENSITY VERSUS SPACECRAFT RANGE, ASSUMING A UNIFORM ELECTRON NUMBER DENSITY DISTRIBUTION. The 8.0 el/cc average is shown by the horizontal curve.

c. Accuracy of the Interplanetary Electron Content and Number Density

The variation in electron content due to measurement errors can be estimated from the scatter in the electron content near zero range (Figs. 5-4 and 5-5) where the interplanetary electron content has little effect. In the range of 0 to 10 Gm, the rms variation in

content is $\pm 3.15 \times 10^{16}$ el/m^2 for Pioneer VI and $\pm 2.65 \times 10^{16}$ el/m^2 for Pioneer VII. Since there is some interplanetary variation in this region, the variation of content in the 0 to 10 Gm range interval can be considered an upper limit for measurement variation. The very much larger variations in content in the 10 to 100 Gm ranges, which can be seen in Figs. 5-4 and 5-5, are therefore real, as are also the density variations computed from these contents. The computed variation for a least squares best fit line in the 10 to 100 Gm range is $\pm 11.65 \times 10^{16}$ el/m^2 for Pioneer VI and $\pm 15.53 \times 10^{16}$ el/m^2 for Pioneer VII, very significantly larger than the 2.5 to 3 $\times 10^{16}$ el/m^2 in the 0 to 10 Gm range.

The density data in the 0 to 10 Gm range (Figs. 5-5 and 5-6) are disregarded for several reasons. Small variations in the measurement of electron content result in large changes in density near zero range. The same size variation in content has progressively less effect on the density at greater range. For example, a $\pm 2.5 \times 10^{16}$ el/m^2 variation in electron content results in a 5 el/cc density variation at 5 Gm range, but only 0.5 el/cc at 50 Gm.

For Pioneer VI, the intercept for the straight line in Fig. 5-4 represents a content larger than the data points measured near the range origin, as discussed above. Therefore, the densities computed from Eq. (5.1) plotted in Fig. 5-6 are negative if the interplanetary content is less than the 8.7×10^{16} el/m^2 value of the intercept; this is the case for most of the points near the range origin and a few points far out in range.

$$\text{Density} = \frac{I_{\text{interplanetary}} - I_{\text{intercept}}}{\text{Range}} \qquad (5.1)$$

For Pioneer VII, the content represented by the intercept of the line in Fig. 5-5 is a little too low, which causes the densities near the origin (Fig. 5-7) to be too high.

d. The Interplanetary Density with $1/r^2$ Density Distribution

In this section the interplanetary density calculations are corrected for the decrease in density of the solar wind electrons as it expands radially from the sun. In the interplanetary density analysis

of section V.B.2.a, the solar wind was assumed to be uniform, which induced a moderate spatial dependency in the electron number density.

(1) The $1/r^2$ Density Equation

As the solar wind flows out from the sun, continuity requires that the density fall off as $1/r^2$ from the sun. Thus the interplanetary electron content from earth to the spacecraft depends on the spacecraft location, as given in Eq. (5.2); this is derived in Appendix E.

$$I = \frac{(N_o \times GEOR)}{\operatorname{sinc}\left(\frac{ESP}{\pi}\right)\left(\frac{RS}{RD}\right)\left(\frac{SUNR}{RD}\right)} + I_o \qquad (5.2)$$

- $(N_o \times GEOR)$: electron content for uniform density
- $\operatorname{sinc}\left(\frac{ESP}{\pi}\right)$: due to ray path cutting closer to sun because of ESP angle
- $\left(\frac{RS}{RD}\right)$: due to change of earth-sun range from reference distance
- $\left(\frac{SUNR}{RD}\right)$: due to spacecraft distance from sun
- I_o: near-earth content

I = the integrated electron content between the earth and the interplanetary spacecraft

I_o = a constant integrated electron content due to part of the ionosphere which was not removed from the interplanetary content

RD = the reference distance from the sun at which the density N_o is to be normalized. For this experiment, RD = 1 AU (149.5 Gm)

N_o = the interplanetary density at a distance RD from the sun

GEOR = geocentric range of the spacecraft. For this experiment, 0.1 to 100 Gm

ESP = earth-sun-probe (spacecraft) angle. For this experiment, 0 to 40°

RS = range of earth from the sun, 147 to 152 Gm

SUNR = range of the spacecraft from the sun, 120 to 165 Gm

Equation (5.2) is plotted versus earth-spacecraft range in Fig. 5-8 with a density N_o of 5 el/cc for the trajectories

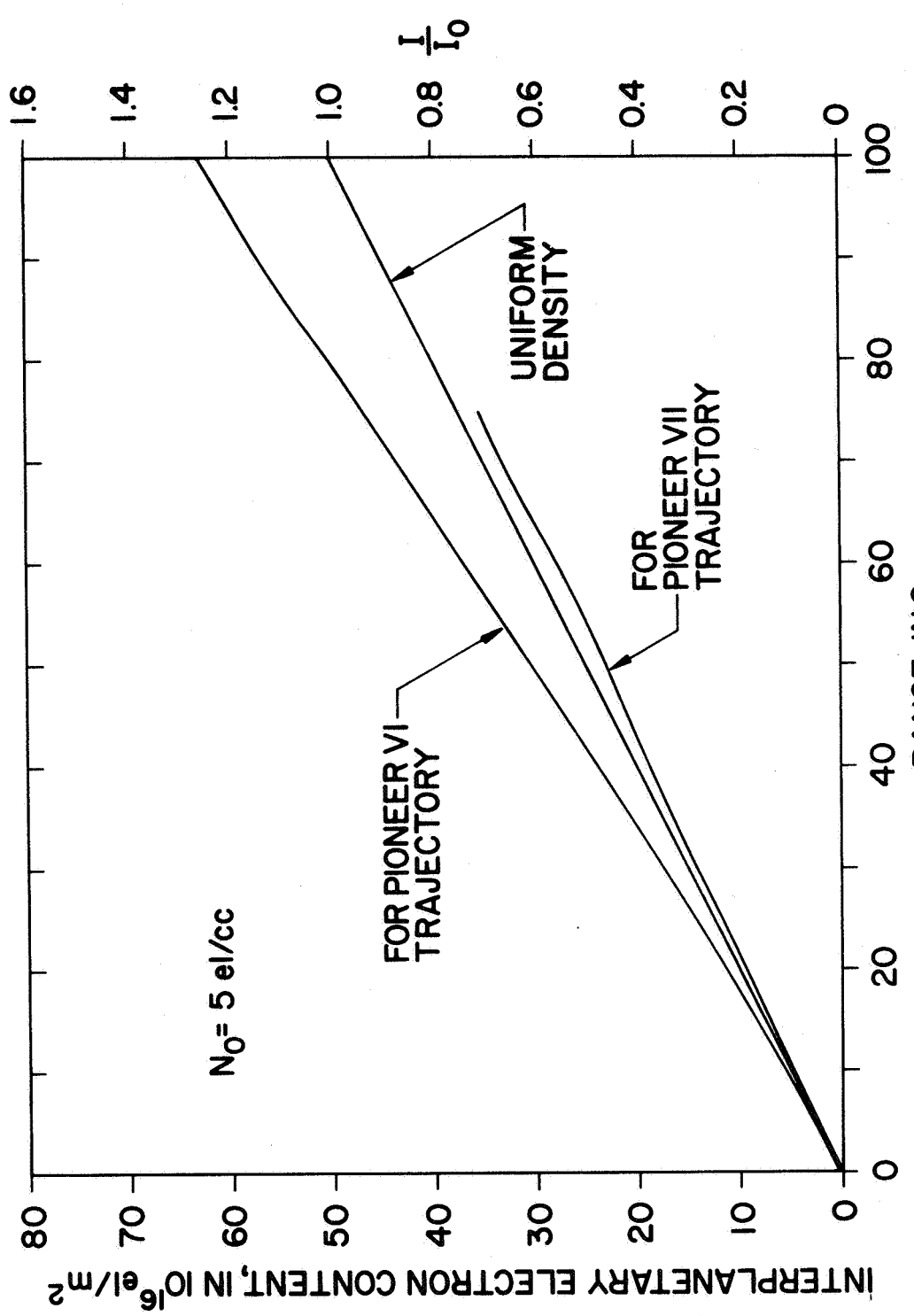

FIG. 5-8. INTERPLANETARY ELECTRON CONTENT VERSUS (GEOCENTRIC) SPACECRAFT RANGE, FOR AN ELECTRON NUMBER DENSITY DEPENDENCE OF $1/r^2$ FROM THE SUN. The content is calculated for the Pioneer VI trajectory and for the Pioneer VII trajectory, with a density of 5 el/cc at 1 AU. Electron content for a uniform density distribution of 5 el/cc is shown for comparison.

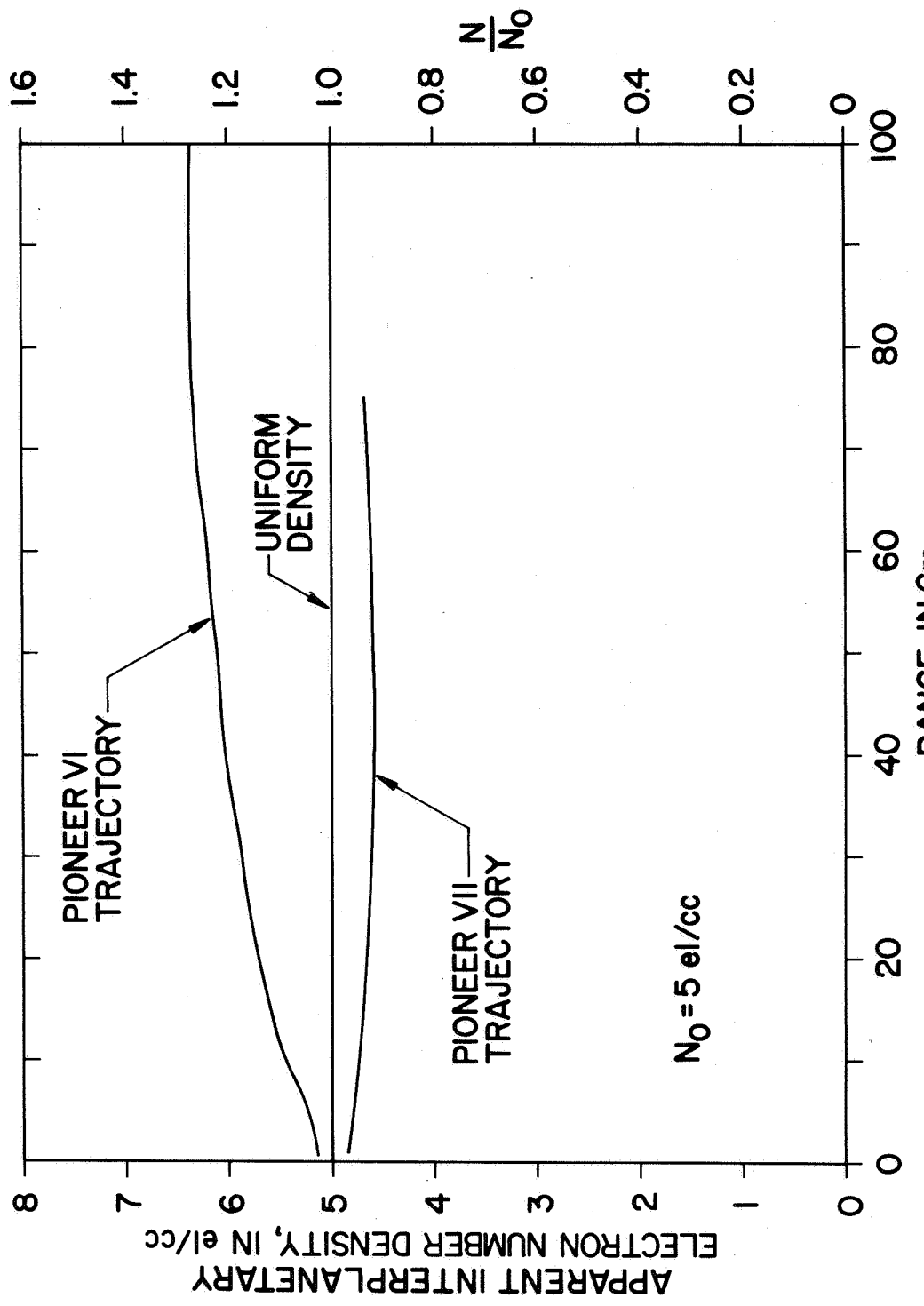

FIG. 5-9. APPARENT ELECTRON NUMBER DENSITY OBTAINED FROM DIVIDING THE ELECTRON CONTENT CURVES IN FIG. 5-8 BY THE SPACECRAFT RANGE.

of Pioneer VI and VII. The electron content curve for a uniform density of 5 el/cc is shown for comparison. The electron content curve for Pioneer VI is practically a straight line, but it has a 25 percent greater slope than the electron content for a uniform density. That is, the Pioneer VI flight in toward the sun (trajectory in Fig. 4-2) gives a higher electron content than would a uniform density, because the density is higher closer to the sun. Thus the average electron number density inferred from the slope of the electron content line, assuming a uniform density, is about 25 percent too large.

The interplanetary electron number density computed from each Pioneer VI interplanetary content point will increase with range, up to 25 percent over the density at 1 AU, as the spacecraft gets closer to the sun. Figure 5-9 shows the increase in average density along the propagation path as a function of spacecraft range for Pioneer VI. This plot is the electron content of Eq. (5.2) divided by the earth-spacecraft range, with an N_o of 5 el/cc. The constant density of 5 el/cc, which is independent of range, is shown for comparison.

Pioneer VII was launched away from the sun, where it encounters a density less than at 1 AU. The measured electron content is about 10 percent less than would be measured if the density were uniform, as can be seen in Fig. 5-8. The density computed from the slope of the straight line fitted to the Pioneer VII interplanetary electron content versus range, is about 10 percent too low.

(2) Pioneer VI and VII Interplanetary Density with the $1/r^2$ Density Dependence

The electron content curve of Eq. (5.2) is fitted to the Pioneer VI interplanetary electron content data in Fig. 5-4. The electron content curve for the $1/r^2$ density (solid curve) is nearly a straight line, so it falls almost on top of the straight line fitted to the data (dashed line) for the uniform density assumption. However, the density at 1 AU computed from this curve is 4.26 el/cc, about 25 percent less than the 5.47 el/cc computed previously for the uniform density. The interplanetary electron number density computed from each electron content point is plotted versus range in Fig. 5-10, where the solid line in the figure is the 4.26 el/cc. The rms density variation from the

mean is ±3.61 el/cc, with densities ranging from a minimum of 1.3 el/cc to a maximum of 17.2 el/cc, in the 10 to 100 Gm range interval. The negative densities in Fig. 5-10 are caused by the large intercept on the electron content curve, as explained in section V.B.2.c.

The average electron number density, normalized to 1 AU, is 8.72 el/cc for Pioneer VII, as compared with 8.02 el/cc computed from the uniform density assumption. In the 10 to 100 Gm range interval, the rms density variation from the mean is ±4.05 el/cc; the minimum density measured is 2.2 el/cc while the maximum is 27.4 el/cc.

The average electron number density measured by Pioneer VII is 8.7 el/cc, twice the average density of 4.3 el/cc measured by Pioneer VI. Inspection of the Pioneer VII interplanetary electron number density data (Fig. 5-11) shows a background level around 5 el/cc, close to the Pioneer VI average of 4.3 el/cc. The quiet level of around 5 el/cc is that measured by experimenters with plasma probes; this measurement represents one of the most significant results of this experiment.

Increasing solar activity is responsible for the many large values of electron number density seen in the Pioneer VII data (Fig. 5-11); these values increase the average electron number density over that measured by Pioneer VI. The smoothed (for 1 year) sunspot number in Fig. 5-12 increased from 23 to 43 during the Pioneer VI flight. The smoothed sunspot number had a much higher range, increasing from a predicted 63 to 85 during the data period of Pioneer VII, reflecting the increased average interplanetary electron number density measured by Pioneer VII.

The increased activity of the sun and solar wind is also marked by several large, high density plasma pulses in Pioneer VII data; these pulses are described in the next sections.

C. Plasma Pulses

In all the Pioneer data up to February 1967, only three plasma pulses have been found, each of which is treated here separately. All can be explained by a density pulse traveling radially from the sun with a spherical wavefront.

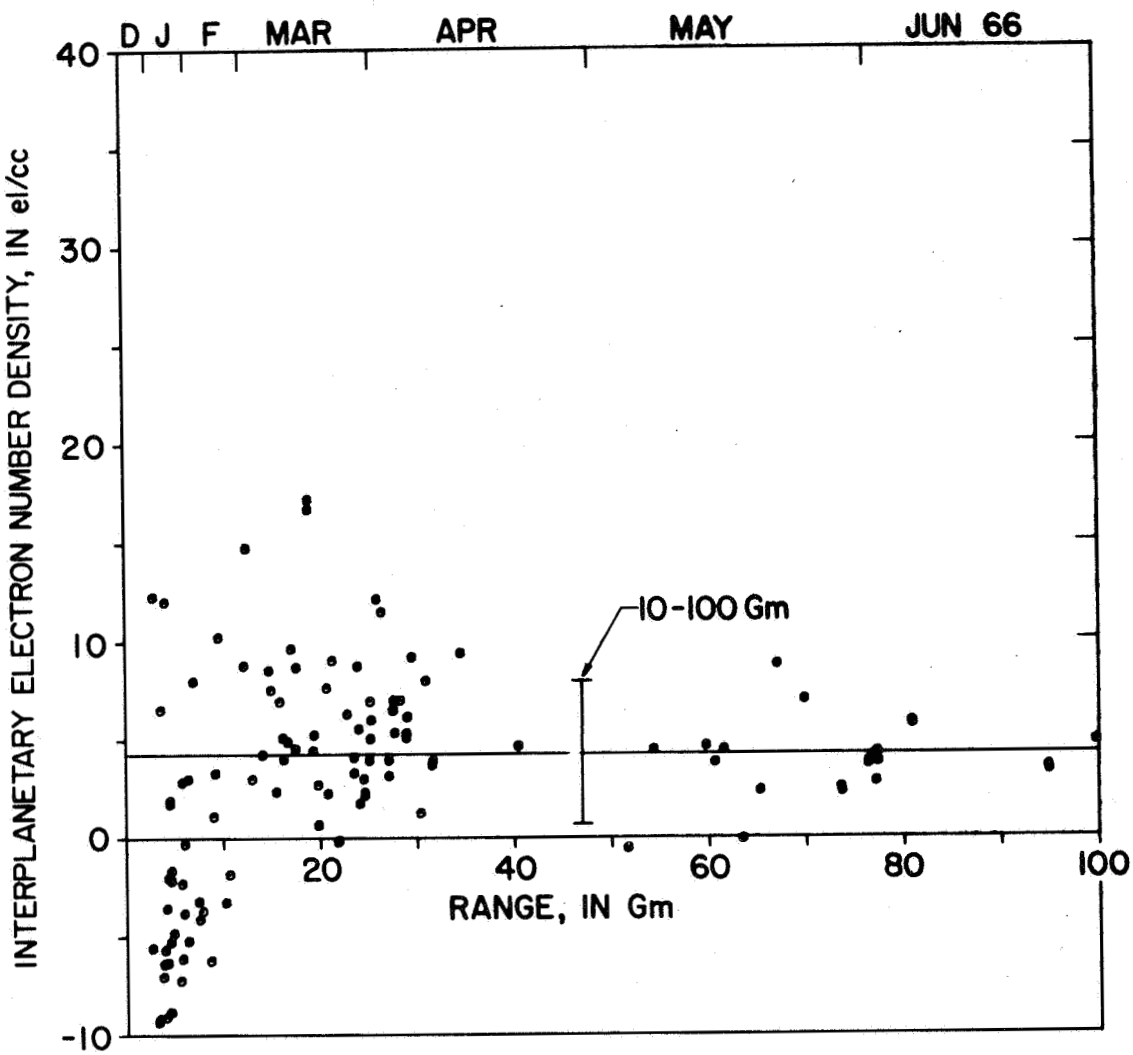

FIG. 5-10. PIONEER VI INTERPLANETARY ELECTRON NUMBER DENSITY VERSUS SPACECRAFT RANGE FROM THE EARTH; THE TIME SCALE ACROSS THE TOP INDICATES WHEN THE MEASUREMENTS WERE MADE. The density is normalized to 1 AU by correcting for the electron number density dependence of $1/r^2$ from the sun. The 4.3 el/cc average is shown by the horizontal curve.

1. Plasma Pulse of 24 October 1966

Most of the Pioneer electron content data looks very similar from day to day, only slowly changing character over the weeks as Pioneer gets farther from earth, and as the ionosphere changes with the time of day that Pioneer is above the horizon.

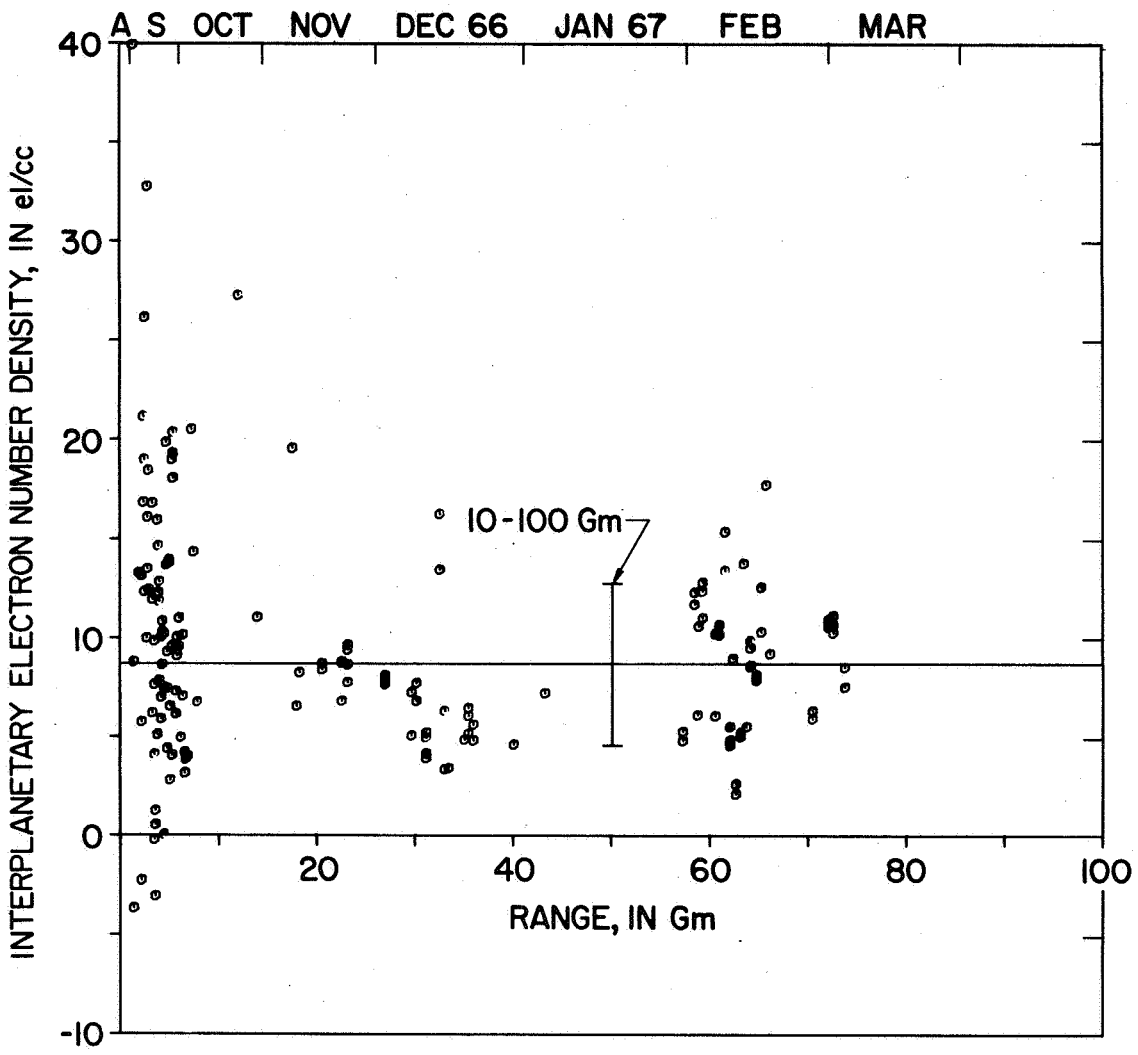

FIG. 5-11. PIONEER VII INTERPLANETARY ELECTRON NUMBER DENSITY VERSUS SPACECRAFT RANGE FROM THE EARTH; THE TIME SCALE ACROSS THE TOP INDICATES WHEN THE MEASUREMENTS WERE MADE. The density is normalized to 1 AU by correcting for the electron number density dependence of $1/r^2$ from the sun. The 8.7 el/cc average is shown by the horizontal curve.

On 24 October 1966, the Pioneer electron content was unusually high, as can be seen in Fig. 5-13, where the electron content of that day is compared with the electron content on several other days. The interplanetary electron content is established by the beacon measurement on

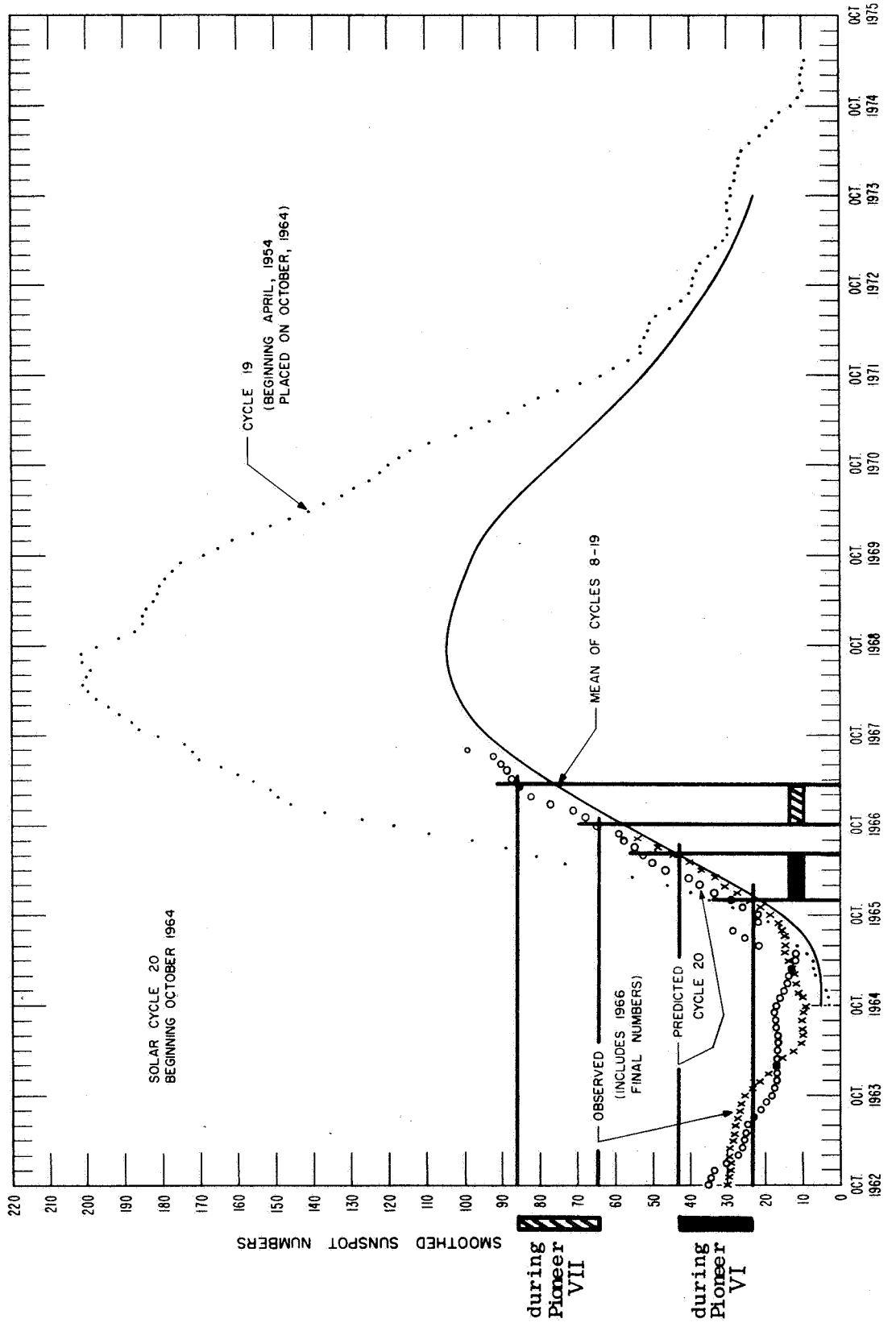

PREDICTED AND OBSERVED SUNSPOT NUMBERS

FIG. 5-12. SMOOTHED SUNSPOT NUMBER.

24 October at 0940. The difference between the electron content on 24 October and the control day of 26 October is plotted (Fig. 5-14) above the line labeled "interplanetary background content."

The electron content in Fig. 5-14 increased until 0500, when it reached a maximum and started to decrease linearly. The content pulse is extended with dashed lines, from which it is estimated that the pulse began at 2130 and ended at 1400 when the content had returned to the background level.

For a first approximation, the pulse will be assumed to be a symmetrical triangle with the trailing edge in Fig. 5-14 defining the pulse. The trailing edge is used because it is observed through the thin undisturbed nighttime ionosphere (0500 is 8 p.m., PST). The leading edge is less reliable because it is observed at low elevation angles through a more variable afternoon ionosphere. This triangular-shaped electron content can be explained by a rectangular density pulse traveling radially outward from the sun, crossing the propagation path shown in Fig. 5-15. The triangle shape of the electron content curve (Fig. 5-14) defines the length of the pulse equal to the length of the propagation path. If the density pulse were shorter than the propagation path, the electron content curve would have a flat top during the time that the density pulse is completely within the path. If the density pulse were longer than the path, the electron content path would also have a flat top during the time that the path is completely within the density pulse.

The peak content of 40×10^{16} el/m^2 above the background level, divided by the length of the propagation path (12.4 Gm), gives a pulse density of 33 el/cc greater than the background level (10 el/cc). The length of the pulse is 10.7 Gm, equal to the radial length of the propagation path. The pulse velocity is 330 km/sec, which is determined from the radial length of the propagation path (10.7 Gm) divided by the time taken to traverse this distance (9 hr). This compares very well with the 300 to 316 km/sec measured throughout this period by the Ames Research Center plasma probe aboard the Pioneer spacecraft (Wolfe, personal communication). The plasma measured at the spacecraft, which is the plasma leaving the propagation path, is coincident with the trailing edge of the

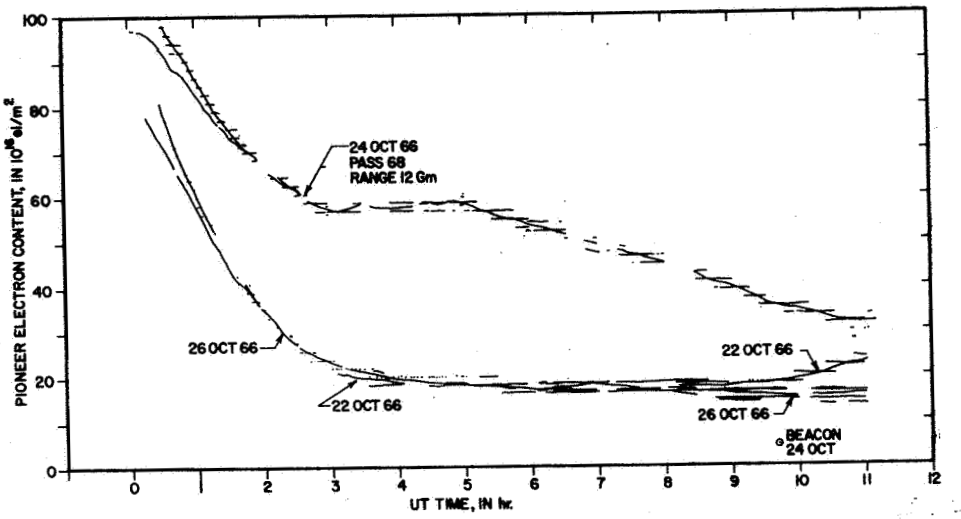

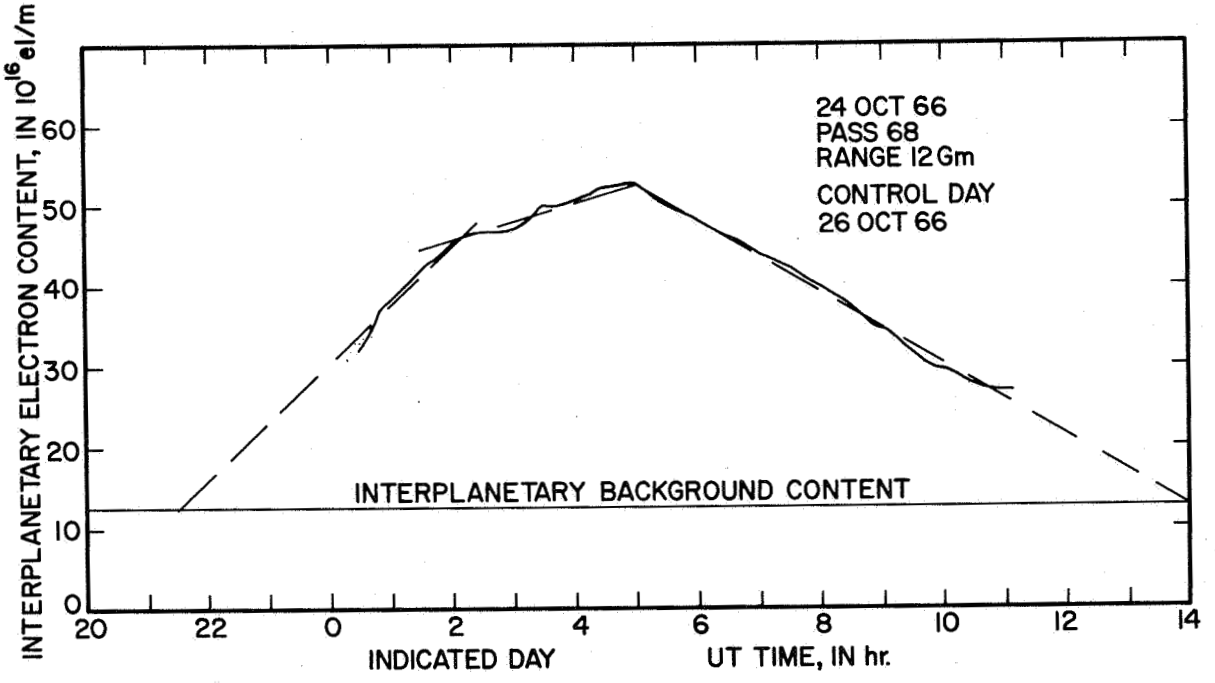

FIG. 5-13. (UPPER GRAPH) THE PULSE OF PIONEER ELECTRON CONTENT (INCLUDING THE IONOSPHERE) on 24 OCTOBER 1966. The content on several days is shown for comparison.

FIG. 5-14. (LOWER GRAPH) THE INTERPLANETARY ELECTRON CONTENT PULSE ON 24 OCTOBER 1966. Notice the vertical scale has been expanded 2 times over the vertical scale of Fig. 5-13.

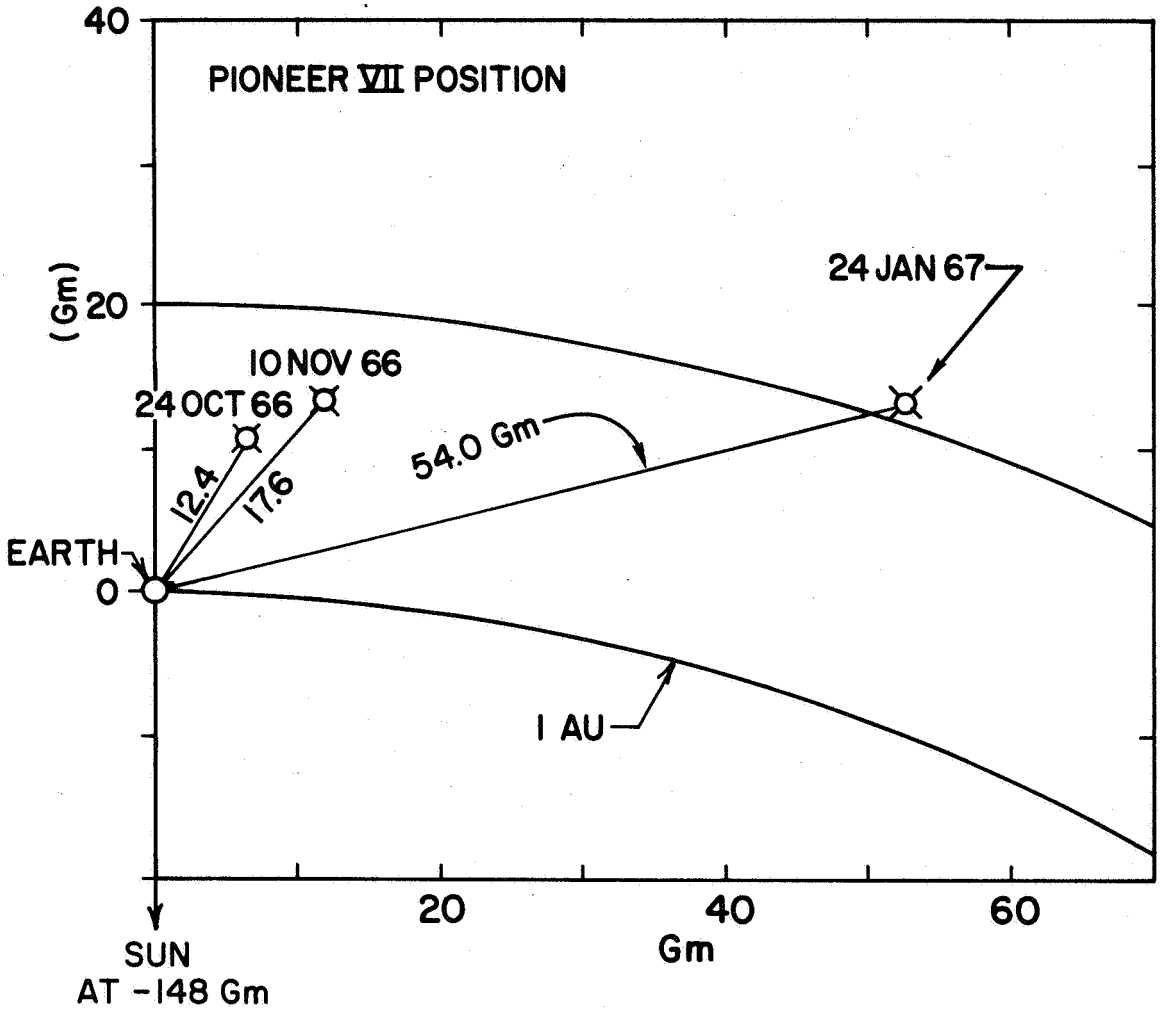

FIG. 5-15. THE POSITION OF THE PROPAGATION PATH BETWEEN EARTH AND THE SPACECRAFT ON THE DAYS WHEN PULSES OF ELECTRON CONTENT OCCURRED. Arcs of solar radius of 150 Gm (1 AU) and 170 Gm are shown for reference.

electron content pulse in Fig. 5-14. When the multiple spikes of plasma density measured by the plasma probe are integrated, they have nearly the same decrease as measured by SCRA's experiment. Thus the event of 24 October can be described by a pulse with a 33 el/cc increase in density, traveling at 330 km/sec, with a length (depth) of 10.7 Gm.

Wolfe describes these pulses as "pile up" of a faster moving plasma running into a slower moving one that had started earlier. This

description fits the solar plasma pulse structure seen by plasma probes, where the density suddenly jumps up to some high value (30 el/cc) with a low velocity (300 to 400 km/sec), and continues for several hours to one and one-half days. Then the velocity rapidly increases to a high value (500 to 700 km/sec) and the density drops to a low value (1 to 5 el/cc). (See Neugebauer and Snyder, 1966, pp. 4475-4478, for a description of Mariner II plasma measurements, with a plot of velocities and densities.)

2. Plasma Pulse of 10 November 1966

Another plasma pulse is shown in Fig. 5-16 where the Pioneer electron content of 10 November 1966 is compared with the content of several other days. The difference between the content of 10 November and the control day of 5 November is shown in Fig. 5-17, where dashed lines are extended to complete the pulse. This pulse of electron content differs from the pulse of 24 October in that it is smaller and it has a flat top instead of being triangular shaped.

The event of 10 November can be explained by a rectangular density pulse, shorter than the propagation path length, traveling radially from the sun. As the density pulse started across the propagation path at 1930 (in Fig. 5-17), the electron content started to increase linearly. The increase continued until 0200, when the trailing edge of the density pulse reached the propagation path. The flat top continued while the density pulse was within the propagation path. The content started to decrease at 0530, when the leading edge reached the end of the propagation path, and continued to decrease until the trailing edge reached the end of the propagation path at 1100. The fraction of the propagation path covered by the pulse is the length of the pulse (the decrease occurring between 0530 and 1100 divided by the length of the propagation path (0200 to 1100), which is (5.5 hr)/(9 hr) = 0.61. Strictly speaking, these time intervals are not lengths, but they offer a simple way to think about the pulse.

The pulse density is the pulse electron content divided by the part of the propagation path occupied by the pulse, that is,

$$\text{Pulse density} = \frac{(30 \times 10^{16}\ \text{el/m}^2)}{(0.61)\ (17.5\ \text{Gm})} = 28\ \text{el/cc}$$

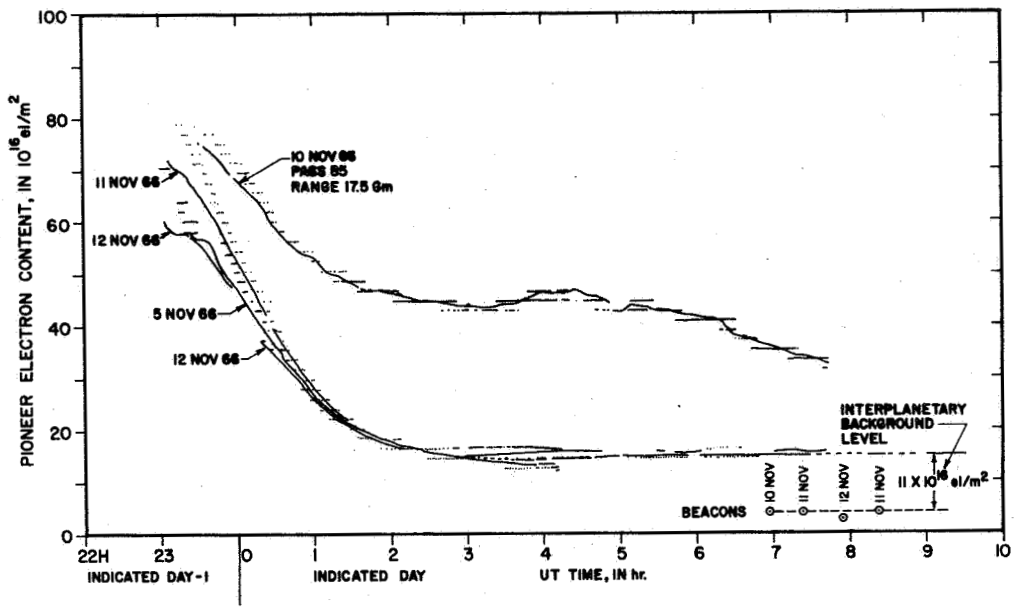

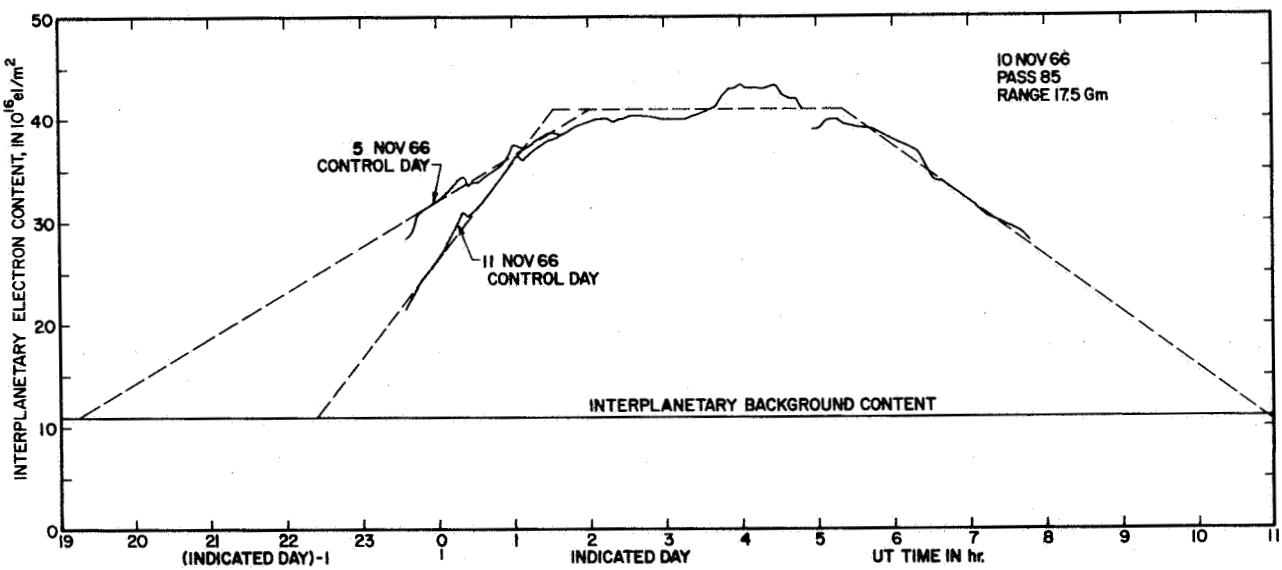

FIG. 5-16. (UPPER GRAPH) THE PULSE OF PIONEER ELECTRON CONTENT (INCLUDING THE IONOSPHERE) ON 10 NOVEMBER 1966. The content on several other days is shown for comparison.

FIG. 5-17. (LOWER GRAPH) THE INTERPLANETARY ELECTRON CONTENT PULSE ON 10 NOVEMBER 1966. Notice the vertical scale has been expanded by a factor of 2 over Fig. 5-16.

For a pulse with wavefront normal to the earth-sun line, the pulse depth is 8.1 Gm which is the fraction of the propagation path covered, measured radially. The pulse has a radial velocity of 420 km/sec, which is the 13.5 Gm (solar) radial depth of the propagation path divided by the 9 hour length of the pulse.

Wolfe has suggested that these pulses have an Archimedian spiral shape, caused by sources of plasma streams rotating with the sun (like a rotating sprinkler). The spiral angle is obtained from Fig. 5-18.

$$\tan \alpha = \frac{\Delta r}{r\Delta\theta} = \frac{(300 \text{ km/sec})}{(150 \text{ Gm})(2.7 \ \mu\text{rad/sec})}$$

$$\alpha = 36.5^\circ$$

In an Archimedian spiral, the plasma is still flowing radially, but it has a wavefront tilted from the normal to a radial line.

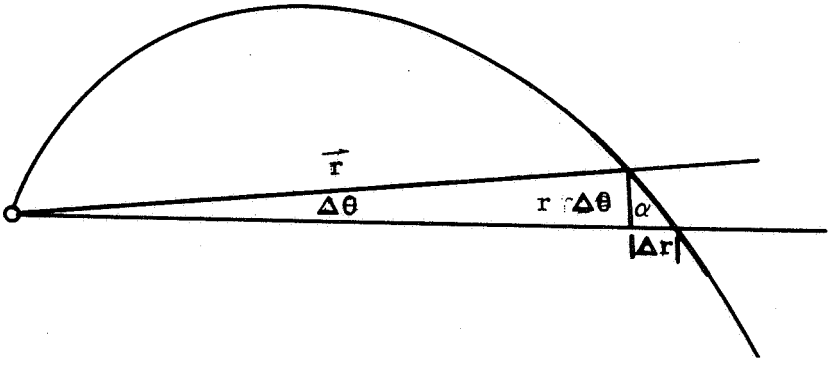

FIG. 5-18. ARCHIMEDIAN SPIRAL ANGLE OF A PLASMA STREAM FROM THE SUN.

The wavefront of the pulse of 10 November might be tilted more toward the propagation path in Fig. 5-15; thus the radial velocity of the plasma could be slower, and the pulse would still cross the propagation path in the 9 hours. If the pulse is traveling at 300 km/sec, a common velocity for dense plasma, the wavefront must be tilted 15° from a wavefront normal to the earth sun line--a tilt much less than the 36°

Archimedian spiral angle. This implies that the source of the pulse is more like a short burst, instead of a continuous stream. The burst generates a pulse with a spherical wavefront, while the continuous source generates an Archimedian spiral. In other words, the source of the pulse on the sun rotates less than the angular dimension of the source.

An element of uncertainty remains on the leading edge of the content pulse in Fig. 5-17. This edge would be steeper than the trailing edge if 11 November had been used as the control day, in which case, the rectangular density pulse model used would no longer fit the data. The uncertainty involved with the control day technique, caused by daily ionospheric variation, is overcome by ATS Faraday measurement of ionospheric content. The ATS method is used in the measurement of the plasma pulse in the next section.

3. Plasma Pulse of 25 January 1967 with Continuous Measurement of the Ionosphere

A technique for continuously monitoring the ionosphere has been in use since the launch of the ATS geostationary satellite, which appears above Stanford's horizon. This technique has been used to subtract the ionospheric content from the Pioneer content for the plasma pulse of 25 January 1967 (Fig. 5-18).

a. Continuous Faraday Rotation Measurement of the Ionospheric Content

The ATS satellite, which has a 137 MHz transmitter, is fixed 37° above the Stanford horizon. The plane of polarization of the linearly polarized 137 MHz transmission is Faraday rotated in the ionosphere, with the amount of rotation Ω proportional to the ionospheric electron content. This is given by

$$\Omega = \frac{K}{f^2} N H \cos\theta \sec\chi \, dh \ (\text{rad}) \qquad (5.3)$$

where

$K = 2.97 \times 10^{-2}$

f = frequency, in Hz

N = electron number density, in el/m^3

H = magnetic field, in A/m

θ = angle between the wave normal and the magnetic field

χ = zenith angle of the ray

$\sec \chi \, dh$ = differential element of path length

An average value can be used for most of the terms under the integral. (See Titheridge, 1966, Fig. 3, p. 1136, for a plot of the typical values for the terms under the integral.) When average values are used, Eq. (5.3) becomes

$$\Omega = \frac{K}{f^2} \overline{H \cos \theta \sec \chi} \int N \, dh$$

The value of the weighted mean $\overline{H \cos \theta \sec \chi}$ is equivalent to the factor under the bar, evaluated at 350 to 400 km height. The exact height chosen is not critical because this factor changes only 1 percent/10 km. The magnetic field falls off as $1/r^3$, so the content for the higher ionosphere (> 2000 km) contributes little to the integral.

The polarization is measured on the ground in the same way used by Garriott with Syncom III (Garriott et al, 1965). In fact, his equipment is being used. The received polarization is the Faraday rotation angle modulo π, with one Faraday half-turn (π radians) at 137 MHz representing 4.4×10^{16} el/m^2 at Stanford. The total Faraday rotation of about 7 half-turns at midday is determined by keeping track of the rotation starting during the night when the total rotation is usually less than one half-turn. The total Faraday rotation is confirmed with beacon satellite measurements of the ionospheric content.

In addition to the ATS measurements at Stanford, a second ATS receiver station in Ely in eastern Nevada provides ionospheric content measurements 600 km east of Stanford. The ionospheric content at points between the two stations is obtained by linear interpolation of the content between these stations. A study of east-west gradients, made with beacon satellite measurements, show that this interpolation produces errors usually less than 1×10^{16} el/m^2 (Koehler, unpublished). The Stanford and Ely ATS measurements on a given day are quite similar (within 10

percent) provided that the time scale of the data measured at one station is shifted 30 minutes to account for the difference in solar time between the stations. This means that data from one station can be used by shifting the time scale of the ionospheric content so that the solar time of the ATS subionospheric point matches the solar time of the Pioneer subionospheric point.

Ionospheric electron contents measured at the Stanford and Ely stations were combined to make the ionospheric electron content curves at the bottom of Fig. 5-19; the content from the stations was then subtracted from the Pioneer electron content to give the pulse of interplanetary electron content shown in Fig. 5-20.

b. Interplanetary Pulse of 25 January 1967

The huge pulse (the largest observed in this experiment) shown in Fig. 5-20 rises from 65×10^{16} el/m^2 at 0200 to 175×10^{16} el/m^2 in only 4 hours. The end of the pulse appears the following day between 2000 and 2200. The leading edge of the electron content pulse shows a precursor before the steep rise at 0200 of the main pulse, then a plateau, followed by a second increase, but not as steep as initially. Clearly, this event is a split pulse with a gap of 1.3 hours.

To obtain a first order estimate of the density pulse, the leading edge of the change in content (ignoring the background content) can be approximated by a linear increase of 110×10^{16} el/m^2, running from 0200 to 0600.

Then the interplanetary electron content curve of 25 January 1967 can be explained by a rectangular pulse similar to the other pulses. It is caused by a rectangular density pulse with a spherical wavefront, traveling radially from the sun. In the ecliptic plane, it looks like the circular band shown in Fig. 5-21. The pulse begins to cross the earth end of the propagation path at 0200 (ignoring the precursor) until the trailing edge reaches earth at 0600, at which time the pulse is totally within the propagation path. This position is shown in Fig. 5-21 at 0600, when the electron content reached its peak at 175×10^{16} el/m^2.

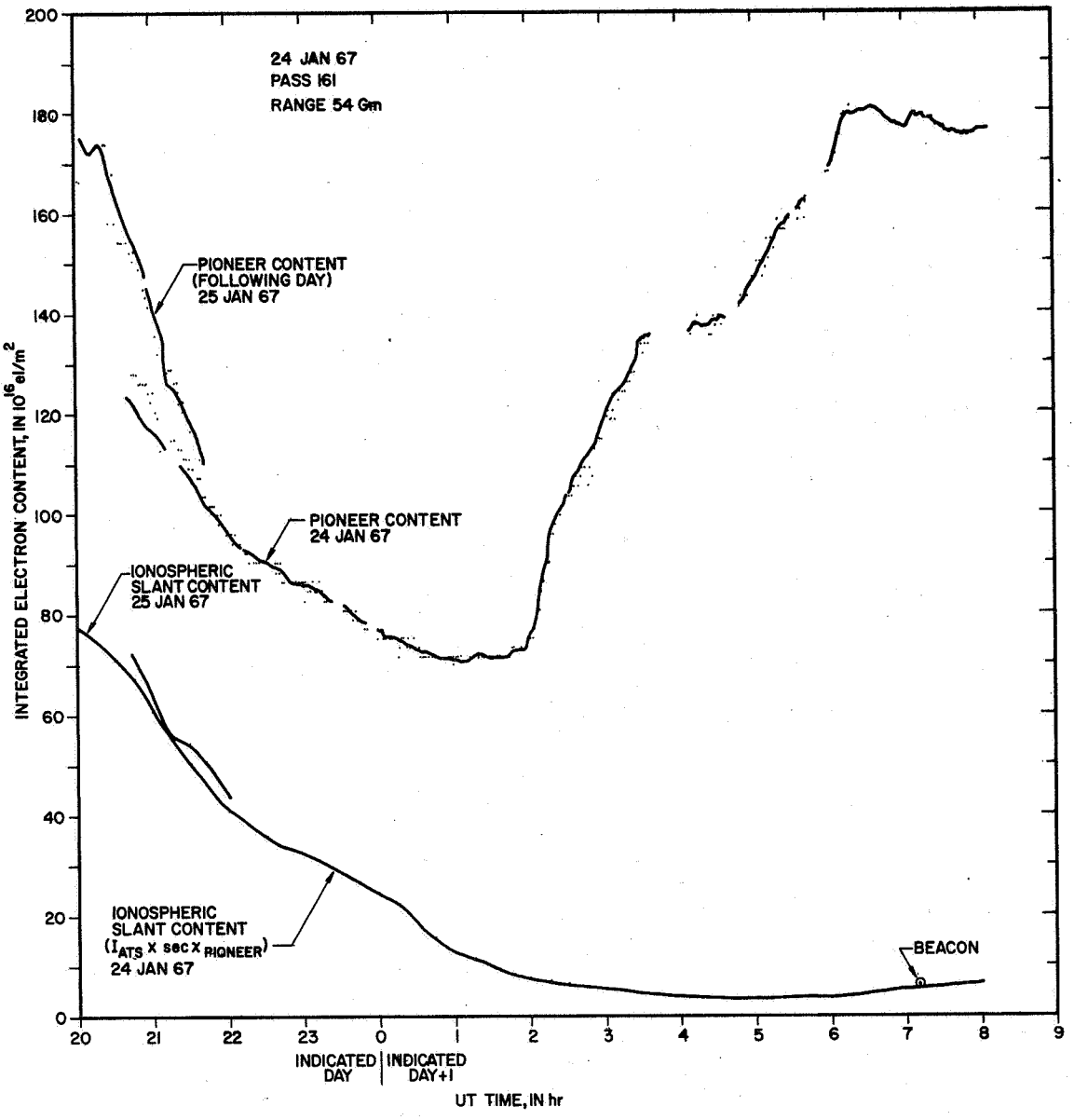

FIG. 5-19. THE PULSE OF PIONEER ELECTRON CONTENT (INCLUDING THE IONOSPHERIC CONTENT) ON 25 JANUARY 1967. The pulse starts at 0200 and ends during the next pass at 2200 (left-hand side of plot). The ATS Faraday rotation measurements of the ionospheric content, projected along the Pioneer propagation path, is shown by the lower curve.

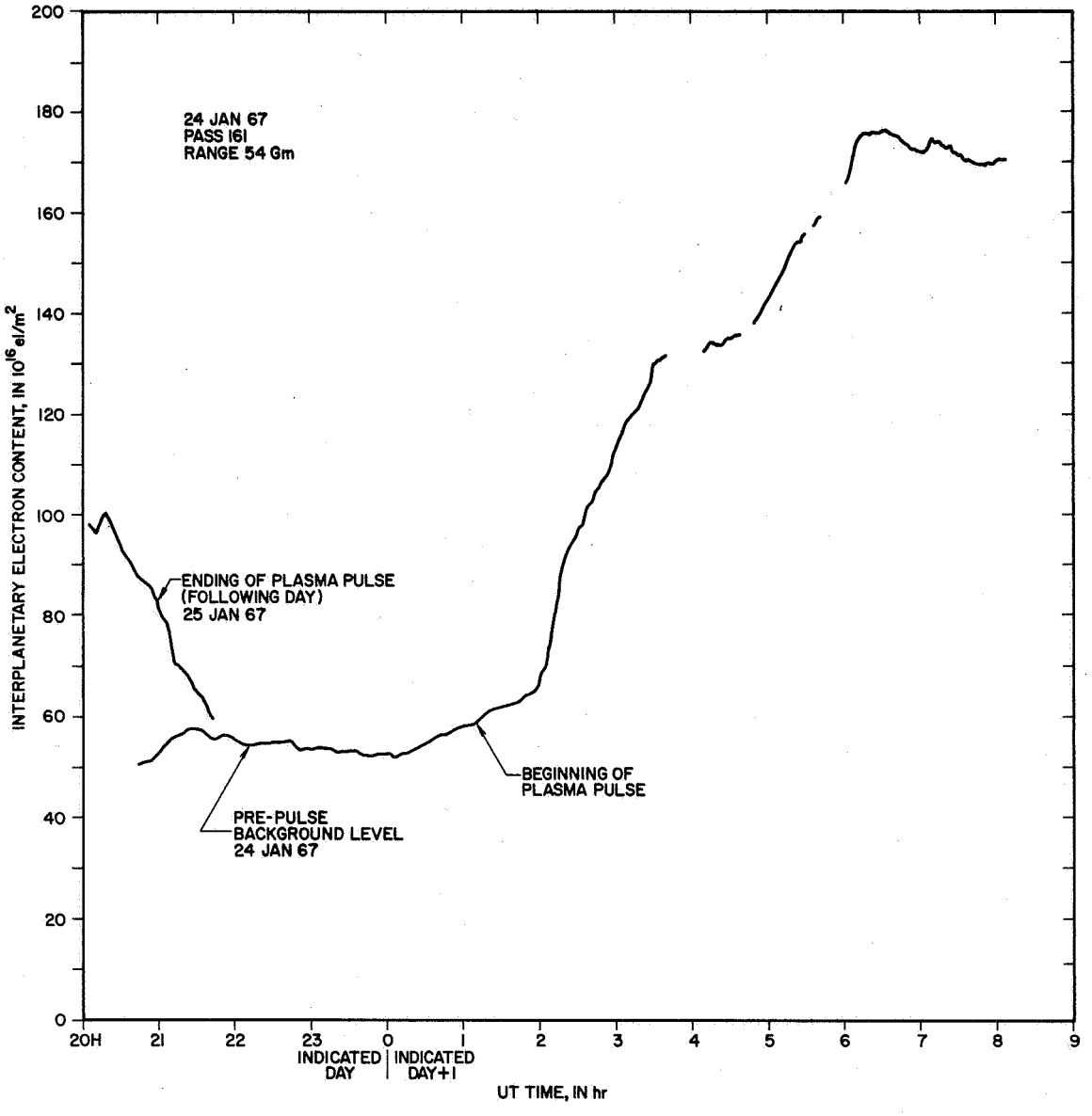

FIG. 5-20. THE INTERPLANETARY ELECTRON CONTENT PULSE OF 25 JANUARY 1967, BEGINNING AT 0200 AND ENDING DURING THE NEXT PASS AT 2200 (LEFT-HAND SIDE OF GRAPH).

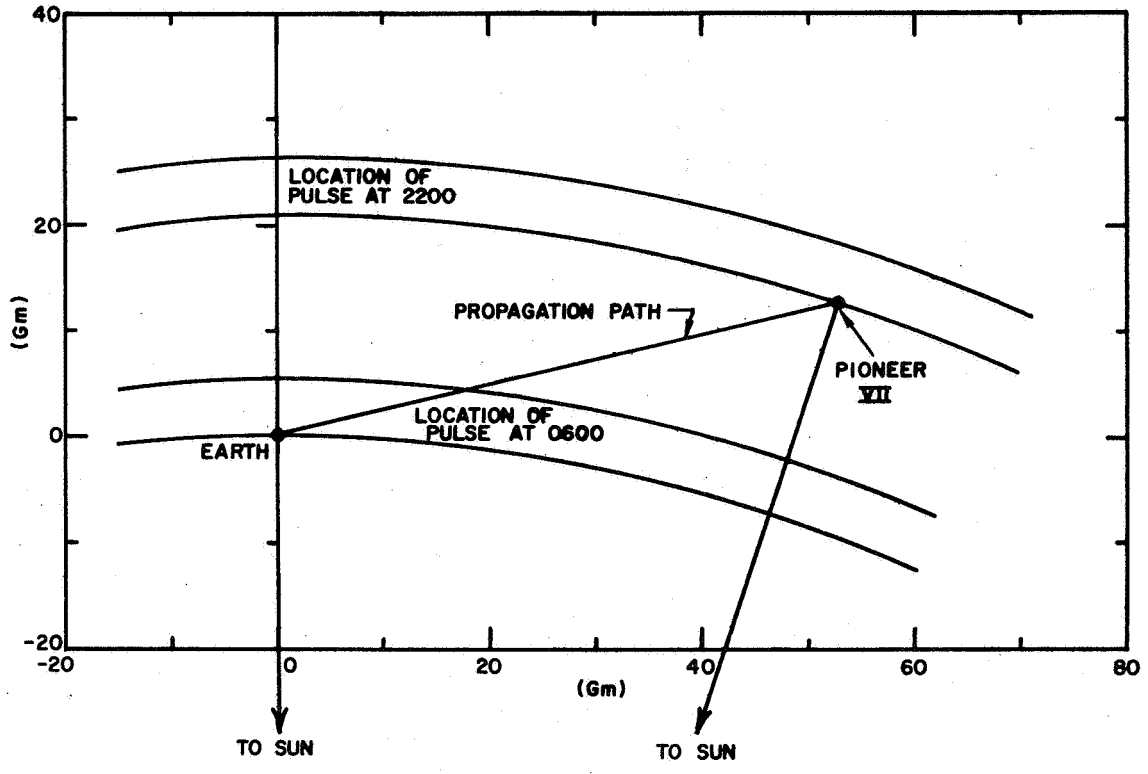

FIG. 5-21. THE DENSITY PULSE OF 25 JANUARY 1967. The location of the spherical shaped pulse at 0600 and at 2200 is shown in the ecliptic plane, relative to the earth-Pioneer propagation path. The pulse is traveling radially from the sun.

The pulse travels outward until the trailing edge crosses the spacecraft end of the propagation path at 2200 (this position is shown in Fig. 5-21), at which time the pulse has just left the propagation path and the electron content has returned to the pre-pulse level of 55×10^{16} el/m^2. The parameters of this pulse are derived from the interplanetary electron content curve (Fig. 5-20).

The transit time of the pulse across the propagation path is the time the trailing edge crosses the earth (0600) to the time it crosses the spacecraft (2200), a period of 16 hours. The pulse velocity in the radial direction is the solar radial distance between earth and the spacecraft, divided by the transit time, which is

$$\text{Pulse velocity} = \frac{20.9 \text{ Gm}}{16 \text{ hr}} = 350 \text{ km/sec}$$

The pulse width is the ratio of the time for the pulse to cross the earth end of the propagation, to the transit time, times the solar radial distance of the spacecraft

$$\text{Pulse width} = \left(\frac{4 \text{ hr}}{16 \text{ hr}}\right)(20.9 \text{ Gm}) = 5.2 \text{ Gm}$$

This is the pulse width shown in Fig. 5-21.

The average pulse density over the background level is the increase in content from 65 to 175 $\times$ 10^{16} el/m^2, divided by the length of the propagation path covered by the pulse, at 0600, which is

$$\text{Density} = \frac{110 \times 10^{16} \text{ el/m}^2}{19.5 \text{ Gm}} = 56 \text{ el/cc}$$

Thus this pulse is a spherical pulse 5.2 Gm thick, with an average density of 56 el/cc, traveling radially outward from the sun at 350 km/sec.

The missing part of the electron content curve (0800 to 2000) can be filled in from the geometry in Fig. 5-21. As the pulse travels outward, the propagation path becomes progressively less oblique, so that the fraction of the path covered by the pulse steadily decreases. In addition, the density decreases because of the $1/r^2$ expansion. Both of these effects reduce the electron content as the pulse progresses outward, as shown in the reconstructed electron content curve in Fig. 5-22.

It is expected that the plasma data from the ARC plasma probe on Pioneer VII and the plasma data from Anchored IMP at the earth end of the propagation path will confirm this description of this event.

D. Summary and Areas for Further Study

1. Summary

Interplanetary electron content measurements have successfully been made, and the average interplanetary electron number density has been computed from the total of 300 interplanetary content measurements. The

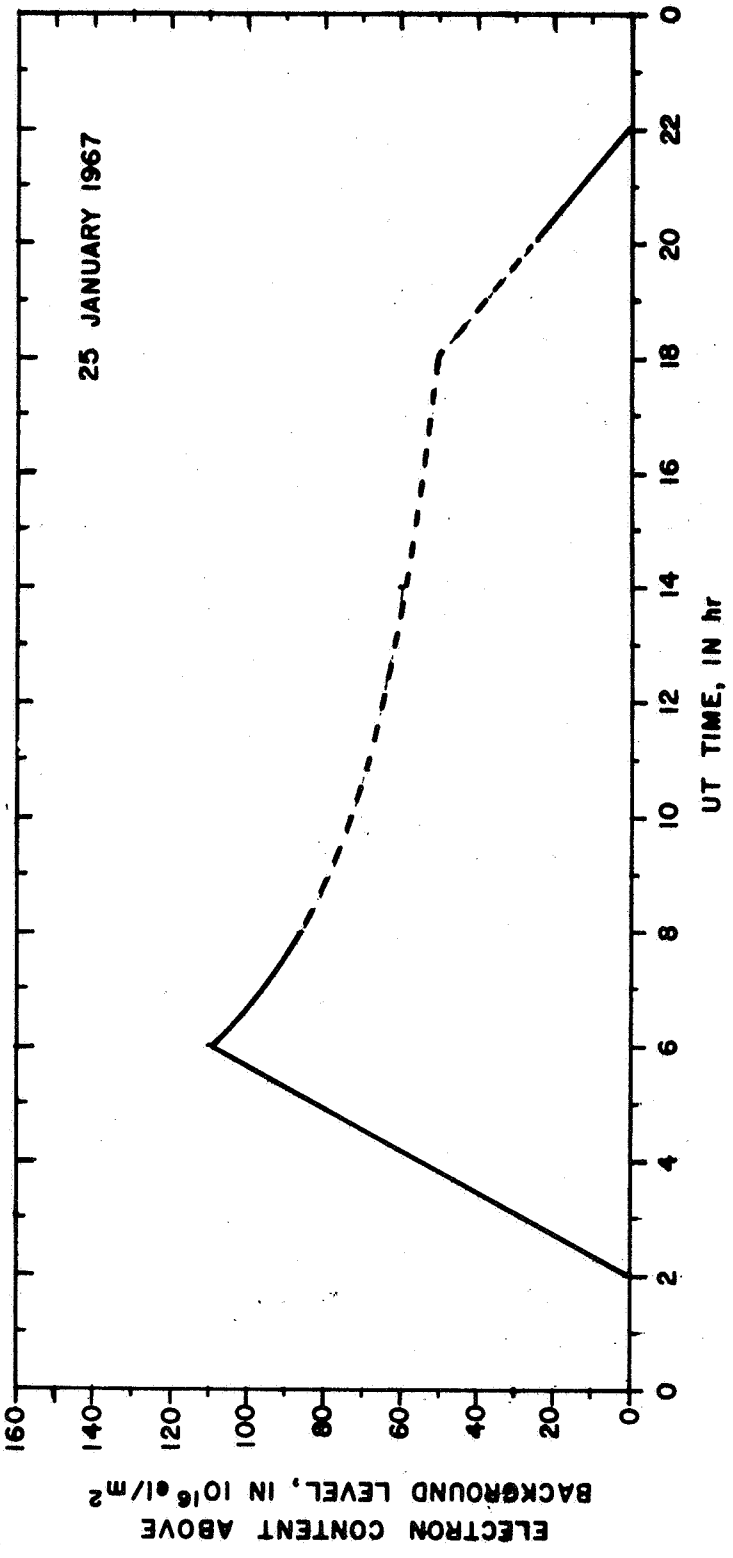

FIG. 5-22. THE RECONSTRUCTED ELECTRON CONTENT CURVE FOR 25 JANUARY 1967. The dashed portion of the curve, which occurred when Pioneer was not visible from Stanford, was deduced from the geometry of Fig. 5-21.

average density at 1 AU, measured from December 1965 through May 1966, was 4.3 ± 3.6 el/cc. Later, from August 1966 to March 1967, when the solar activity was higher, the average density was 8.7 ± 4.0 el/cc.

Several large increases in electron content of 30 to 110 $\times 10^{16}$ el/m^2, which were caused by dense plasma pulses traveling out from the sun, were detected. These pulses can be explained by a common type of model--a rectangular pulse increase of density, with a spherical wavefront traveling radially from the sun. The pulse velocity ranges from 300 to 400 km/sec which is near the minimum solar wind velocity (300 km/sec). The pulse is 5 to 10 Gm thick and has a density (over a background level) of 30 to 55 el/cc.

The Pioneer electron content measured between the earth and the Pioneer deep space probe includes the ionosphere. The interplanetary content was obtained by means of the first order improvement on the Pioneer data by subtracting the ionospheric content measured from beacon satellite signals at individual points in time.

Continuous measurement of the interplanetary content marked the second order improvement on Pioneer data obtained by subtracting a continuous record of the ionospheric content from the Pioneer content. The ionospheric content was continuously determined from the measurement of Faraday rotation of the signals from the ATS geostationary satellite.

2. Areas for Further Study

Interplanetary electron content measurements are continuing with Pioneer VII, with two additional Pioneer spacecraft scheduled to be launched. Measurements will also be made with Mariner on a voyage to Venus. Improvements can be made in the analysis of the data already obtained and in the measurement and analysis of all the data that will be obtained.

These improvements are:

a. Plasma density and velocity data at the spacecraft from ARC's plasma probe on Pioneer and at the earth end of the propagation path from MIT's plasma probe on Anchored IMP can be combined with electron content measurements to determine more accurately the structure of the interplanetary plasma.

b. Greater attention should be given the rate of change of content, since this quantity is closely associated with the nature of data from the plasma probe measurements.

c. The electron content could be measured out to a range of 2 AU if the 50 MHz noise generated by Pioneer spacecraft (scheduled to be launched) were reduced, and the loop bandwidth of the receiver and audio phase lock loops were narrowed. When the spacecraft reached a range of 2 AU, it would begin to return, and the electron content measurements could be continued until the spacecraft failed.

d. The second order effects of the ionosphere on the Pioneer data could be reduced by changing the 49.8 MHz polarization, and by corrections in the Pioneer-ATS data reduction (see Appendix A). An additional ATS station would further reduce the effects of spatial variations in the ionosphere.

APPENDIX A

SECOND ORDER EFFECTS ON GROUP AND PHASE PATH

1. Problem: Divergence between Group Path and Phase Path Determination of Electron Content

On many of the daily plots the phase path determination of electron content diverges below the group path determination. An example is shown in Fig. A-1. On Pioneer VI, this divergence was thought to be due to a

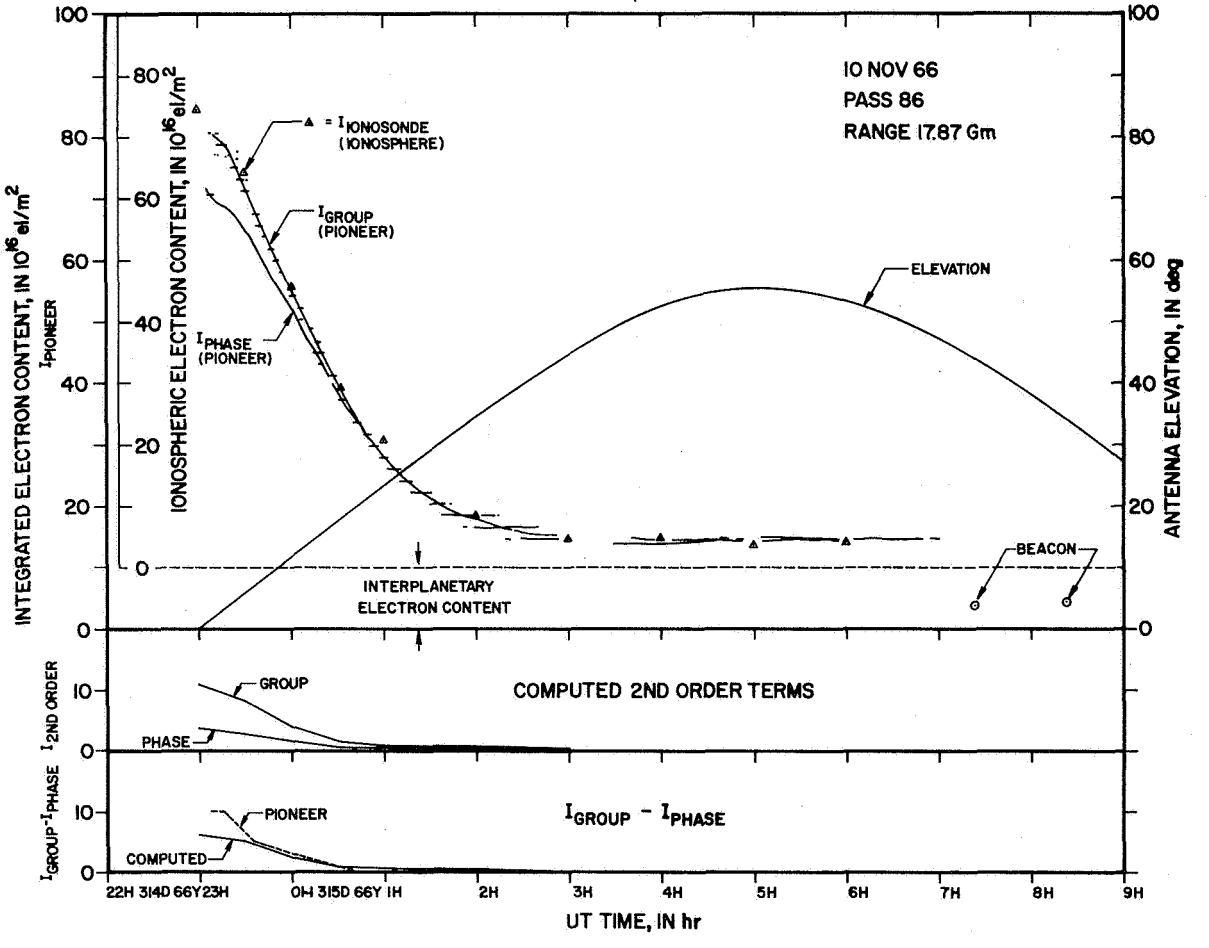

FIG. A-1. UPPER PLOT: PIONEER ELECTRON CONTENT MEASUREMENTS ON A DAY WHEN THE PHASE PATH CONTENT DIVERGED BELOW THE GROUP PATH CONTENT. Middle plot: The computed second order component of the group path content and the phase path content. Lower plot: The difference between the computed second order group path content and phase path content, compared with the difference between the Pioneer group path and phase content.

small error in the calibration of our spacecraft receiver modulation phase meter. The phase path calibration was unquestioned, because the phase path is measured by counting cycles of RF phase, and there is no calibration involved in counting. When this divergence also appeared with our second spacecraft, Pioneer VII, we suspected that the group path calibration was correct and that the cause of the divergence lay elsewhere. The validity of the group path calibration was confirmed when a huge pulse of interplanetary electrons crossed the propagation path, and the electron content increased by 60×10^{16} el/m^2, with no divergence between the group and phase paths, as shown in Fig. 5-18. This huge pulse has a total height of 110×10^{16} el/m^2, but an interruption in the middle of the pulse for 30 minutes prevented the comparison of the group and phase path over more than half the pulse's height.

We had used only the first order terms in Eqs. (A.1) and (A.3) in our conversion of Pioneer group and phase path data to electron content. The neglected second order terms in this conversion are important where the electron number density is large, which is the case in the ionosphere during the day. The second order group and phase path through the ionosphere were calculated on a day when this divergence occurred (Fig. A-1) and the divergence was found to be caused by the second order terms.

2. Second Order Group and Phase Path Theory

The second order approximation to the group path and phase path was calculated for a ray passing through a plane-stratified ionosphere; the ionosphere is tilted to be parallel to the earth at the point where the ray path intersects the densest part of the ionosphere (Ross, 1965). The approximation included ray bending. For a ray path extending far from the earth, the second order equation for the incremental phase path ΔP is

$$\Delta P = \Delta P_o \left[1 \mp |Y_L| + \frac{1}{4} \beta \bar{X} + \frac{1}{4} \beta \bar{X} \tan^2 \chi \right] \qquad (A.1)$$

1st order

magnetic field term (2nd order)

2nd order term due to non-linearity

2nd order term due to bending

where ΔP_o = the first order incremental phase path

$$\Delta P_o = \frac{1}{2} h \bar{X} \sec \chi \qquad (A.2)$$

χ = the ray zenith angle at the ionospheric point

$h \bar{X}$ = X averaged over the height h, times the height

$$= \frac{80.6}{f^2} \int_0^h N \, dh$$

N = electron number density as a function of height, in electrons/m^3

f = frequency of the ray, in Hz

The second order incremental group path $\Delta P'$ is

$$\Delta P' = \Delta P_o \left[1 \mp 2 |Y_L| + \frac{3}{4} \beta \bar{X} + \frac{3}{4} \beta \bar{X} \tan^2 \chi \right] \qquad (A.3)$$

1st order

magnetic field term (2nd order)

2nd order term due to nonlinearity

2nd order term due to bending

The source of the second order group path terms is the same as for the phase path, but the second order group path terms are a factor of 2 or 3 times larger than those for the phase path. It is this factor of 2 or 3 that causes the first order analysis of electron content from the phase path and group path to diverge, as they do in Fig. A-1.

The density distribution factor β is combined with X for a ray path far beyond the earth's ionosphere to give

$$\beta \bar{X} = \frac{\overline{X^2}}{\bar{X}} = \frac{80.6}{f^2} \frac{\int N^2 \, dh}{\int N \, dh} \qquad (A.4)$$

Equation (A.4) for $\beta \bar{X}$ evaluated at 50 MHz over the density distribution of Fig. A-2 is

$$\beta \bar{X} = \left(\frac{80.6}{f^2}\right)(0.7\ N_{max}) = 2.26 \times 10^{-14}\ N_{max} \qquad (A.5)$$

where N_{max} = maximum electron number density in the ionosphere.

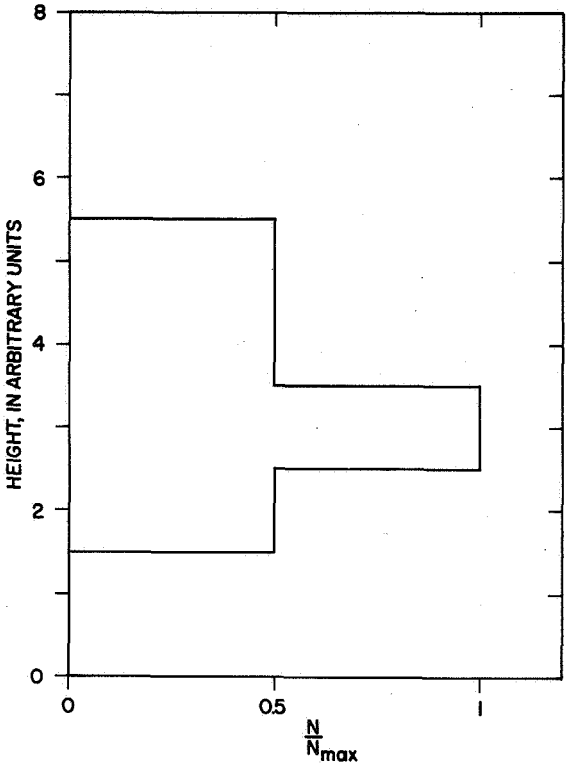

FIG. A-2. MODEL IONOSPHERIC DENSITY DISTRIBUTION USED TO CALCULATE β.

3. The Ionospheric Portion of the Pioneer Plot

The beacon measurement of the ionosphere at 0725 establishes the interplanetary electron content, i.e., the difference between the Pioneer curve and the beacon point, at 10×10^{16} el/m^2. A line, which is drawn at 10×10^{16} el/m^2 to represent the interplanetary content (assumed constant), forms the base line for the ionospheric content.

4. The Ionospheric Model Used To Compute the Second Order Effects

We need the ionosphere for the day of the plot in Fig. A-1 in order to compute the second order effects. The ordinary wave penetration frequency f_o is read from Stanford ionosonde records to determine N_{max} through the equation

$$f_o^2 = 80.6\ N_{max}$$

The N_{max} data are shifted in time to correspond to the solar time (local mean time) at the Pioneer subionospheric point. The slant ionospheric content I_{slant} along Pioneer's ray path through a slab ionosphere is

$$I_{slant} = I_{vert} \sec \chi = N_{max}\ T \sec \chi$$

I_{slant} for a 300 km slab thickness and the time shifted N_{max} from the ionosonde is plotted with Δ's in Fig. A-1, with the interplanetary content line used as a base line. The good fit of I_{slant} to the ionospheric part of the Pioneer plot shows that I_{slant} and N_{max} are good enough to be used to calculate the second order effects.

5. Computed and Measured Differences between Group and Phase Path

Equation (A.1) shows that the incremental phase path length is longer by the amount of the second order factors than that determined from the first order theory. If the electron content I is calculated from the measured phase path, by using the first order theory, the content will be too great by the amount of the second order factors. Similarly, the electron content determined from the group measurements will be too great by the amount of the second order factors in Eq. (A.3), a factor approximately 3 times larger than for the phase path. The amount that the electron content is too great, computed from the second order factors, is plotted in the middle graph of Fig. A-1. It can be seen that the content determined from the phase path diverges below the content determined from the group path, just as the Pioneer group path and phase path content do in the upper plot.

The difference between the computed second order terms of the group path content and of the phase path content is plotted in the bottom graph of Fig. A-1. This difference is compared with the difference between the measured Pioneer group path and phase path determination of electron content. The computed difference is almost equal to the measured difference above 6° antenna elevation, which shows that the divergence between the Pioneer group path and phase path determinations of electron content is caused by second order effects neglected in the analysis of Pioneer data.

6. Discussion

The technique that can be used to compensate for the second order effects depends on the time of day and the antenna elevation angle. The size of error and the method for correction are listed below in order of increasing difficulty.

a. Nighttime, with any elevation. The ionosphere is so thin (on the order of 5×10^{16} el/m^2) that the second order terms are negligible.

b. Daytime, with elevation above 30°. Right-hand circular polarization should be used in order to propagate the ordinary wave (upper sign) on 49.8 MHz, instead of the currently used left-hand circular (or eliptical), which propagates the extraordinary wave (lower sign). Then the magnetic field term Y_L in Eqs. (A.1) and (A.3) would have the upper sign (minus) and would tend to cancel the other second order terms. This change would reduce the second order errors from about 7 percent to about 1 percent of the ionospheric content. For example, the error would be reduced from 2 to 0.3×10^{16} el/m^2 for a daytime ionospheric content of 30×10^{16} el/m^2.

c. Daytime, with elevation between 10° and 30°. The second order corrections would have to be computed in this region. Changing polarization does little to cancel the much larger second order bending term in Eqs. (A.1) and (A.3). The $\tan^2 \chi$ factor, ranging from 6 at 10° elevation to 2 at 30° elevation, makes the bending term dominate the other second order terms.

The corrections can be calculated from the ATS determination of ionospheric electron content. The shape factor β, used in these corrections, can be estimated from the ionospheric content combined with N_{max} determined from ionograms. Time or spatial shift in the ionospheric data must be incorporated so that the solar time of the ionospheric data and the solar time of the Pioneer subionospheric point correspond. The validity of the second order factors can be checked in the same way as in the bottom graph of Fig. A-1.

d. Daytime, with elevation less than 10°. The second order theory presented here is evidently inadequate in this region. Ross suggests the use of a spherically stratified ionosphere as the next level of improvement.

APPENDIX B

IN-FLIGHT MODULATION PHASE METER CALIBRATION

The receiver modulation phase meter aboard the spacecraft is periodically calibrated from the ground. The calibration procedure begins by stepping the modulation phase at the transmitter every 20° (sometimes 30°) through 360°. The receiver modulation phase meter output is plotted versus time (Fig. B-1) from a Pioneer data tape. Each step in the phase meter output is identified with the transmitter modulation phase setting that caused it. First the transmitter modulation phase is written along the time axis. Then a line, with a 1.5 minute offset to correct for earth-spacecraft propagation time, connects the modulation phase setting with its corresponding step in the phase meter output.

The phase meter output versus modulation phase data from Fig. B-1 is plotted in Fig. B-2. The calibration procedure above establishes the

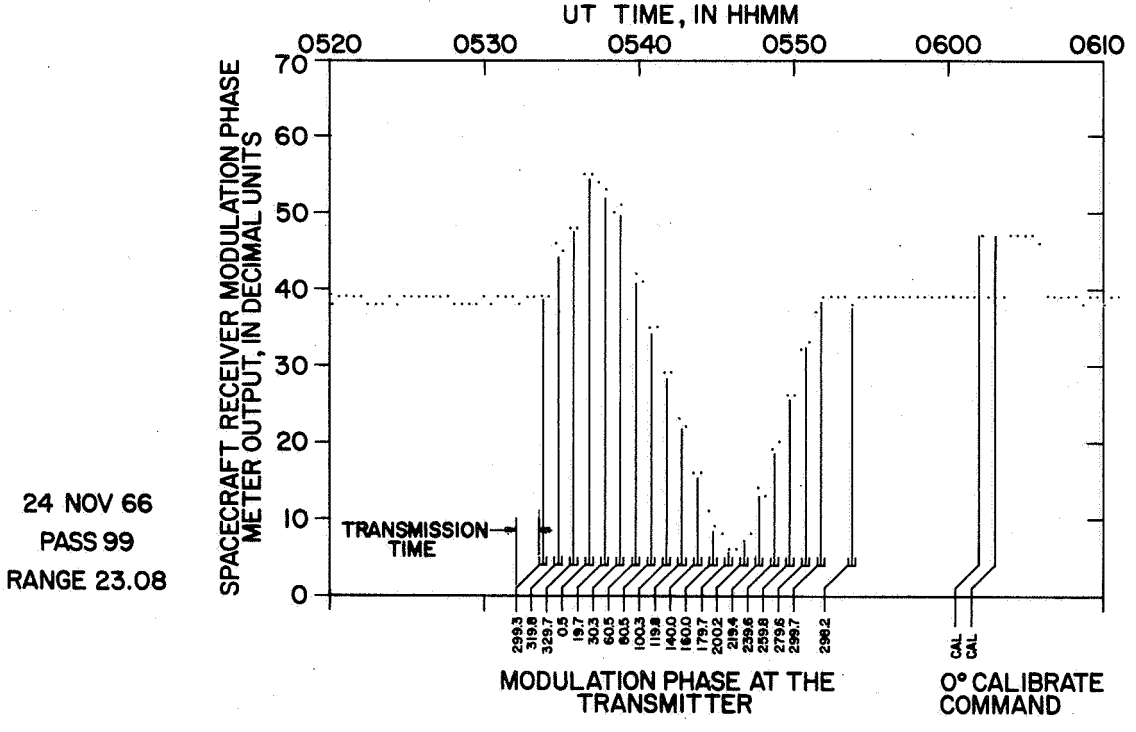

FIG. B-1. SPACECRAFT RECEIVER MODULATION PHASE METER OUTPUT VERSUS TIME. The settings of the transmitter modulation phase are indicated along the time axis. The zero phase calibration command is marked CAL.

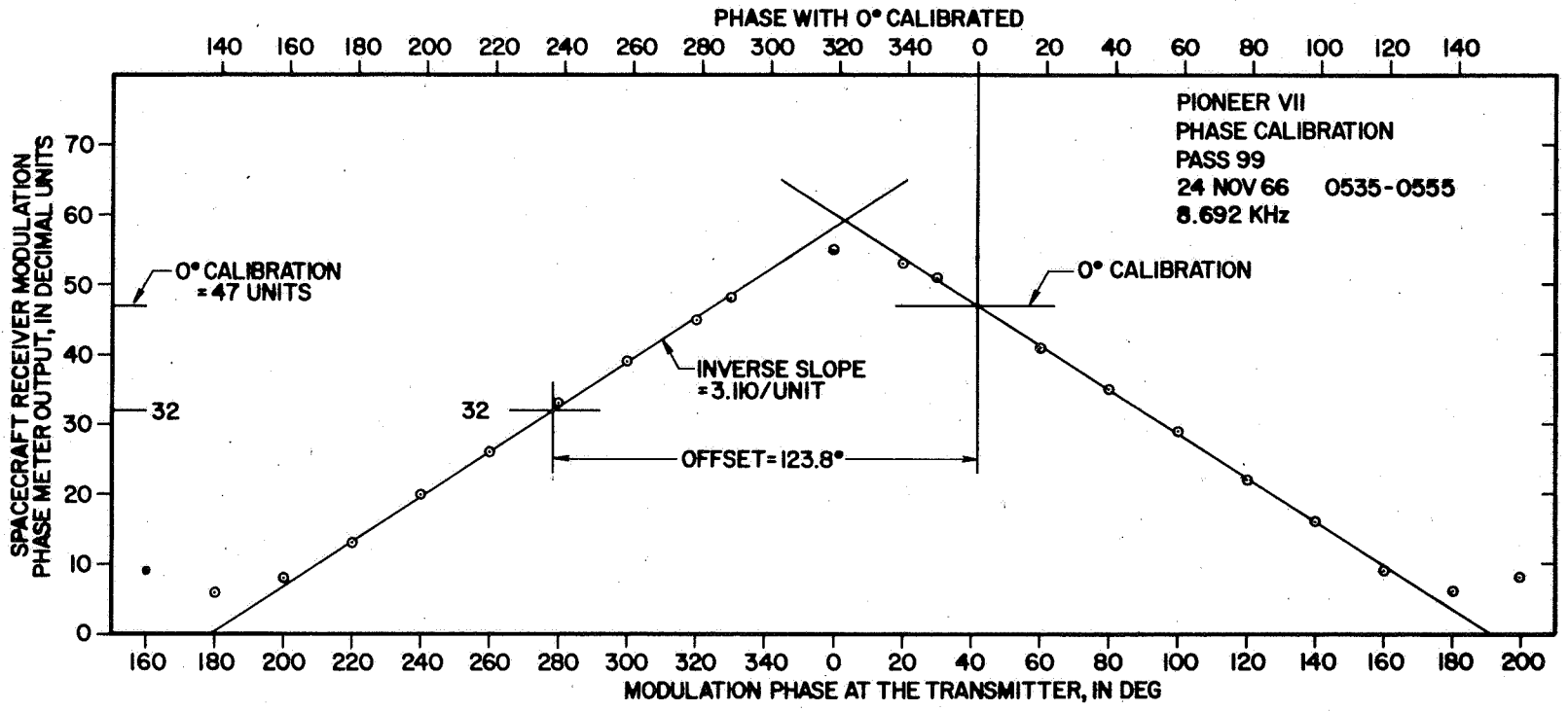

FIG. B-2. PHASE METER OUTPUT VERSUS TRANSMITTER MODULATION PHASE (LOWER SCALE) AND 0° CORRECTED MODULATION PHASE (UPPER SCALE).

shape of the phase meter curve. However, the electron content between the ground transmitter and the spacecraft causes a shift in the modulation phase. A calibration command sent to the spacecraft establishes 0° phase input at the receiver; the resulting phase meter output is 47, and is located on the negative slope of the 8.692 kHz modulation frequency. (The phase meter output is on the positive slope for 0° modulation phase input for 7.692 kHz, as shown in Fig. 4-9.) The modulation phase scale is shifted horizontally to match 0° with the 47 on the phase meter output to obtain the 0° corrected modulation phase scale at the top of Fig.B-2.

. Two parameters are scaled from the calibration in Fig. B-2 to be used in scaling Pioneer group path data: (1) offset--the phase between the center of the phase meter output (32) on the positive slope, and the 0° phase calibrate point, in deg, and (2) phase step--a line is fitted to the center 2/3 of the positive slope, and the inverse slope of this line is the phase step, in deg/unit. The use of the offset minimizes the effect of an error in slope or a change in slope, since the phase meter is kept near center scale.

In plotting Fig. B-2 from the data of Fig. B-1, we assumed that the electron content is constant for the duration of the measurement. This assumption is no longer true at the slower bit rates, where the group path (phase meter) sampling rate is so slow that changes in electron content can occur during the several hours required for a calibration. The changes in electron content can be determined from the phase path measurement, or by returning the modulation phase back to some reference between each phase point, and used to cancel the changes which occurred during the calibration.

The two parameters scaled from the calibration in Fig. B-2 are used in the following equations, which convert the phase meter measurements to electron content.

$$I = k \, \Delta\phi \qquad (3.13)$$

$$\Delta\phi = -(\text{phase meter output} - 32)\ (\text{phase step}) + \text{offset}$$

$$+ \text{Xmit phase (in } \pm \text{ deg)}$$

where

$$k = \begin{cases} 0.599 \times 10^{16} \text{ el/m}^2\text{-deg (for 8.692 kHz)} \\ 0.677 \times 10^{16} \text{ el/m}^2\text{-deg (for 7.692 kHz)} \end{cases}$$

Xmit phase = modulation phase introduced at the transmitter exciter. The number of cycles of modulation phase are added to the Xmit phase as multiples of 360°.

APPENDIX C

OTHER PIONEER DATA PRESENTED ON THE COMPUTER PLOT

A typical computer plot is shown in Fig. C-1. The electron content curves on the bottom half of the plot have been explained in Chapter V. The two remaining quantities presented here are the "rate of change" of electron content, and the "amplitude" of the 49.8 and 423.3 MHz carriers.

1. Rate of Change of Integrated Electron Content

The middle plot in Fig. C-1 is the time differentiation of the phase path electron content. The differentiation is actually the change of electron content in one minute, and has a quantization level given by

$$\frac{3.755 \times 10^{14} \text{ el/m}^2\text{/RF cycle}}{60 \text{ sec}} = 0.63 \times 10^{13} \text{ el/m}^2\text{/sec}$$

The plotting program has a plot protection feature that not only prevents the curve from continuing off scale, but continues the curve beginning from the opposite end of the scale, and plotting a small x to indicate that the point is off scale.

2. Carrier Amplitude

a. The Amplitude Plot

The carrier amplitudes are plotted in the upper graph of the computer-drawn chart, with the solid line denoting the 49.8 MHz carrier amplitude, and the dotted line indicating the 423.3 MHz carrier amplitude. Plot protection keeps the curve on scale, just as for the rate of change curve, should the signal exceed the scale limits of -20 to +10 dB. Whenever there is no signal at the receiver, the curve goes off the bottom of the scale and reappears near the top as a straight line of x's (49.8 MHz) or dots (423.3 MHz).

Zero dB on the amplitude scale is unity signal-to-noise ratio in the 45 kHz noise bandwidth IF amplifier. While the limiter action of the receiver causes the "carrier amplitude" actually to be signal-to-noise ratio, it is proportional to the signal level if the noise is constant.

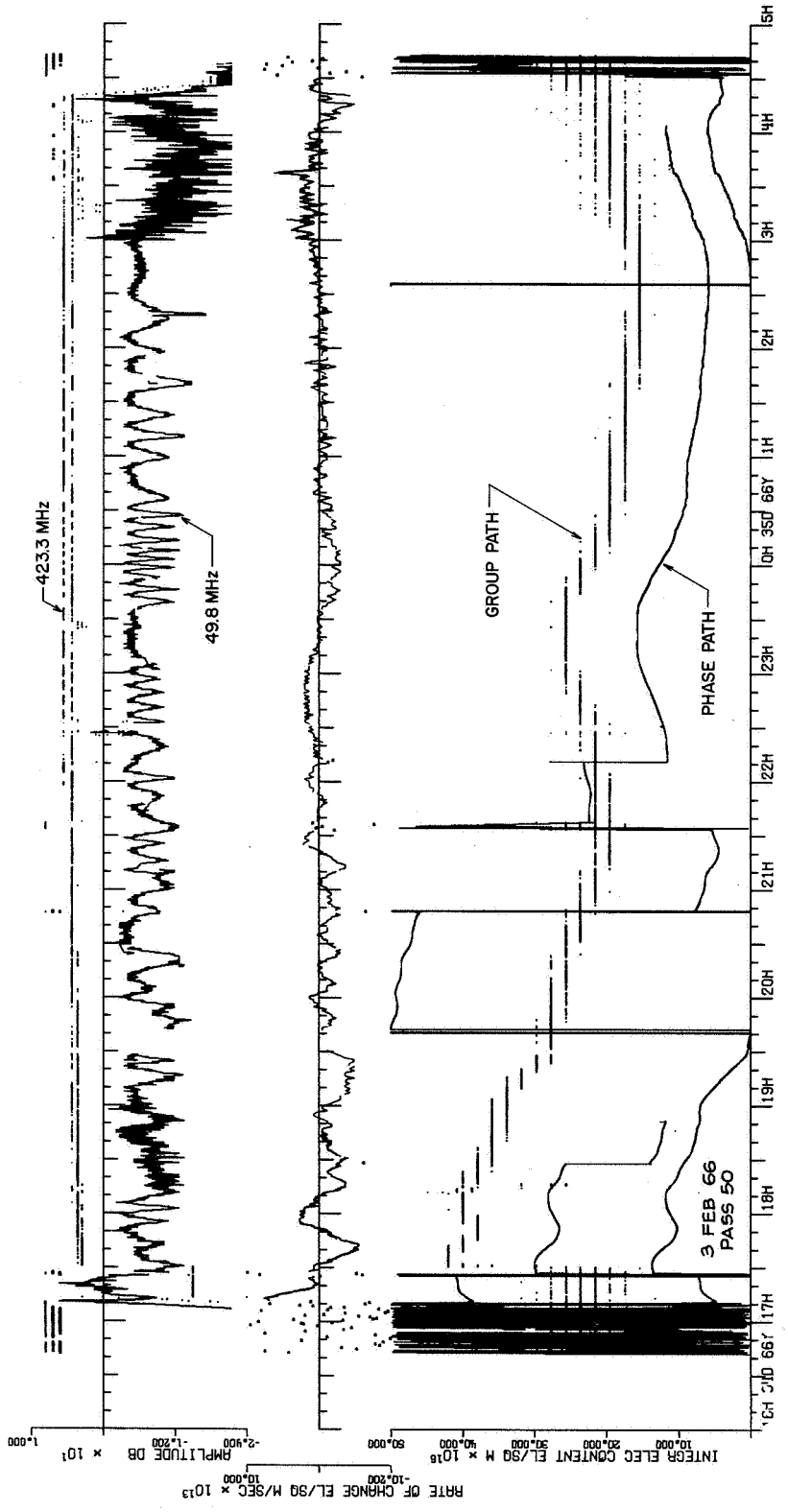

FIG. C-1. EXAMPLE OF A COMPUTER DRAWN CHART OF PIONEER DATA FOR ONE DAY. The horizontal axis is UT time, in hours.

(See Jaffe and Rechtin, 1955, pp. 68-69, for an explanation of the limiter action.) This amplitude is the output of the "amplitude phase detector" in Fig. 4-14, and is filtered by a 0.3 Hz low-pass filter, prior to being sampled for telemetry (see Table 4-3 for the sample interval).

b. Faraday Fading in the 49.8 MHz Amplitude Plot

The rectified sine wave pattern with a changing period, apparent in the 49.8 MHz plot in Fig. C-1, is Faraday fading. The fading rate ranges from 1 per 5 minutes to 1 per 6 hours.

Charts for two days which had particularly clear Faraday fading were chosen to see if the fading could be used for a measure of the ionospheric electron content. The range of the Pioneer spacecraft at this time was only 3 Gm, which minimized interplanetary variations in content. The Faraday rotation was calculated from the Pioneer electron content, assuming that all the changes were in the ionosphere. The similarity between the calculated Faraday fading pattern, and the actual fading pattern were striking. The fades in the amplitude were easily identified. However, a reversal in rotation produced the same pattern as a slowdown, making the rotation direction ambiguous. The amplitude pattern in Fig. C-1 at 2320 is a Faraday reversal, and at 0050 is a Faraday slowdown, with no reversal. Without the direction of rotation, it is not possible to tell whether the content is increasing or decreasing.

Other problems associated with the use of the Faraday fading were that many records do not have distinct Faraday fades; and beyond 10 Gm range, the telemetry falls to 64 bps, which gives us an amplitude sample once every 2 minutes, which is insufficient to resolve the faster fades (see the amplitude pattern in Fig. 5-1 for an example).

APPENDIX D

OTHER METHODS CONSIDERED FOR DETERMINING THE IONOSPHERIC ELECTRON CONTENT

1. Bottomside C-2 Ionosonde

A C-2 vertical ionosonde at Stanford makes an ionogram once every 15 minutes, and has produced readable ionograms for about 80 percent of the time for which there are Pioneer data. The limitations in using the ionograms to determine the total ionospheric electron content to be subtracted from Pioneer electron content are evaluated below.

A vertical incidence ionosonde is a radar pointing vertically; it transmits a series of pulses as the carrier frequency slowly sweeps from 1 to 20 MHz. The range of the reflection from the ionosphere (virtual height) is plotted versus frequency to make an ionogram. Above the penetration frequency, the radio wave passes through the ionosphere without reflection.

a. Integrated Bottomside Electron Content

The ionograms (ionosonde records) can be analyzed for the density and integrated content up to the height of the maximum density. See Davies (1965), pp. 124-125, for a short explanation of the analysis technique, or Thomas (1959) for a thorough explanation. Since no radio wave reflections occur from above the height of the maximum density, the electron content can be determined only up to this height, which includes roughly 25 percent of the total content. Small ionogram scaling errors in the region of the maximum density cause large errors in the analyzed electron content. Use of the bottomside electron content alone did not seem very promising to obtain the total ionospheric electron content.

b. Maximum Density and Equivalent Slab Thickness

The maximum density N_{max} is related to the ordinary wave penetration frequency f_o by

$$f_o^2 = 80.6\ N_{max}$$

If the ionosphere always had the same shape, i.e., the same shape density profile versus height, and simply changed density by a scale factor, the electron content would be proportional to the maximum density.

Vertical ionospheric electron content I, determined from beacon satellites, is plotted in Fig. D-1 versus N_{max}, determined from Stanford ionograms. The beacon data at closest approach (with an elevation over 30°) are paired with the nearest (< 8 min away) C-2 data, for the Pioneer VI period from December 1965 through June 1966. The least squares best fit straight line drawn on this plot has a slope T, related to I by

$$I = N_{max} T$$

T is interpreted as the equivalent slab thickness of the ionosphere with a uniform density N_{max}; T has a value of 300 km determined from Fig. D-1.

Electron content deviates up to $\pm 8 \times 10^{16}$ el/m^2 from the line drawn in Fig. D-1. This uncertainty increases to ± 10 to 24×10^{16} el/m^2 when the vertical content is multiplied by sec x (1.2 to 3) to obtain the slant content required for Pioneer. A second order fit was within $\pm 1.5 \times 10^{16}$ el/m^2 of the straight line in Fig. D-1. On an hourly basis these points looked even more scattered.

The thickness $T = I/N_{max}$ for each point is plotted in Fig. D-2, which vividly demonstrates that T is not a function of N_{max}.

The use of the slab thickness to determine the ionospheric content is valuable when the Pioneer electron content is large compared with the uncertainty in slab thickness determined ionospheric content. The Pioneer electron content is largest at large ranges, and the uncertainty in ionospheric electron content is lowest at night--5 to 10 times less than the daytime content. This slab thickness method is very questionable during the day, especially at the shorter Pioneer ranges. In all cases, one must not seek significance in changes smaller than the uncertainties in the ionospheric content.

2. Incoherent Electron Backscatter Ionospheric Density Profile

Another way to obtain the ionospheric electron content is with the incoherent electron backscatter radar which is adjacent to Stanford's

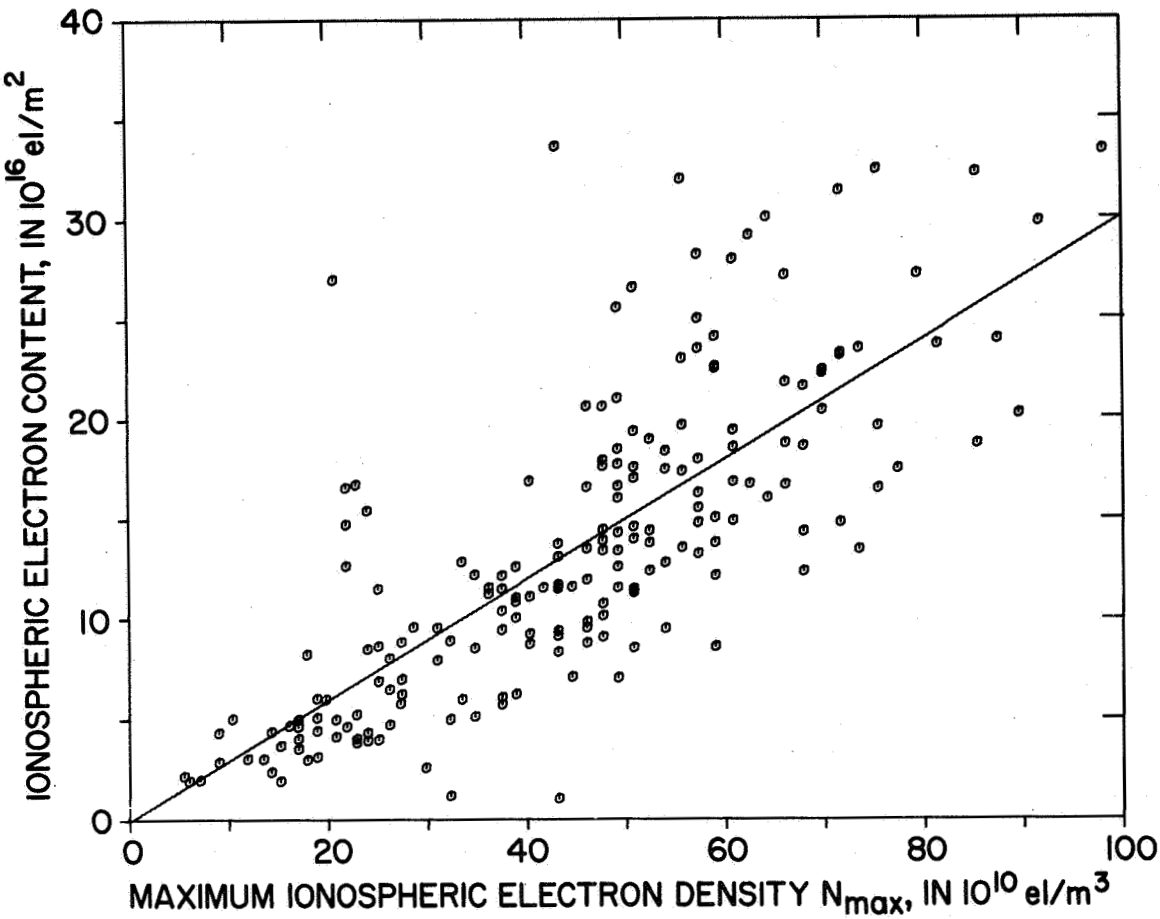

FIG. D-1. BEACON SATELLITE MEASUREMENTS OF IONOSPHERIC ELECTRON CONTENT I VERSUS SIMULTANEOUS MEASUREMENTS OF MAXIMUM IONOSPHERIC ELECTRON DENSITY N_{max} FROM C-2 IONOGRAMS. These measurements were made at Stanford.

Big Dish. Once every 15 minutes this radar can produce a very impressive looking electron density profile from 220 to 1000 km height. The density profile below 220 km, which is obscured by ground clutter, can be determined from a true height analysis of C-3 ionograms. The density profile is integrated to obtain the ionospheric integrated electron content.

The L band (1.3 GHz) radar has 5 MW peak power and 125 kW average power. Its 88 ft diameter dish can be left pointing vertically or it can follow Pioneer across the sky. The power scattered back by the electrons is of a noise-like character, and well below the radar receiver

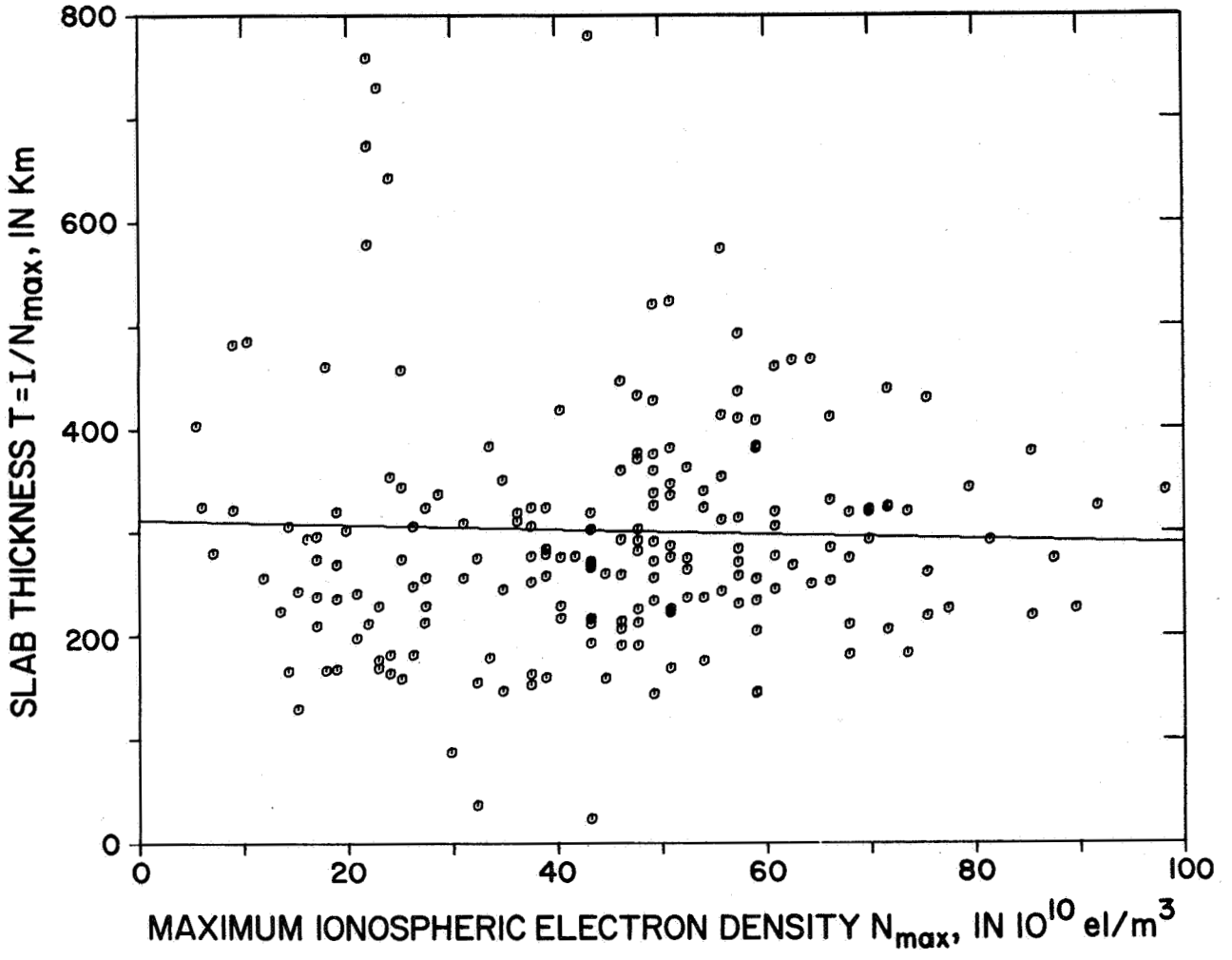

FIG. D-2. SLAB THICKNESS (I/N_{max}) VERSUS N_{max}, FROM THE DATA OF FIG. D-1.

system noise. An on-line SDS 930 digital computer averages 70,000 returns in the 15 minute integration time to bring the signal up out of the noise to produce one ionogram.

a. Experience with the Backscatter Radar

To date, operational difficulties, primarily system noise synchronous with the radar PRF, have made the radar less reliable than other methods for determining electron content.

Comparison of the radar electron content with beacon content gave a scatter of ±20 percent. One day when the radar pointed along

ATS's path and the total content reached 25×10^{16} el/m^2, there was good agreement between the radar and ATS, within $\pm 2 \times 10^{16}$ el/m^2.

b. General Data Reduction

The data first of all require penetration frequencies, read from C-3 bottomside ionograms, to scale the radar ionograms. A true height analysis of the C-3 data is desirable to obtain the lower ionospheric density profile which is obscured by the radar ground clutter. At present, 40 radar ionograms and C-3 true height analyses have to be combined manually for one day's ionosphere, then multiplied by the Pioneer's sec χ, to take care of Pioneer's slant ray path through the ionosphere. These operations should be done by a computer.

c. Basic Limitations

The radar can be programmed to track Pioneer, as does the Big Dish. As the zenith angle increases, the radar range of the ionosphere increases, and the smaller radar return is noisier. The trade-off is between error due to different ray paths, and measurement error due to noise. The smaller nighttime ionosphere gives a much smaller return and hence less accurate results than does the denser daytime ionosphere. Alternatively, the integration time must be longer to bring the smaller nighttime signal up out of the noise.

When compared with ATS, perhaps the most serious limitation of the radar is the 15 minute interval between ionograms. This can be reduced to 5 minutes in the daytime, but the results are noisy.

d. Areas for Improvement

The radar cross-section of the electron is a function of density and temperature. Currently the average electron cross-section at the peak density is implicitly used through the use of C-3 determined peak density to calibrate the radar ionogram. A study is necessary to see if this average is satisfactory for the rest of the ionosphere. If not, the following measures can be taken.

The density dependence of electron cross-section can be taken into account by iteration of the radar return weighted by the density dependence of the electron radar cross-section. The electron temperature can be inferred from the shape of the spectrum of the return. Higher

temperature means higher electron velocity, which increases the doppler spread of the return signal. A Cooley-Tukey spectrum analysis of the returns can be implemented on the SDS computer which is connected to the radar; but new, more flexible analog sampling equipment is necessary, costing $10,000 to $20,000.

e. Uses of the Radar

The radar method is much too complicated (to operate and analyze) and expensive compared with the ATS Faraday rotation method to justify its routine use at the present time. Should ATS fail, the radar should be used.

Pioneer data are nearly worthless without a constant monitor of the ionospheric part of Pioneer's electron content. The ionospheric profile could be used to improve the ATS data analysis and to correct the second order effects of Pioneer's ray path. However, a study should be made of models for second order corrections before using the radar for measuring the profile. Perhaps an approximate model would suffice, since the corrections are second order.

APPENDIX E

INTEGRATED ELECTRON CONTENT WITH $1/r^2$ SOLAR WIND DENSITY DEPENDENCE

The electron number density obtained from dividing the interplanetary electron content by the range (Chapter V.B.2.b.) assumes a uniform solar wind density distribution. Continuity requires the solar wind density to fall off as $1/r^2$, as it flows out from the sun. In this appendix the interplanetary electron number density is computed for a $1/r^2$ density distribution, and normalized to a 1 AU solar range. The electron number density for Pioneer VI is about 25 percent greater for the uniform assumption than for the normalized, $1/r^2$ model; for Pioneer VII, it is about 10 percent less. See Section V.B.2.d.(1).

The electron density with a $1/r^2$ heliocentric density distribution is integrated along the propagation path between the earth and a deep space probe (Fig. E-1) to obtain the integrated electron content I. This equation for I can be solved for the density N_o normalized to 1 AU (or any reference distance) for a given value of electron content.

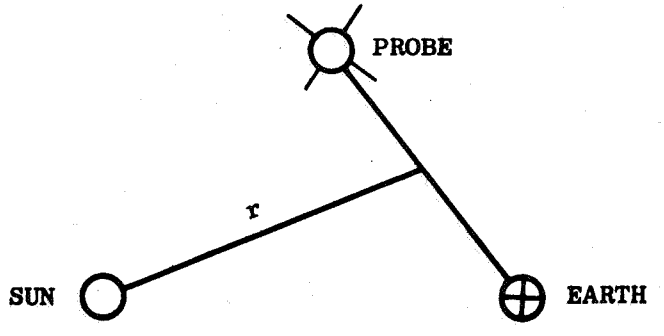

FIG. E-1. PROPAGATION PATH BETWEEN THE EARTH AND A DEEP SPACE PROBE.

The geometry of a line in polar coordinates is shown in Fig. E-2. The equation for a straight line in polar coordinates is

$$r = \frac{b}{\cos \theta}$$

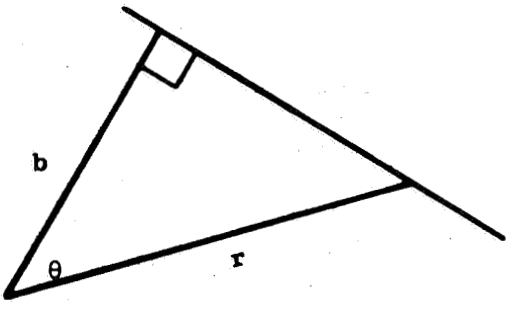

FIG. E-2. GEOMETRY OF A LINE IN POLAR COORDINATES.

Other relations used in this appendix are

$$\frac{\ell}{b} = \tan \theta$$

$$\ell = b \tan \theta$$

$$d\ell = b \sec^2\theta \, d\theta = \frac{b}{\cos^2\theta} \, d\theta$$

The interplanetary density N is

$$N = \frac{N_o}{(r/r_o)^2}$$

where N_o is the density at range r_o.

Figures E-1 and E-2 are combined in Fig. E-3.

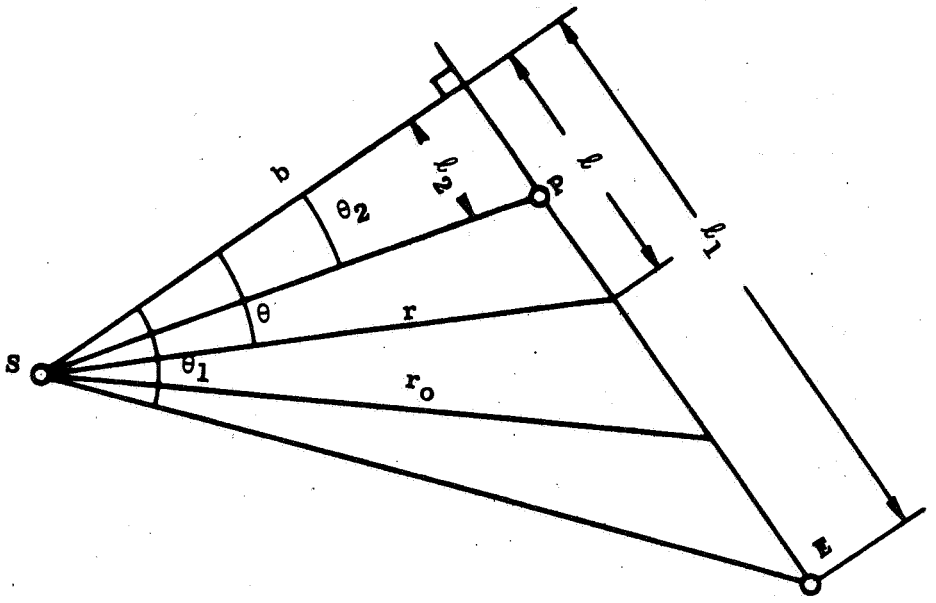

FIG. E-3. GEOMETRY FOR INTEGRATING $1/r^2$ DENSITY ALONG THE PROPAGATION PATH.

The density is integrated between E and P to get the integrated electron number density I.

$$I = \int_{\ell_1}^{\ell_2} N \, d\ell = \int_{\ell_1}^{\ell_2} \frac{N_o}{(r/r_o)^2} \, d\ell$$

$$= \int_{\theta_1}^{\theta_2} \frac{N_o}{\left[\frac{b/\cos\theta}{r_o}\right]^2} \cdot \frac{b}{\cos^2\theta} \, d\theta = \frac{N_o r_o^2}{b} \int_{\theta_1}^{\theta_2} d\theta$$

$$I = \frac{N_o r_o^2}{b} (\theta_2 - \theta_1) \qquad \text{(E.1)}$$

Next, this equation for I is expressed in terms of the quantities listed in our Pioneer ephemeris. The angle $\theta_2 - \theta_1$ is the ephemeris listed angle ESP (Earth-Sun-Probe). Only b remains to be determined in terms of the ephemeris parameters labeled in Fig. E-4.

$$b = RS \sin SEP \tag{E.2}$$

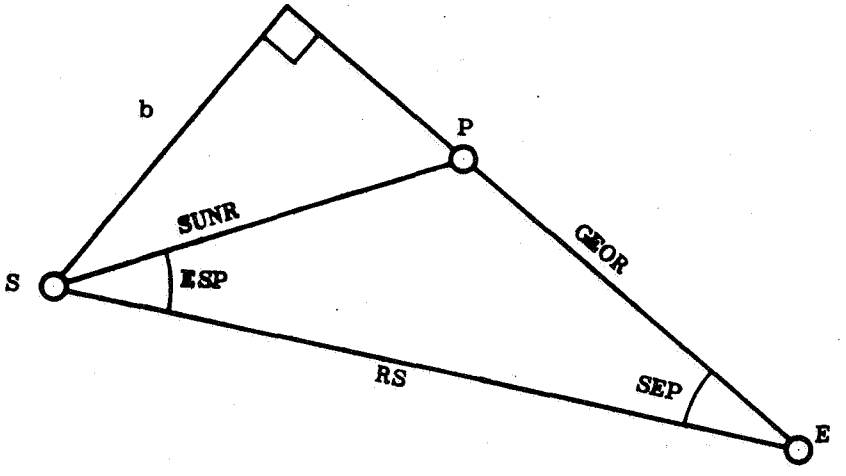

FIG. E-4. EPHEMERIS TERMS DEFINED.

Using the law of sines,

$$\frac{GEOR}{\sin ESP} = \frac{SUNR}{\sin SEP}$$

$$\sin SEP = \frac{SUNR}{GEOR} \sin ESP$$

Substitute this equation for sin SEP into Eq. (E.2) for b.

$$b = RS \left(\frac{SUNR}{GEOR}\right) \sin ESP$$

Next, substitute this equation for b, and the angle ESP for $\theta_2 - \theta_1$ into Eq. (E.1) for I.

$$I = \frac{N_o r_o^2}{b} (\theta_2 - \theta_1) = \frac{N_o r_o^2 \, ESP}{RS \, \frac{SUNR}{GEOR} \sin ESP}$$

$$= \frac{N_o \, GEOR}{\left(\frac{\sin ESP}{ESP}\right)\left(\frac{RS}{r_o}\right)\left(\frac{SUNR}{r_o}\right)}$$

Finally, substitute RD for r_o, the reference distance for N_o,

$$I = \frac{N_o \, GEOR}{\text{sinc}\left(\frac{ESP}{\pi}\right)\left(\frac{RS}{RD}\right)\left(\frac{SUNR}{RD}\right)} \qquad (E.3)$$

This equation for the integrated electron content I is a function of spacecraft position. Solving for N_o gives the electron number density, normalized to 1 AU (for RD = 1 AU). Equation (E.3) is plotted in Fig. 5-8 for the Pioneer VI trajectory, and shows that the content with the $1/r^2$ density distribution to be 25 percent higher than for the uniform distribution. For Pioneer VII the content is 10 lower.

The $1/r^2$ solar wind density dependence implicitly assumes that the solar wind velocity is constant; the following development confirms the assumption. The velocity change of a particle traveling at the solar wind velocity (300 km/sec) is determined from its gain in potential energy as the particle travels from 0.8 to 1.12 AU. The potential energy gained by a body going out from the sun is

$$\Delta PE = \int_{R_1}^{R_2} -F(r) \, dr = \int_{R_1}^{R_2} G \, m_1 m_2 \, dr = \frac{G \, m_1 m_2}{1/2}\left(\frac{1}{R_1} - \frac{1}{R_2}\right) \qquad (E.4)$$

where

G = gravitational constant = 6.67×10^{-11} $m^3/kg\text{-}sec^2$

m_1 = mass of the sun = 2×10^{30} kg

m_2 = mass of the body going away from the sun

Next, the kinetic energy lost by a body that changes its velocity from v_1 to a lower velocity v_2 is

$$\Delta KE = \frac{1}{2} m_2 v_1^2 - \frac{1}{2} m_2 v_2^2 = \frac{m_2}{2} \left(v_1^2 - v_2^2 \right)$$

Express v_2 in terms of v_1 and substitute into the above equation for ΔKE

$$v_2 = v_1 + \Delta v$$

$$\Delta KE = \frac{m_1}{2} \left[v_1^2 - (v_1 + \Delta v)^2 \right] = -m_1 v_1 \Delta v + \frac{m_1 \Delta v^2}{2} \qquad \text{(E.5)}$$

The second term is small, compared with the first. The kinetic energy lost, Eq. (E.5), is set equal to the potential energy gained in Eq. (E.4).

$$-m_2 v_1 \Delta v = G\, m_1 m_2 \left(\frac{1}{R_1} - \frac{1}{R_2} \right)$$

$$\Delta v = -1.0 \text{ km/sec}$$

The solar wind velocity is reduced by only 1.0 km/sec or 0.33 percent of the minimum solar wind velocity of 300 km/sec. The slowing down is even less for higher solar wind velocities. This small velocity change has an insignificant effect on the interplanetary electron density.

BIBLIOGRAPHY

Bhonsle, R. V., A. daRosa, and O. K. Garriott, "Measurements of the Total Electron Content and the Equivalent Slab Thickness of the Midlatitude Ionosphere," Radio Science, Journal of Research NBS/USNC-URSI, 69D, No. 7, July 1965, 929-937.

Of interest in determining the ionospheric electron content from the maximum density.

Davies, K., Ionospheric Radio Propagation, National Bureau of Standards Monograph 80, U. S. Govt. Printing Office, 1965.

This book gives a brief introduction into very wide range of ionospheric topics with many useful results. Good extensive references are supplied with each pin-pointed to a particular topic, so that once you are introduced to the topic, it is easy to go further.

Eshleman, V. R. et al, "The Interplanetary Electron Number Density from Preliminary Analysis of the Pioneer 6 Radio Propagation Experiment," J. Geophys. Res., 71, 13, 1 July 1966, 3325-3327.

A brief description of Stanford's Pioneer experiment with some results.

Garriott, O. K., "The Determination of Ionospheric Electron Content and Distribution from Satellite Observations, Part 2: Results of the Analysis," J. Geophys. Res., 65, 4 April 1960, 1151-1157.

The Faraday rotation technique is used to analyze Sputnik III transmissions to obtain ionospheric electron content from Sept. 1958 through Apr. 1959.

Garriott, O. K. and F. De Mendonça, "A Comparison of Methods Used for Obtaining Electron Content from Satellite Observations," J. Geophys. Res., 68, 17, 1 Sept. 1963, 4917-4927.

See 4920-1 Sec. D for Doppler methods. The accuracy of the Doppler analysis is compared with other techniques described in the article.

Garriott, O. K., F. L. Smith, and P. C. Yuen, "Observations of Ionospheric Electron Content Using a Geostationary Satellite," Plan. Space Sci., 13, 1965, 829-838.

A brief introduction to Faraday rotation with the Syncom III geostationary satellite; the electron content measured on a number of days at Hawaii and at Stanford are presented.

Jaffe, R. and E. Rechtin, "Design and Performance of Phase Lock Circuits Capable of Near Optimum Performance over a Wide Range of Input Signal and Noise Levels," IRE Trans. on Inform. Theory, March 1955, 66-76.

The signal-to-noise characteristics of a bandpass limiter, clearly presented on pp. 68-69, are useful in understanding the significance of the 'carrier amplitude' data from Stanford's Pioneer radio propagation experiment.

Koehler, R., "A Phase Locked Dual Channel Spacecraft Receiver for Phase and Group Path Measurements," Stanford Electronics Laboratories Rpt. SU-SEL-65-007, Feb. 1965; or NASA Contractor's Rpt. NASA CR-323, Nov. 1965.

This instruction book for the Stanford Pioneer receiver used in this experiment includes some of the design considerations, especially the signal strength and phase lock loop design.

Lawrence, R. S., C. G. Little, and J. H. A. Chives, "A Survey of Ionospheric Effects upon Earth-Space Radio Propagation," Proc. IEEE, 52, 1, Jan. 1964, 4-27.

VHF, 40-1000 MHz, effects of the ionosphere; the first 3 pages, pp. 4-6, describe all the effects needed to understand the first order group and phase path effects used in this study; it is a quick reference for the ionospheric effects at VHF without always having to rederive it as is necessary with Ratcliffe (1959).

Lazarus, A. J., H. S. Bridge and J. Davis, "Preliminary Results from the Pioneer 6 M.I.T. Plasma Experiment," J. Geophys. Res., 71, 15, 1 Aug. 1966, pp. 3787-3790.

Martin, F. T., Beacon Explorer B (BE-B) Project Development Plan, Revision 1, Goddard Space Flight Center, Sept. 1964.

Some details about the beacon satellites.

McCraken, K. G. et al, "Anisotropic Cosmic Radiation Fluxes of Solar Origin," J. Geophys. Res., 71, 13, 1 July 1966, 3297-3304.

One of the Pioneer cosmic ray experiments.

Ness, N. F., C. S. Scearce, S. Cantarano, "Preliminary Results from the Pioneer 6 Magnetic Field Experiment," J. Geophys. Res., 71, 13, 1 July 1966, 3305-3313.

Neugebauer, M., C. W. Snyder, "The Mission of Mariner II: Preliminary Observations, Solar Plasma Experiment," Science, 138, 3545, 7 Dec. 1962, 1095-1097.

Neugebauer, M., C. W. Snyder, "Mariner 2 Observations of the Solar Wind; 1. Average Properties," J. Geophys. Res., 71, 1966, 4469-4484.

Includes graphs of 3 hour averages of solar wind velocity and density from 27 August 1962 to 28 December 1962.

Ratcliffe, J. A., The Magneto-Ionic Theory and its Applications to the Ionosphere, Cambridge University Press, London, 1959.

The Appleton-Hartree equations are derived with several different approaches with the derivation in Chap. 2 as the basis for the rest of the book; Chap. 8, pp. 75-6 for the quasi longitudinal approximation which is usually used, and Chap. 11, p. 103 for group velocity; Chap. 12, pp. 108-113 for ionosonde type effects in the ionosphere; Chap. 13 includes the magnetic field on ionograms; Chap. 7, pp. 65-6 is concerned with polarization which is developed one step earlier than the taking-off point for most articles about the ionosphere -- this allows the resolving of puzzling points about polarization.

Ross, W. J., "Second-Order Effects in High-Frequency Transionospheric Propagation," J. Geophys. Res., 70, 3, 1 Feb. 1965, 597-612.

The second-order terms are retained in the index of refraction equation for group and phase paths through a plane stratified ionosphere which is tilted to be parallel to the earth at the ionospheric point.

Simpson, J. A. et al, "Anisotropy and Fluctuations of Solar Proton Fluxes of Energies 0.6-100 Mev Measured on the Pioneer 6 Space Probe," J. Geophys. Res., 71, 13, 1 July 1966, 3289-3296.

One of the cosmic ray experiments aboard Pioneer.

Thomas, J. O., "The Distribution of Electrons in the Ionosphere," Proc. IRE, 47, Feb. 1959, 162-175.

A clear explanation of a true height ionogram analysis technique.

Titheridge, J. E., "Continuous Records of the Total Electron Content of the Ionosphere," J. of Atmos. and Terres. Phys., 28, 1966, 1135-1150.

A Faraday rotation angle system is described which uses a 1 rps rotating antenna and a 2 Hz phase meter and produces a direct record of Faraday rotation.

Wolfe, J. H. et al, "The Compositional, Anisotropic, and Non-Radial Flow Characteristics of the Solar Wind," J. Geophys. Res., 71, 13, 1 July 1966, 3329-3335.

One of the Pioneer plasma probe experiments.

UNCLASSIFIED
Security Classification

DOCUMENT CONTROL DATA - R & D

(Security classification of title, body of abstract and indexing annotation must be entered when the overall report is classified)

1. ORIGINATING ACTIVITY (Corporate author)	2a. REPORT SECURITY CLASSIFICATION
Stanford Electronics Laboratories Stanford University, Stanford, California	Unclassified
	2b. GROUP

3. REPORT TITLE

INTERPLANETARY ELECTRON CONTENT MEASURED BETWEEN EARTH AND THE PIONEER VI AND VII SPACECRAFT USING RADIO PROPAGATION EFFECTS

4. DESCRIPTIVE NOTES *(Type of report and inclusive dates)*

Scientific Report

5. AUTHOR(S) *(First name, middle initial, last name)*

Richard L. Koehler

6. REPORT DATE	7a. TOTAL NO. OF PAGES	7b. NO. OF REFS
May 1967	113	21

8a. CONTRACT OR GRANT NO.	9a. ORIGINATOR'S REPORT NUMBER(S)
NSR 05-020-109	
b. PROJECT NO. NAS 2-3908 NsG 377	SU-SEL-67-051
c.	9b. OTHER REPORT NO(S) *(Any other numbers that may be assigned this report)*
d.	

10. DISTRIBUTION STATEMENT

Reproduction in whole or in part is permitted for any purpose of the United States Government.

11. SUPPLEMENTARY NOTES	12. SPONSORING MILITARY ACTIVITY

13. ABSTRACT Radio signals at 50 and 425 MHz are sent from Stanford to deep space probes to determine the electron number density, structure, and time variability of the interplanetary medium. The electron content (the number of electrons in a square meter column along the path of propagation) introduces a small difference in the time it takes the 50 and 425 MHz signals to reach the spacecraft; this time difference is caused by the frequency dependence of the velocity of propagation in a plasma. The time difference, determined from phase shift of the modulation on both signals, provides a measure of the total electron content in the path. In addition, the number of cycles of phase shift of the radio frequency carriers are counted to provide a high resolution measurement of the change in electron content along the path. Total contents of up to 200×10^{16} el/m^2 have been measured, a substantial portion of which was located in the dense ionosphere surrounding the earth. To obtain the interplanetary content, the ionospheric portion must be subtracted. Differential doppler measurement of beacon satellite signals provide the ionospheric electron content several times during one Pioneer pass. Faraday rotation of signals from a geostationary satellite (Applied Technology Satellite) provides continuous measurement of electron content through the ionosphere. The interplanetary content is divided by the spacecraft range to give the average number density. An average interplanetary number density of 4.3 el/cm^3 with an ams variation of ±3.6 was determined from 125 Pioneer VI interplanetary electron content measurements, made from December 1965 through May 1966. The average determined from 170 Pioneer VII measurements made from August 1966 to March 1967 is 8.7 ±4.0 el/cm^3. The higher average at the later date occurred because interplanetary space was filled more frequently with denser plasma caused by

DD FORM 1 NOV 65 1473

Security Classification

14. KEY WORDS	LINK A		LINK B		LINK C	
	ROLE	WT	ROLE	WT	ROLE	WT
INTERPLANETARY ELECTRON CONTENT INTERPLANETARY ELECTRON DENSITY PIONEER VI SPACECRAFT PIONEER VII SPACECRAFT GROUP PATH PHASE PATH IONOSPHERIC ELECTRON CONTENT PLASMA PULSES BISTATIC SOFT TARGET RADAR						

ABSTRACT (Continued)

increasing solar activity. The quiet level for Pioneer VII was about 5 el/cm^3, which is near the average for Pioneer VI; these values are in agreement with measurements made locally in interplanetary space by plasma probe experimenters. All of the above measurements apply to regions of interplanetary space which are within 20 percent of the distance of earth from the sun. Three sudden, large increases in the electron content were observed: 24 October 1966, 10 November 1966, and 25 January 1967. They are explained by a model with a rectangular-shaped increase in electron number density with a spherical wavefront traveling radially from the sun at 300 to 400 km/sec. The increase in density ranged from 30 to 55 electrons/cm^3 above the background density, extending over a region from 5 to 10×10^6 km along a solar radial.